UNIVERSITY OF CALIFORNIA, SAN DIEGO

Spatiotemporal Regulation of Protein Kinase C Signaling:

Control of Normal Cellular Dynamics and Mis-regulation in Cancer

A dissertation submitted in partial satisfaction of the

requirements for the Doctor of Philosophy

in

Biomedical Sciences

by

Lisa Leon Gallegos

Committee in Charge:

Professor Alexandra C. Newton, Chair
Professor Joan Heller Brown
Professor Seth J. Field
Professor Roger Y. Tsien
Professor Nicholas Webster

2009

The dissertation of Lisa Leon Gallegos is approved and it is acceptable in quality and form for publication on microfilm and electronically:

Chair

University of California, San Diego

2009

Dedication

To Betty Blake:
the original thinker, talker, tinkerer.
We miss you.

Table of Contents

Signature page iii

Dedication page iv

Table of Contents v

List of Figures vi

Acknowledgements ix

Vita xii

Abstract of the Dissertation xiii

Chapter 1 Cellular Control of Protein Kinase C Signaling 1

Chapter 2 Targeting Protein Kinase C Activity Reporter to Discrete Intracellular Regions Reveals Spatiotemporal Differences in Agonist-dependent Signaling 32

Chapter 3 A Single Residue in the C1 Domain Sensitizes Novel Protein Kinase C Isoforms to Cellular Diacylglycerol Production 79

Chapter 4 A Putative Cancer Driver Mutation in Protein Kinase C βII Decreases Diacylglycerol-dependent Signaling and Prevents Apoptosis in the Context of Oncogenic K-Ras 109

Chapter 5 Protein Kinase Cα Interacts With and Phosphorylates SAP97/DLG1 to Promote Cytoskeletal Rearrangements 136

Chapter 6 Summary and Conclusions 187

List of Figures

Figure 1.1. Primary structure of protein kinase C (PKC) family members 20

Figure 1.2. Reversible, genetically-encoded, FRET-based reporters for visualizing PKC activity and DAG accumulation..... 21

Figure 1.3. Differential activation signatures of PKC at the plasma membrane and at the Golgi, as read out using targeted FRET-based reporters. 22

Figure 1.4. Examples of PKC regulation at the cellular level in response to lipid second messenger signaling 23

Figure 2.1. Targeting C Kinase Activity Reporter (CKAR) 53

Figure 2.2. Targeted CKAR retains specificity and reversibility in monitoring PKC activity in live cells 54

Figure 2.3. Localized PKC activity in COS 7 cells 55

Figure 2.4. PKC response to UTP in COS 7 cells. 57

Figure 2.5. Ca^{2+} release is responsible for early phase of the UTP-stimulated PKC response..... 58

Figure 2.6. Localized persistence in PKC activity follows DAG persistence 60

Figure A1.1. Validating targeting of CKAR to sub-cellular locations 71

Figure A1.2. Validation of targeting of GolgiCKAR and PMCKAR using Brefeldin A. 73

Figure A1.3. Partial cleavage of MitoCKAR..... 74

Figure A1.4. Validating specificity of targeted CKARs. 75

Figure A1.5. Kinetics of PdBu distribution into intracellular membranes. 76

Figure A1.6. Gö6983 accumulation in intracellular membranes. 77

Figure A1.7. Untargeted DAGR reports differences in DAG production at peripheral membranes compared to juxtanuclear membranes. 78

Figure 3.1. Residue 22 tunes binding of the C1b domain to DAG membranes *in vitro* and *in vivo* and affects kinase activity. 94

Figure 3.2. Residue 22 affects localization of the C1b domain and full-length PKC..... 95

Figure 3.3. The C1 domain's ability to bind DAG arises from modulation of the width and surface properties of the loops surrounding the hydrophobic DAG-binding cleft..... 96

Table 3.1 Binding constants for the interaction of the C1b domain with membranes…..97

Figure A2.1. FRET ratios reflecting C1b translocation can be adjusted to accurately account for differences in the ranges of individual cells 106

Figure A2.2. Brefeldin A treatment disperses Golgi-localized C1b domains 107

Figure A2.3. Raw counts from kinase assay demonstrate that the DAG-sensitizing mutation does not affect PKC activity in the presence of Ca^{2+} 108

Figure 4.1. Val 144 is conserved amongst C1b domains of conventional PKC isoforms. 125

Figure 4.2. Mutation of Val 144 to Met in the C1b domain of PKCβ decreases the affinity for PdBu- and DAG-containing membranes..... 126

Figure 4.3. Mutation of Val 144 to Met in full-length PKCβII increases the concentration of UTP required to promote phosphorylation of CKAR, a PKC activity reporter 127

Figure 4.4. Both PKCβII and PKCβII-V144M promote cell cycle progression in cells containing oncogenic K-Ras 128

Figure 4.5. PKCβII V144M promotes survival in colon cancer cell lines containing oncogenic K-Ras mutations, but has no effect in a colon cancer cell line containing wild-type K-Ras 129

Figure 4.6. Model describing potential mechanism whereby inactivating PKC mutations contribute to tumor progression 130

Table 4.1 Mutations in PKC family members present in colon tumor samples or colon cancer cell lines harboring oncogenic K-Ras mutations…….131

Figure 5.1. The PDZ ligand of PKCα interacts with the 3rd PDZ domain of both DLG1 and PSD95. 164

Figure 5.2. The PDZ ligand of PKCα contributes to the interaction between MAGUK scaffolds and PKCα. 165

Figure 5.3. CFP-DLG1 and RFP-PKCα form ring-shaped, actin-rich clusters in COS7 cells in a PKC activity-dependent, PDZ ligand-independent manner. 166

Figure 5.4. Endogenous DLG1 and PKCα staining is enriched at podosomes. 169

Figure 5.5. Inhibition of conventional PKC reverses podosome formation.. 170

Figure 5.6. Generation of a phospho-specific antibody to PKC phosphorylation site, Thr656 (rat numbering), located in the hinge region of DLG1 and other MAGUK scaffolds.. 171

Figure 5.7. PDZ interaction is not essential for phosphorylation of expressed DLG1.. 172

Figure 5.8. Phosphorylation of Thr 656 occurs at podosomes. 173

Figure 5.9. Endogenous PKCα and DLG1 co-localize at leading edge of migrating astrocytes in activity-dependent manner..... 176

Figure 5.10. Inhibiting cPKCs impairs astrocyte migration. 177

Figure 5.11. Endogenous DLG1 is phosphorylated at the midbody of COS7 cells undergoing cytokinesis. 178

Figure 5.12. Purified GST-tagged BRCT domains from Ect2 bind phospho-Thr656... 179

Figure 5.13. Model describing potential molecular mechanism by which PKCα/DLG1 signaling scaffold promotes cytoskeletal rearrangements. 181

Figure 6.1. Summary of thesis work examining spatio-temporal dynamics of PKC signaling. 198

Acknowledgements

Most importantly, I thank my husband, Arturo Gallegos, for love and support of every kind not only during graduate school, but throughout the 12 years we have been together. I especially thank him for giving me every reason to believe that we can do anything together.

I thank my parents, Edward and Karen Leon, and sisters and brothers, Tina, Lynda, Anthony, and Mychael for stimulation, instruction, support, and unconditional love through fun times, good times, and hard times. I also thank my husband's family, Arturo, Irma and Lilia, for their friendship, love, and unconditional support. I thank extended family, especially Raymond and Betty Blake and Reyes and Katy Leon, for providing additional support throughout my life.

I thank members of the Newton lab, past and present, for instruction, guidance, and good company during the past 5 years. Many thanks to Maya Kunkel, my primary mentor, friend and colleague for guidance on matters related to science and life in general. Thanks to senior lab members Charles King, Tianyan Gao, and Gloria Reyes for scientific mentorship and fellowship. I also thank past and present graduate students Daniel Dries, Angela Scott, John Brognard, Christine Gould, and Matt Niederst, Audrey O'Neill, Noel Warfel, and Alyssa Wu for helpful discussions and/or shared experiences that enriched my graduate education and guided me on my career path. In particular, I thank Dan and John for scientific collaborations from which I learned a great deal and Audrey for collaborating with me on my most recent project.

I thank mentors on my thesis committee and throughout the department (in particular members of Jack Dixon's Lab) for critical scientific feedback and/or career

advice. I also thank mentors in the scientific community who have provided helpful discussions interpreting data, teaching me new techniques, or helping orient me in the scientific literature (in particular Mark Dell'Acqua). Many thanks to collaborators Randy Hall, Erin Garcia, C. J. Allison, John Brognard, and Tony Hunter for sharing data and ideas featured in this thesis.

I thank members of the Biomedical Sciences Graduate program for friendship and support. I especially thank Gina Butcher and Leanne Nordeman for their guidance throughout graduate school on administrative and other matters. I thank members of my entering class, Lindsay Lewellyn, Ben Sachs, Tom Gallegos, and Jason Goode, and their families, for their friendship and shared experiences. I also thank friends outside of the BMS community (especially Katy Warren) for their balancing perspectives.

Finally, I extend sincere gratitude to my inspiring mentor, Alexandra Newton, for providing a wonderful environment for graduate research in her lab. Throughout personal trials and professional obligations, she has been an upbeat, resilient, intelligent, even-tempered, professional, and caring mentor, friend, and role model. Graduate experiences vary widely from person-to-person and from lab-to-lab, and I am fully aware of how incredibly lucky I am to have had the amazingly rich graduate experience that I have had under her guidance.

The text of chapter 1 is, in part, a reprint of the material as it appears in IUBMB Life, 2008, Gallegos LL and Newton AC. I was the author of this literature review.

The text of Chapter 2 is, in full, a reprint of the material as it appears in the Journal of Biological Chemistry, 2006, by Gallegos LL, Kunkel MT, and Newton AC. I was the primary author and researcher.

The text of Chapter 3 is, in full, a reprint of the material as it appears in the Journal of Biological Chemistry, 2007, by Dries DR, Gallegos LL, and Newton AC. I was the co-primary author and researcher.

Vita

2003 Bachelor of Science, New Mexico State University

2009 Doctor of Philosophy, University of California, San Diego

Publications

Gallegos, LL, Newton AC. Spatiotemporal dynamics of lipid signaling: Protein kinase C as a paradigm. IUBMB Life. Volume 60, Number 12, December 1, 2008. Pgs: 782-789.

Dries, DR*, Gallegos, LL*, Newton AC. *equal authors. A single residue in the C1 domain sensitizes novel protein kinase C isoforms to cellular diacylglycerol production. Journal of Biological Chemistry. Volume 282, Number 2, January 12, 2007. Pgs: 826-830.

Gallegos, LL, Kunkel, MT, Newton AC. Targeting protein kinase C activity reporter to discrete intracellular regions reveals spatiotemporal differences in agonist-dependent signaling. Journal of Biological Chemistry. Volume 281, Number 41, October 12, 2006. Pgs: 30947-30956.

ABSTRACT OF THE DISSERTATION

Spatiotemporal Regulation of Protein Kinase C Signaling:

Control of Normal Cellular Dynamics and Mis-regulation in Cancer

by

Lisa Leon Gallegos

Doctor of Philosophy in Biomedical Sciences

University of California, San Diego, 2009

Professor Alexandra C. Newton, Chair

Protein kinase C (PKC) is an archetypal mediator of cellular signaling. PKC consists of 10 Ser/Thr kinases that participate in a wide range of cellular processes, including proliferation, apoptosis, learning and memory, and cell migration. PKC signaling is controlled by lipid second messengers and protein scaffolding. For proper cellular PKC signaling, location and timing of activation are critical. Aberrant PKC

signaling is known to occur in disease states, notably cancer. The goal of this thesis is to examine how spatial and temoral specificity are achieved in cellular PKC signaling, and how this regulation is altered in cancer. Understanding the nuances of PKC regulation in cells and mis-regulation in disease will undoubtedly inform efforts to therapeutically target this enzyme family.

Chapter 1

Cellular Control of Protein Kinase C Signaling

Signal transduction networks convert external cues into cellular actions. Receptors are activated by agonists; these in turn stimulate the production of second messengers, which turn on signaling cascades in cells, in many cases by promoting phosphorylation of substrates by kinases. Often the initial signal from low concentrations of agonist is amplified into the production of relatively higher concentrations of cellular metabolites (1), or is converted into a large-scale cellular response, such as migration toward a chemo-attractant (2). Connectivity in cellular signaling has long been studied in terms of linear cascades of signaling proteins acting on effector proteins. However, it is increasingly clear that timing and localization are critical determinants of whether proteins will act on effectors, and whether the actions of protein complexes will couple to a biological effect. Signal transduction cascades are subject to myriad forms of regulation that are as diverse as can be imagined. Not surprisingly, the mis-regulation of signaling is the root of most diseases, notably cancer (3,4). Because kinases lie at the crux of signal amplification, they have long been attractive therapeutic targets for modulating signaling in disease processes (5). The protein kinase C (PKC) family of Ser/Thr kinases is one such kinase family that has been extensively studied in the context of normal cellular signaling and is also a target in the treatment of disease.

PKC

The PKC family of Ser/Thr kinases comprises 10 members in the AGC kinase branch of the kinome (6). PKC was initially discovered as a lipid-independent proteolytic product by Nishizuka and colleagues in 1977 (7). Subsequently, it was found that the full-length enzyme is stimulated by the products downstream of phospholipase C (PLC)-catalyzed hydrolysis of PIP_2, DAG and Ca^{2+} (8,9); this milestone finding recently

celebrated its 25th anniversary (10). Following on the heels of this seminal discovery, the connection was made that PKC was the long sought-after receptor for the tumor-promoting high-affinity DAG analogs, phorbol esters (11), a finding which catapulted the enzyme to the forefront of signaling research. All 10 mammalian PKC isoforms contain a highly-conserved kinase core at the carboxyl terminus and an amino-terminal autoinhibitory pseudosubstrate peptide, but differ by, and are classified according to, their divergent amino-terminal regulatory regions (Figure 1.1). Conventional PKC (cPKC) isoforms (α, alternative splice variants βI and βII, and γ) contain a Ca^{2+}-sensitive C2 domain and two tandem DAG-sensitive C1 domains; novel PKC (nPKC) isoforms (δ, θ, ε, and η) contain a Ca^{2+}-insensitive C2 domain and two tandem DAG-sensitive C1 domains; and atypical PKC (aPKC) isoforms (ζ and ι(human)/λ(mouse)) contain a single C1 domain that is insensitive to DAG and a PB-1 domain that is a protein-protein interaction module (reviewed in (6,12)).

PKC isoforms are processed by a series of ordered phosphorylation events to mature into the catalytically-competent species (reviewed in (6)). Maturation is initiated by phosphorylation at PKC's activation loop threonine by the upstream kinase, phosphoinositide-dependent kinase-1 (PDK-1), and then requires mammalian target of rapamycin complex 2 (mTORC2) for phosphorylation/autophosphorylation at two carboxyl-terminal sites, the hydrophobic and turn motifs (reviewed in (6,13,14)). In most systems, the maturation of cPKC and nPKC isoforms is constitutive, such that monitoring the phosphorylation state of PKC is not often indicative of acute activation. Once catalytically competent, PKC resides in an inactive state in the cytosol with the inhibitory peptide lodged into its active site. For cPKC and nPKC isoforms, high-affinity Ca^{2+}-

and/or DAG-mediated membrane binding provides the energy required to expel the inhibitory peptide from the active site and allow PKC to phosphorylate downstream substrates. For aPKC isoforms, acute activation in response to growth factor signaling has been demonstrated, but the exact mechanism remains ambiguous (15); regulation by protein-protein interactions may be more important (16).

PKC signaling in response to lipid second messengers

Lipids acutely control the structure, function, and localization of an abundance of signaling proteins. Under unstimulated conditions, the enrichment of specific lipids in distinct subcellular organelles lays the framework for poising signaling proteins to efficiently respond to second-messenger signaling. A generally accepted model places phosphoinositide-4,5-bisphosphate (PIP_2) enrichment at the plasma membrane, phosphoinositide-4-phosphate at the Golgi, and phosphoinositide-3-phosphate at endosomes (reviewed in (17)); recent reports have placed basal diacylglycerol (DAG) enrichment at the Golgi (18-20) and phosphatidylserine (PS) enrichment at the cytoplasmic side of both the plasma membrane and endosomes (21). Within this framework of organization, cells have a variety of mechanisms to stimulate and regulate production of relatively short-lived lipid second messengers which can promote activating conformations and direct signaling proteins to new locations. Signaling proteins simultaneously sense the cellular address of the appropriate lipid ‘zip codes’ and respond to stimulated production of specific lipid second messengers through one or more specialized membrane-targeting domains. For example, modules such as PKC conserved region 1 (C1) domains target proteins to DAG; PKC conserved region 2 (C2) domains to specific phospholipids; pleckstrin homology (PH) and Epsin N-terminal

homology (ENTH) domains to specific phosphoinositides; and Bin/Amphiphysin/Rvs (BAR) domains to highly-curved lipid structures (22,23). Such lipid signaling modules, as described above, control the spatiotemporal dynamics of PKC.

1. Lipid second messengers control the dynamics of PKC signaling

The crux of PKC activation occurs at the level of lipid second messenger production and turnover. For conventional isozymes, the most common pathway for lipid second messenger production involves a G_q-coupled receptor triggering PIP_2 hydrolysis by PLCβ isoforms. This produces DAG and IP_3, which transiently elevates intracellular Ca^{2+}. PLCδ is acutely activated downstream of Ca^{2+} release, which may also contribute to PKC signaling mediated by G_q (reviewed in (24,25)). PLCγ and ε activated downstream of receptor tyrosine kinase and G_{12} signaling, respectively, are potential activators of PKC; PLCε is a particularly interesting potential activator of PKC since it contains intrinsic feed-forward mechanisms to hydrolyze phosphoinositides in a prolonged manner (reviewed in (25)). Phosphatidic acid phosphatase (PAP) may also play a role in generating basal DAG by dephosphorylating phosphatidic acid (PA) (18), although it remains to be tested whether this pathway contributes to acute, receptor-mediated DAG production. Termination of signaling occurs when receptors are internalized and degraded to halt signaling to PLC, and DAG is converted into PA by the action of DAG kinases (reviewed in (26)).

The effects of lipid second messenger production and turnover on signaling occur on a time scale that is amenable to live cell imaging. Thus, many live cell imaging studies have monitored the agonist-evoked membrane translocation of fluorescently-tagged PKC isoforms (27). Additional studies using fluorescence resonance energy

transfer (FRET)-based reporters for DAG production (Diacylglycerol Reporter, DAGR) and PKC activity (C Kinase Activity Reporter, CKAR; Figure 1.2) have revealed that stimulated changes in second messenger levels correlate with PKC activity. For example, plasma membrane-targeted CKAR revealed phase-locked oscillations of Ca^{2+} and endogenous PKC activity in Hela cells upon stimulation of endogenous histamine receptors (28,29). In Chapter 2, we present studies using live cell imaging to demonstrate that variations in lipid second-messengers lead to differences in PKC activity at discrete cellular organelles (30). Specifically, in COS7 cells, UTP stimulation of endogenous P2Y receptors results in an acute activation of endogenous PKC at the plasma membrane, followed by sustained activity at the Golgi (Figure 1.3). The duration of PKC activity at the two locations is driven by persistence in localized DAG production, as revealed in independent experiments by plasma membrane- and Golgi-targeted DAGR. These studies and others demonstrate that localized regulation of second messenger production and turnover largely determine the extent of stimulated PKC signaling at a given cellular location.

2. Ligand affinity tunes cellular PKC activation

Lipid binding modules of the same class often bind ligand with different intrinsic affinities, which influences the cellular concentration required to activate or localize a particular signaling protein. Differential affinities of the C1 domains of novel vs. conventional PKC isoforms for DAG-containing membranes serve as a case in point. Specifically, nPKC isoforms bind DAG-containing membranes with two orders of magnitude higher affinity than do cPKC isoforms (31). This higher intrinsic affinity of the C1 domain allows nPKC isoforms to be activated by cellular concentrations of DAG

alone, while cPKC isoforms require both Ca^{2+} (via C2) and DAG (via C1) to achieve the high-affinity membrane binding necessary to expel the inhibitory pseudosubstrate peptide from the active site (32). In Chapter 3, we present a study in which we discover a single amino acid substitution in the C1b domain (Tyr123 in human PKCβ isoforms, Trp252 in human PKCδ) that underlies the difference in DAG sensitivity between cPKC and nPKC isoforms (19). Thus, the residue at this position (which we refer to as position 22 in the C1b domain) serves as a switch between low vs. high-affinity DAG binding for the C1b domains of PKC isoforms. In Chapter 4, we also describe a putative cancer driver mutation occurring in a human colon tumor that decreases binding of the C1b domain of PKCβII to membranes in response to DAG. This mutation increases the threshold for PKC activation, which decreases apoptosis in colon cancer cell lines by dampening a pro-apoptotic feedback loop involving K-Ras.

High-affinity DAG binding influences not only the selective activation of PKC isozymes, but also their cellular localization. As first shown with nPKCθ in Jurkat T cells (18), reducing basal DAG production by inhibiting either PLC or PAP blocked localization of this isoform to the Golgi. Consistent with this report, we show in Chapter 3 that converting the C1b domain of nPKCδ to a low-affinity DAG binding domain (by mutating Trp22 to Tyr) blocked basal Golgi localization of the isolated C1 domain as well as full-length PKCδ in COS7 cells. Conversely, changing Tyr22 to Trp in the C1b domain of cPKCβ, converting it to a high-affinity DAG binding domain, was sufficient to localize this conventional C1 domain to the Golgi. Note that introduction of the same mutation into the C1b domain of full-length cPKCβII did not target it to Golgi, although it partially precluded the requirement of Ca^{2+} for activation *in vitro* (19). This result

suggests that determinants outside the C1 domain (likely the C2 domain) govern cellular targeting of cPKC isoforms. Also, while the Golgi is a major site of nPKC activity (18,31), it is entirely possible that stimulated DAG production at other regions of the cell can temporarily draw nPKC isoforms away from the Golgi (e.g. to the plasma membrane (33)).

Ca^{2+}-dependent interactions with anionic phospholipids via the C2 domains of cPKC isoforms also occur with variable affinities; however, these differences are fairly subtle. PKCα, β, and γ have similar intrinsic affinities for Ca^{2+} (PKCα=PKCγ>PKCβ), and their Ca^{2+}-dependent membrane affinities (PKCβ>PKCα=PKCγ) are also similar (both measurements within a two-fold difference) (34-36). Collectively, the differences in Ca^{2+} affinity and Ca^{2+}-dependent membrane affinity do not affect the on-rate of the isolated C2 domains in response to stimulation of purinergic receptors in PC12 cells, but they somehow affect the residence time at the membrane, with the C2 domain from PKCα persisting longer at the membrane (200 s) than that of PKCγ (72 s) or β (48 s) (36). This effect appears to be governed additionally by the anchoring of PIP_2 at a site in the C2 domain distal to the Ca^{2+}-dependent membrane binding site, even though the presence of PIP_2 in binding assays does not dramatically augment the two-fold range in binding affinities amongst the C2 domains *in vitro* (36). Certainly, further cellular consequences of these fine binding differences remain to be determined. Nevertheless, in cells, lipid-dependent membrane binding affinity has been proven to affect isoform-specific PKC signaling both by setting the threshold for activation and determining localization.

3. Coincident selectivity for multiple ligands within the same domain refines localized PKC responses.

Lipid signaling domains may have selectivity for more than one ligand. For example, while the C2 domains of cPKC isoforms bind anionic phospholipids non-specifically in the presence of Ca^{2+}, the preferential recognition of PIP_2 with a basic patch on the C2 domain distal to the Ca^{2+}-dependent binding site (37) directs cPKC isoforms to the PIP_2-rich plasma membrane (38). In an elegant series of experiments in which PIP_2 production was artificially and selectively increased at the plasma membrane by an inducible Rapamycin-FK506-binding protein system, the residency time of cPKC isoforms at the plasma membrane was increased even though generation of DAG was normal under these conditions (39). It would be interesting to test whether PIP_2 was the sole mediator of plasma membrane targeting by selectively targeting PIP_2 production to a different site (e.g. at the Golgi) and determining if this is sufficient to bring cPKC isoforms to a non-traditional location. Additionally, it remains to be tested whether the interaction with PIP_2 serves solely as a mechanism to refine targeting, or if it can provide a contribution toward the high-affinity binding necessary to release the pseudosubstrate peptide from the active site.

It is well established that the C1 domains of the DAG-responsive mammalian PKC isoforms also have selectivity for PS over other anionic phospholipids (40). Although some studies have suggested a role for PS in disrupting interactions between the C1 and C2 domains to confer conformational flexibility and greater accessibility to DAG (41), there is a stereo-specific enhancement in DAG-dependent membrane binding to the isolated C1b domain of PKCβ by L-phosphatidyl serine, indicating that the PS-responsive determinant for PKC activation is intrinsic to isolated C1 domains (40). While it remains to be tested whether acute or localized differences in PS influence PKC

activity on a cellular level, the recent generation of a specific fluorescent tool for visualizing cellular PS should greatly assist in determining how cellular PKC activity is affected by this lipid cofactor (21).

4. The presence of multiple signaling domains in the same protein enhances PKC signaling.

In the context of the full-length protein, the binding of lipid second messengers to a domain can be enhanced by the presence of other modules in the protein. The C1 domain, in full-length cPKC isoforms, is assisted in its search for DAG by the Ca^{2+}-dependent membrane binding of the C2 domain (32). The C2 domain pre-targets the enzyme to the plasma membrane, allowing the C1 domain to search in two dimensions for DAG. While the C2 domain of nPKCs is unresponsive to Ca^{2+}, it does assist with protein-protein interactions that can further refine the localization of DAG-dependent signaling. Specifically, the C2 domains of both cPKC and nPKC isoforms contain sequences that interact with the receptor for activated C kinase (RACK) family of protein scaffolds (reviewed in (42)). Additionally, the C2 domain of nPKCδ (and possibly that of nPKCθ) has the ability to bind phospho-tyrosine, but the biological consequence of this has yet to be determined (43). However, unlike cPKC isoforms, engagement of the novel C2 domain is not required to provide energy to release the pseudosubstrate peptide to acutely activate nPKC isoforms; DAG-dependent membrane binding of the novel C1 domain is sufficient for activation (31). Other protein-protein interaction modules also greatly affect localization of PKC activity, and will be discussed later.

5. Lipid binding modules can be selectively revealed in the full-length PKC.

While the presence of other domains in the full-length protein can heighten and refine the response to lipid second messengers, lipid binding domains can also be masked in the context of the full-length protein. While this is much more of a paradigm for another C1 domain-containing protein, β-chaemerin (44), it has been proposed that the C1 domains of specific cPKC isoforms are masked under certain cellular conditions. This phenomenon was first described for cPKCγ, when Oancea and Meyer showed that the isolated C1 domain translocated to cellular membranes with exogenous DAG far more quickly than did the full-length PKCγ, while, in response to Ca^{2+}, the isolated C2 domain translocated to membranes with the same kinetics as the full-length protein (45). They postulated that the region N-terminal to the C1 domain encompassing the pseudosubstrate acts as a clamp to keep the C1 domain inaccessible to DAG; the clamp is released when the C2 domain engages membranes. For cPKCα, it was recently shown that acidic residues in the C-terminal tail bind basic residues in the C2 domain, and that this interaction maintains PKCα in a closed conformation that masks the C1a domain; the C1a domain is presumably revealed when the basic patch on the C2 domain engages PIP_2 in the membrane. (46). This model is strengthened by the evidence that, while mutation of residues in either charged region to Ala residues sensitizes the enzyme to exogenous DAG, swapping the residues in the basic and acidic patches restores DAG insensitivity. For PKCα, another inter-domain interaction between the C1 and C2 domains has been demonstrated (41,47) and is thought to regulate accessibility of the C1 domain to DAG. Ultimately, C1 domain masking appears to occur by isoform-specific mechanisms, or not at all in the case of cPKCβII (40), and it is still unclear whether inter-domain interactions affect cPKC isoforms on a cellular level. Nevertheless, the ability of cPKC isoforms to

selectively hide their C1 domains could have cellular consequences. One possible outcome is that this orders the response to Ca^{2+} and DAG, such that the C2 domain must respond to Ca^{2+} before the C1 domain can sense DAG. This effect would allow the C2 domain selectivity to more efficiently govern the localization of the cPKC response: since the C2 domain prefers the PIP_2-rich plasma membrane (38), ordering the response could help override the slight basal preference of the tandem C1 domains for internal membranes (unpublished data).

While the mechanism of domain masking in cPKC isoforms may be isozyme-specific, there appears to be a consensus that the C2 domain of nPKC isoforms is an autoinhibitory module that impedes DAG-dependent membrane binding. Both nPKCε and nPKCδ respond faster to C1 ligands when the C2 domain is physically removed (31,48). In cells, unmasking the C1 domain of nPKCε (and the *A. californica* homolog, Apl nPKCII) appears to depend upon phosphatidic acid (PA) (49,50). Specifically, blocking the formation of PA desensitizes nPKCε to receptor-mediated translocation (50). Recently, it was shown that PA binds the C1b domain of Apl nPKCII to both relieve suppression from the C2 domain and synergize with DAG to recruit Apl nPKCII to cellular membranes, an effect mediated by a single Arg residue at position 273 in the full-length Apl nPKCII (51). Because this critical determinant is conserved in the C1b domain of mammalian nPKCε, the mechanism is likely conserved. Thus, the PKC family provides examples of how inter-domain interactions in the context of a full-length protein can restrain the response of isolated domains and provide a further element of regulation in cells.

6. Competition from other proteins for the same ligand results in context-dependent PKC responses.

Another factor that can govern lipid-dependent signaling on a cellular level is the expression of several different proteins in a cell that are responsive to a common ligand. It is possible that the expression of a protein with affinity for a particular ligand will out-compete proteins responding to the same ligand in the same cell. This effect has been demonstrated for PKC isoforms during receptor-mediated stimulation. That is, while nPKC isoforms bind DAG with higher affinity than do cPKC isoforms, nPKCε is prevented from translocation to plasma membrane in response to DAG by the faster, Ca^{2+}-assisted response of cPKCα in histamine-stimulated HEK cells (33). However, when Ca^{2+} is chelated, nPKCε can now respond at the plasma membrane. Furthermore, when exogenous DAG is added to the same cells, nPKCε alone translocates to the plasma membrane; but, upon photolysis of caged Ca^{2+}, cPKCα displaces nPKCε. Titration of cPKCα expression showed a concentration-dependent suppression of nPKCε translocation in response to receptor-mediated stimulation, further supporting the idea of competition between the two isoforms for DAG-dependent membrane binding. In addition to competing with each other, isoforms in the PKC family also have competition from the growing list of proteins that contain a C1 domain and respond to cellular DAG, including protein kinase D, RasGRP, β-chaemerin, and Munc18 (reviewed in (52)). While the importance of this competition for the same ligand remains to be fully investigated, it is interesting to speculate that the unique protein expression profile of different cell types could lead to the ability of a protein to respond to DAG production at a given location in one cell type, but be out-competed and respond differently in another

cell type. Thus, the spatio-temporal dynamics of lipid-dependent PKC signaling can be regulated by diverse mechanisms (Figure 1.4).

Signaling of PKC in protein complexes

Protein scaffolds have clearly-defined roles in regulating signaling cascades. The mitogen activated protein kinase (MAPK) cascade is a classical example of a scaffold-coordinated signaling cascade, whereby three to four kinases in the pathway are sequentially activated to promote a cellular response (reviewed in (53)). This signaling pathway was originally shown to be coordinated by the Ste5p scaffold in yeast; via this scaffold, the MAPK cascade mediates mating responses to pheromones (54,55). More recently, it was discovered that Ste5p is not simply a static scaffold; rather, it also plays an allosteric role in the activation of the members of the MAPK cascade (56). Other scaffolds for the MAPK family have also since been discovered in mammalian cells (e. g. (57)), and have been proposed to act as a "switch" for regulating whether the MAPK cascade will produce a graded or binary ("all-or-none") response to extracellular stimuli (58).

In addition to the extensive ways in which cellular lipids interplay with the lipid-binding modules in PKC isoforms to regulate signaling, many studies support that PKC isozymes are also present in discrete complexes with other signaling proteins. These protein complexes are found associated with specific structures in cells and perform highly specific functions. The following examples of regulation of PKC in protein complexes unveil another level of complexity in the regulation of this enzyme family, and underscore the need for sensitive tools to study the activity of PKC isozymes in a cellular context. While additional protein complexes involving PKC isozymes have been

described, these particular examples are either prototypical or provide clues to how PKC might be activated in ways that depart from classical lipid-dependent signaling.

1. InaD: the prototypical scaffold coordinating PKC activity in the eye.

InaD was originally discovered in a screen for molecules affecting phototransduction in the eye of the model organism, *D. melanogaster* (59). In this system, photo-activated rhodopsin, a G_q coupled receptor, activates Ca^{2+} influx via TRP Ca^{2+} channels in a mechanism involving NORPA, a PLCβ orthologue, and eye-PKC, a PKC isoform in drosophila most closely resembling conventional mammalian isozymes (reviewed in (60)). InaD is a protein scaffold consisting of five distinct PDZ (PSD-95/DLG/ZO-1) domains, and it coordinates the binding of eye-PKC, NORPA, and the TRP Ca^{2+} channel via interactions with C-terminal PDZ ligands of the signaling proteins (59,61-64). The formation of this complex is important for the phosphorylation of both InaD and the TRP calcium channel by eye-PKC (65). Loss of either the scaffold InaD or eye-PKC results in deficits in light adaptation (61,66). This is the seminal example of a PKC isoform being coordinated into a protein complex mediating a cell type-specific signal transduction cascade.

2. Par6-atypical PKC-Par3 complex: a conserved module in cell polarity.

The establishment of intracellular asymmetry, or polarity, in cells is critical for directed migration, asymmetric cell division, neuronal differentiation, and epithelial cell polarity (reviewed in (67)). Genetic screens in *C. elegans* for proteins involved in asymmetric cell division uncovered seven proteins critical for cell polarity: Par1-6 and aPKC (68,69). Immunocytochemistry revealed co-localization of Par3, Par6, and aPKC in the anterior cortex of asymmetrically dividing cells (70), and it was demonstrated that

these proteins form a complex (71). Soon afterward, it was discovered that this polarity module exists in *D. melanogaster*, *X. lavies*, and mammalian cells, and that it appears to be critical in all of the aforementioned cellular functions requiring polarized distribution of proteins (72-75). In mammalian epithelial cells, the Par6-aPKC-Par3 module localizes apically, and is essential for maintaining separation between apical and basolateral domains. A few substrates of aPKC in this context are known, such as Par-1 and Lgl, and phosphorylation by aPKC is required to exclude these proteins away from apical cellular regions containing aPKC complexes (76-78). This interaction is mutually exclusive; for example, Par-1 is a kinase that phosphorylates Par3 and excludes Par6-aPKC-Par3 complexes away from basolateral cellular regions containing Par-1 (79,80). While the details of precisely how aPKC is activated in this complex remain obscure, a mode of activation involving release of inhibitory constraints of Par6 on aPKC by the binding of Par6 to the Rho family GTPase, CDC42, has been proposed (81-83).

3. PKCε-14-3-3 complex: a mode of lipid-independent PKC activation in cytokinesis

14-3-3 proteins are a highly-conserved family of phospho-peptide binding proteins that have numerous well-defined roles in mediating the downstream effects of phosphorylation (reviewed in (84)). Recently, it has been demonstrated that this family of proteins can also act to promote activity of a specific member of the PKC family, PKCε, and that this protein complex is involved in the completion of cytokinesis (85). The binding of 14-3-3 proteins to PKCε was discovered in a yeast two-hybrid screen for PKCε-specific interacting partners. According to this study, the binding of 14-3-3 proteins to PKCε is controlled by p38 MAPK, GSK3, and autophosphorylation. Recruitment of GSK3 to PKCε is controlled by p38 MAPK; subsequent phosphorylation

of PKCε by GSK3 and autophosphorylation creates 14-3-3 binding sites (Ser 346, Ser 368) in the hinge region of PKCε between the regulatory and catalytic domains. The binding of 14-3-3 promotes lipid-independent activity of PKCε, ostensibly by "propping open" this kinase in the active conformation. This promotes PKCε activity localized at the midbody during cytokinesis. Blocking PKCε activity, or mutating these phosphorylation/autophosphorylation sites to Ala, significantly delays exit of cells from cytokinesis (85). This provides an exciting example of how an initial lipid-dependent signaling event might be maintained by protein-protein interactions upon depletion of the upstream lipid second messenger.

4. PKCα-PICK-1 complex: a PDZ interaction controls cerebellar LTP

PICK-1 (protein interacting with C kinase-1) was originally identified in a yeast two-hybrid screen for proteins interacting with PKCα (86). This protein contains a BAR domain for membrane remodeling and a PDZ domain for recruiting proteins with PDZ ligands. PKCα contains a unique C-terminal PDZ ligand, the last residues of which encode "-QSAV," which mediates its interaction with PICK-1 (87). PKCα is important for cerebellar long-term depression (LTD), a major form of synaptic plasticity that is thought to be critical for certain types of motor learning, as evidenced by defects in LTD when PKCα is knocked out in mice (88). Furthermore, these studies have shown that the PDZ ligand of PKCα is required for its roles in cerebellar LTD, as deficits can be rescued by full-length PKCα but not by PKCα missing sequences encoding the C-terminal PDZ ligand (88). Phosphorylation of the AMPA receptor subunit GluR2 at Ser 880 by PKCα is important for LTD (89). PICK-1 is a prime candidate for mediating the effects of

PKCα in cerebellar LTD, since targeted mutation of PICK1, the GluR2 C-terminal PDZ ligand, or the GluR2 PKC phosphorylation site eliminates cerebellar LTD in mice (90). However, other scaffolds interacting with PKCα's C-terminal PDZ ligand have not yet been investigated and may play a role in PKCα-specific effects in the brain and in other cell types.

In Chapter 5, we describe a study in which a search for additional scaffolds for PKCα's C-terminal PDZ ligand results in the discovery of a PKCα-DLG1-Ect2 signaling module that directs cytoskeletal rearrangements. Furthermore, recent comprehensive studies on PDZ ligand-PDZ domain interactions have found that specificity determinants on PDZ ligands upstream from the C-terminal Val or Ile residue are truly optimized in an unrestricted fashion across all amino acid residues; this has revolutionized classification of proteins containing PDZ ligands. Thus, the conservation of a hydrophobic Val or Ile residue at the C-terminus of a protein strongly suggests the presence of a PDZ ligand (91). Three other PKC isoforms, βI, ζ, and ι, also harbor a C-terminal Val residue, with residues upstream conserved across species. Thus, it is likely that PKCα is not the sole PKC isoform with the potential to interact with PDZ domain-containing scaffolds.

Preface

This thesis examines the spatio-temporal dynamics of signaling by PKC. Specifically, I describe studies employing diverse techniques to address cellular factors controlling PKC signaling in normal cellular processes and in disease. In Chapter 2, we describe targeting a FRET-based reporter for PKC signaling to intracellular organelles to monitor PKC activity in response to GPCR signaling. In Chapter 3, we describe a single

residue in the C1b domain of novel and conventional PKCs, the identity of which dictates differences in DAG sensitivity and resulting differences in activation and cellular location amongst the two classes of PKC. In Chapter 4, we describe an ongoing study to examine how mutations in PKC in colon cancer contribute to progression of tumorigenesis. Specifically, we have characterized a mutation in the C1b domain of PKCβII that desensitizes it to lipid signaling to disengage a feedback loop which normally promotes apoptosis in colon cancer cells harboring oncogenic K-Ras mutations. Finally, in Chapter 5, we describe another ongoing study involving a novel signaling scaffold composed of PKCα, DLG1 and Ect2 which promotes cytoskeletal rearrangements, likely via Rho family GTPases, and which may be involved in tumor metastasis. In summary, the work described in this thesis establishes that PKC has unique activation signatures at specific intracellular locations, unveils the molecular mechanism allowing novel PKC isozymes to respond to agonist-evoked changes in DAG, characterizes how a cancer driver mutation controls PKC function, and presents a novel mechanism for cytoskeletal control by PKCα.

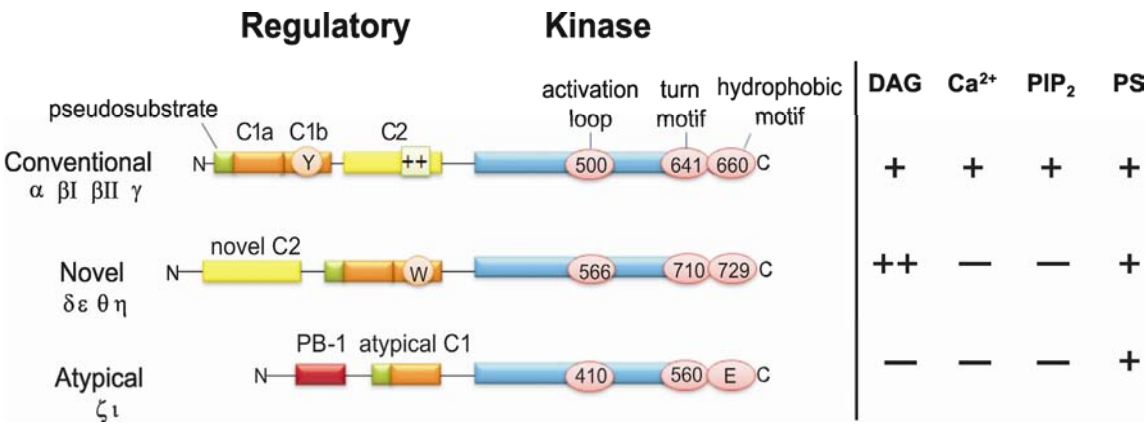

Figure 1.1. Primary structure of protein kinase C (PKC) family members. All PKC isoforms contain an autoinhibitory pseudosubstrate peptide (green) and a carboxy-terminal kinase core (blue). The kinase core contains three phosphorylation/autophosphorylation sites (pink) critical for maturation: the activation loop, turn motif, and hydrophobic motif (numbering shown for cPKCβ, nPKCδ, and aPKCζ; note that the hydrophobic motif site is a Glu in aPKC isoforms). PKC isoforms are grouped according to their regulatory domains: cPKC isoforms contain two tandem DAG-sensitive C1 domains (orange) and a Ca^{2+}-sensitive C2 domain (yellow); nPKC isoforms contain two tandem DAG-sensitive C1 domains and a novel, Ca^{2+}-insensitive C2 domain; and aPKC isoforms contain a PB-1 (phox and bem-1) protein-protein interaction module (red) and an atypical, DAG-insensitive C1 domain. The C1 domains of all PKC isoforms interact with PS, and the C2 domains of cPKC isoforms interact non-specifically with anionic phospholipids, including PS. Critical features underlying responsiveness to second messengers are highlighted: Tyr (Y) at position 22 in the C1b domain of cPKC isoforms confers weak DAG responsiveness; Trp (W) at position 22 in the C1b domain of nPKC isoforms confers strong DAG responsiveness; and a basic patch (++) in the C2 domain of cPKC isoforms (located distal to the Ca^{2+}-dependent lipid binding site) specifically recognizes PIP_2.

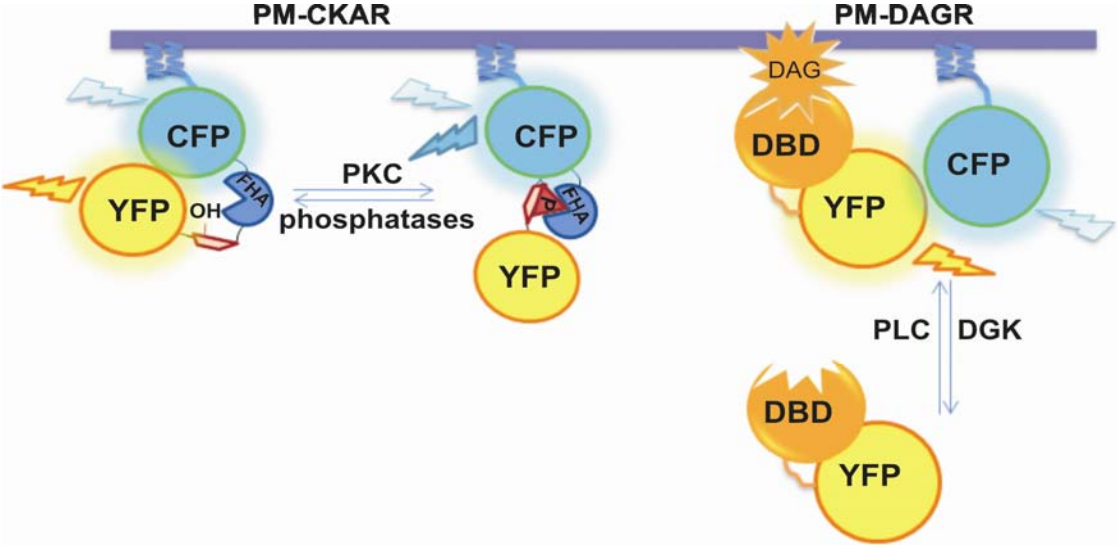

Figure 1.2. Reversible, genetically-encoded, FRET-based reporters for visualizing PKC activity (C Kinase Activity Reporter, CKAR) and DAG accumulation (Diacylglycerol Reporter, DAGR). For CKAR, phosphorylation of the PKC-specific substrate peptide allows the forkhead-associated (FHA) domain to interact with it, which decreases FRET between donor cyan fluorescent protein (CFP) and acceptor yellow fluorescent protein (YFP) molecules. For DAGR, the CFP donor is tethered to a membrane and the YFP acceptor is linked to a DAG binding domain (DBD); FRET increases with DAG production as the DBD translocates to the membrane. Shown are plasma membrane-targeted versions of the reporters, PM-CKAR and PM-DAGR.

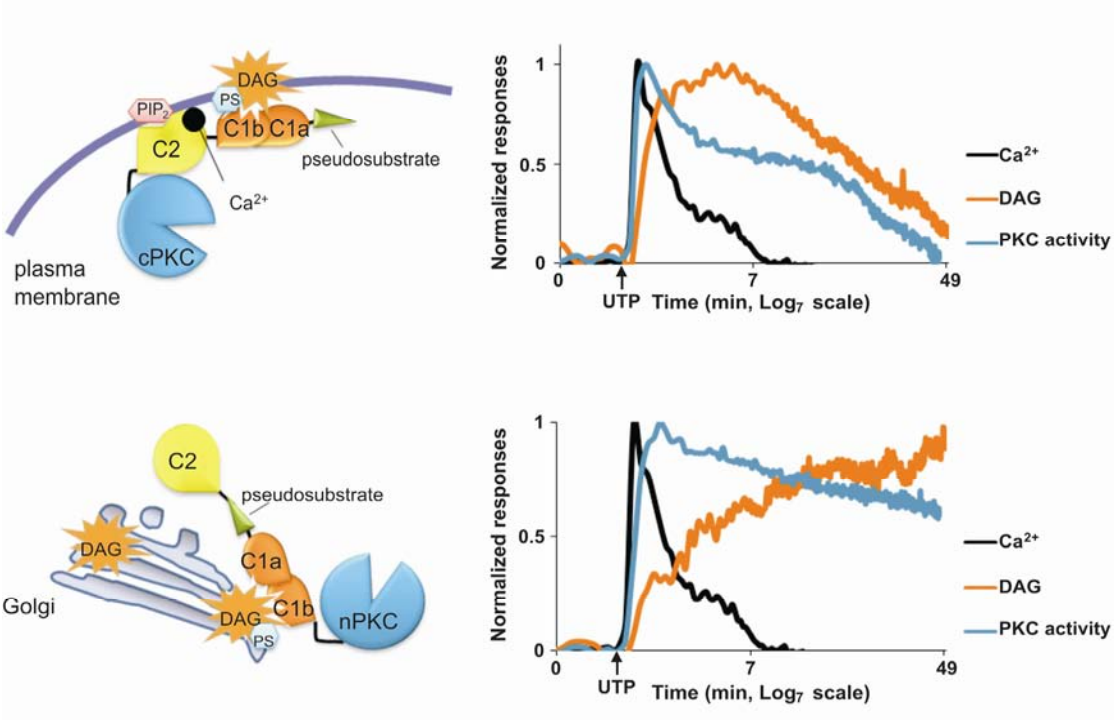

Figure 1.3. Differential activation signatures of PKC at the plasma membrane and at the Golgi, as read out using targeted FRET-based reporters. In response to UTP, the early phase of PKC signaling at the plasma membrane is acutely coupled to Ca^{2+} release, while the duration of signaling is controlled by the rate of DAG turnover. Compared to the plasma membrane, PKC signaling at the Golgi overlaps less with Ca^{2+} and is sustained by prolonged DAG accumulation. These profiles of PKC signaling are consistent with a role for Ca^{2+}-responsive cPKC isoforms at the plasma membrane and high-affinity DAG-binding nPKC isoforms at the Golgi.

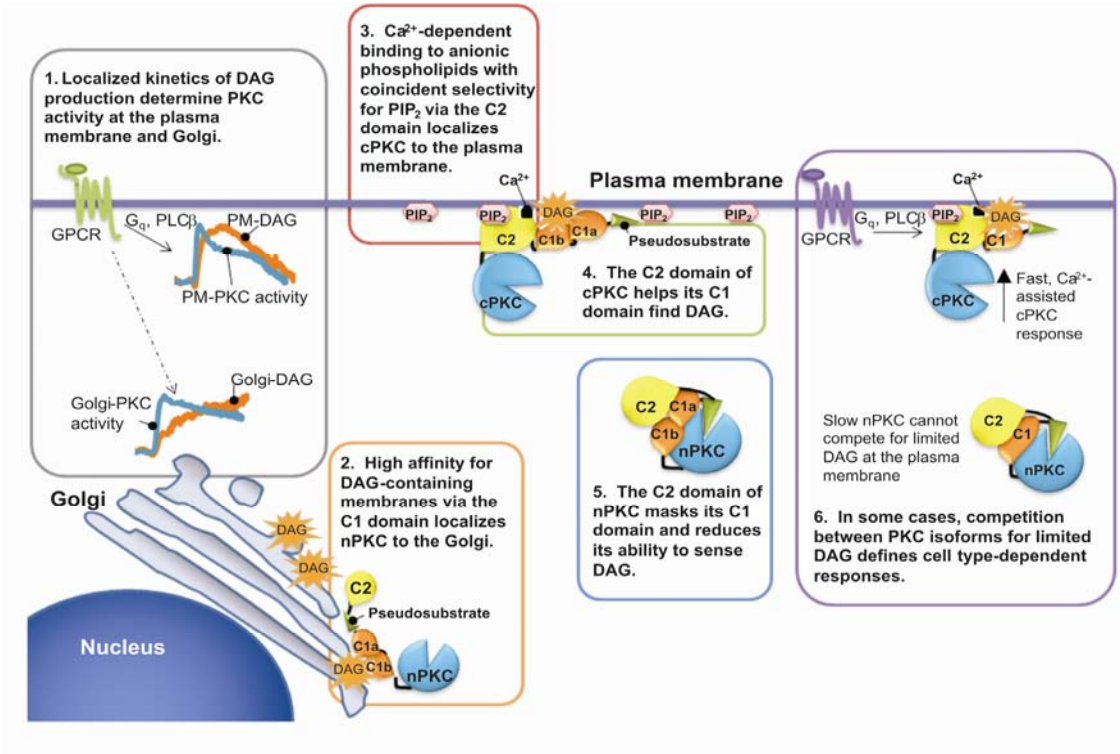

Figure 1.4. Examples of PKC regulation at the cellular level in response to lipid second messenger signaling. 1) Localized kinetics of DAG production determine PKC activity at the plasma membrane and Golgi. 2) High affinity for DAG-containing membranes via the C1 domain localizes nPKC to the Golgi. 3) Ca^{2+}-dependent binding to anionic phospholipids with coincident selectivity for PIP_2 via the C2 domain localizes cPKC to the plasma membrane. 4) The C2 domain of cPKC helps its C1 domain find DAG. 5) The C2 domain of nPKC masks its C1 domain and reduces its ability to sense DAG. 6) In some cases, competition between PKC isoforms for limited DAG defines cell type-dependent responses.

References

1. DeLange, R. J., Kemp, R. G., Riley, W. D., Cooper, R. A., and Krebs, E. G. (1968) *J Biol Chem* **243**(9), 2200-2208

2. Berg, H. C., and Brown, D. A. (1972) *Nature* **239**(5374), 500-504

3. Pawson, T., and Warner, N. (2007) *Oncogene* **26**(9), 1268-1275

4. Blume-Jensen, P., and Hunter, T. (2001) *Nature* **411**(6835), 355-365

5. Pawson, T., and Scott, J. D. (2005) *Trends Biochem Sci* **30**(6), 286-290

6. Newton, A. C. (2003) *Biochem J* **370**(Pt 2), 361-371

7. Inoue, M., Kishimoto, A., Takai, Y., and Nishizuka, Y. (1977) *J Biol Chem* **252**(21), 7610-7616

8. Takai, Y., Kishimoto, A., Kikkawa, U., Mori, T., and Nishizuka, Y. (1979) *Biochem Biophys Res Commun* **91**(4), 1218-1224

9. Creba, J. A., Downes, C. P., Hawkins, P. T., Brewster, G., Michell, R. H., and Kirk, C. J. (1983) *Biochem J* **212**(3), 733-747

10. Newton, A. C. (2004) *Trends Pharmacol Sci* **25**(4), 175-177

11. Castagna, M., Takai, Y., Kaibuchi, K., Sano, K., Kikkawa, U., and Nishizuka, Y. (1982) *J Biol Chem* **257**(13), 7847-7851

12. Sossin, W. S. (2007) *Learn Mem* **14**(4), 236-246

13. Cameron, A. J., De Rycker, M., Calleja, V., Alcor, D., Kjaer, S., Kostelecky, B., Saurin, A., Faisal, A., Laguerre, M., Hemmings, B. A., McDonald, N., Larijani, B., and Parker, P. J. (2007) *Biochem Soc Trans* **35**(Pt 5), 1013-1017

14. Jacinto, E., and Lorberg, A. (2008) *Biochem J* **410**(1), 19-37

15. Neri, L. M., Martelli, A. M., Borgatti, P., Colamussi, M. L., Marchisio, M., and Capitani, S. (1999) *Faseb J* **13**(15), 2299-2310

16. Suzuki, A., Akimoto, K., and Ohno, S. (2003) *J Biochem* **133**(1), 9-16

17. Di Paolo, G., and De Camilli, P. (2006) *Nature* **443**(7112), 651-657

18. Carrasco, S., and Merida, I. (2004) *Mol Biol Cell* **15**(6), 2932-2942

19. Dries, D. R., Gallegos, L. L., and Newton, A. C. (2007) *J Biol Chem* **282**(2), 826-830

20. Villani, M., Subathra, M., Im, Y. B., Choi, Y., Signorelli, P., Del Poeta, M., and Luberto, C. (2008) *Biochem J*

21. Yeung, T., Gilbert, G. E., Shi, J., Silvius, J., Kapus, A., and Grinstein, S. (2008) *Science* **319**(5860), 210-213

22. Hurley, J. H., and Misra, S. (2000) *Annu Rev Biophys Biomol Struct* **29**, 49-79

23. Hurley, J. H. (2006) *Biochim Biophys Acta* **1761**(8), 805-811

24. Drin, G., and Scarlata, S. (2007) *Cell Signal* **19**(7), 1383-1392

25. Rhee, S. G. (2001) *Annu Rev Biochem* **70**, 281-312

26. Merida, I., Avila-Flores, A., and Merino, E. (2008) *Biochem J* **409**(1), 1-18

27. Sakai, N., Sasaki, K., Ikegaki, N., Shirai, Y., Ono, Y., and Saito, N. (1997) *J Cell Biol* **139**(6), 1465-1476

28. Violin, J. D., Zhang, J., Tsien, R. Y., and Newton, A. C. (2003) *J Cell Biol* **161**(5), 899-909

29. Violin, J. D., and Newton, A. C. (2003) *IUBMB Life* **55**(12), 653-660

30. Gallegos, L. L., Kunkel, M. T., and Newton, A. C. (2006) *J Biol Chem* **281**(41), 30947-30956

31. Giorgione, J. R., Lin, J. H., McCammon, J. A., and Newton, A. C. (2006) *J Biol Chem* **281**(3), 1660-1669

32. Newton, A. C. (2001) *Chem Rev* **101**(8), 2353-2364

33. Lenz, J. C., Reusch, H. P., Albrecht, N., Schultz, G., and Schaefer, M. (2002) *J Cell Biol* **159**(2), 291-302

34. Kohout, S. C., Corbalan-Garcia, S., Torrecillas, A., Gomez-Fernandez, J. C., and Falke, J. J. (2002) *Biochemistry* **41**(38), 11411-11424

35. Keranen, L. M., and Newton, A. C. (1997) *J Biol Chem* **272**(41), 25959-25967

36. Guerrero-Valero, M., Marin-Vicente, C., Gomez-Fernandez, J. C., and Corbalan-Garcia, S. (2007) *J Mol Biol* **371**(3), 608-621

37. Corbalan-Garcia, S., Garcia-Garcia, J., Rodriguez-Alfaro, J. A., and Gomez-Fernandez, J. C. (2003) *J Biol Chem* **278**(7), 4972-4980

38. Evans, J. H., Murray, D., Leslie, C. C., and Falke, J. J. (2006) *Mol Biol Cell* **17**(1), 56-66

39. Marin-Vicente, C., Nicolas, F. E., Gomez-Fernandez, J. C., and Corbalan-Garcia, S. (2008) *J Mol Biol* **377**(4), 1038-1052

40. Johnson, J. E., Giorgione, J., and Newton, A. C. (2000) *Biochemistry* **39**(37), 11360-11369

41. Stahelin, R. V., Wang, J., Blatner, N. R., Rafter, J. D., Murray, D., and Cho, W. (2005) *J Biol Chem* **280**(43), 36452-36463

42. Schechtman, D., and Mochly-Rosen, D. (2001) *Oncogene* **20**(44), 6339-6347

43. Benes, C. H., Wu, N., Elia, A. E., Dharia, T., Cantley, L. C., and Soltoff, S. P. (2005) *Cell* **121**(2), 271-280

44. Hall, C., Lim, L., and Leung, T. (2005) *Trends Biochem Sci* **30**(4), 169-171

45. Oancea, E., and Meyer, T. (1998) *Cell* **95**(3), 307-318

46. Stensman, H., and Larsson, C. (2007) *J Biol Chem* **282**(39), 28627-28638

47. Slater, S. J., Seiz, J. L., Cook, A. C., Buzas, C. J., Malinowski, S. A., Kershner, J. L., Stagliano, B. A., and Stubbs, C. D. (2002) *J Biol Chem* **277**(18), 15277-15285

48. Stahelin, R. V., Digman, M. A., Medkova, M., Ananthanarayanan, B., Melowic, H. R., Rafter, J. D., and Cho, W. (2005) *J Biol Chem* **280**(20), 19784-19793

49. Pepio, A. M., and Sossin, W. S. (1998) *Biochemistry* **37**(5), 1256-1263

50. Jose Lopez-Andreo, M., Gomez-Fernandez, J. C., and Corbalan-Garcia, S. (2003) *Mol Biol Cell* **14**(12), 4885-4895

51. Farah, C. A., Nagakura, I., Weatherill, D., Fan, X., and Sossin, W. S. (2008) *Mol Cell Biol*

52. Toker, A. (2005) *EMBO Rep* **6**(4), 310-314

53. Elion, E. A. (2001) *J Cell Sci* **114**(Pt 22), 3967-3978

54. Kranz, J. E., Satterberg, B., and Elion, E. A. (1994) *Genes Dev* **8**(3), 313-327

55. Choi, K. Y., Satterberg, B., Lyons, D. M., and Elion, E. A. (1994) *Cell* **78**(3), 499-512

56. Sette, C., Inouye, C. J., Stroschein, S. L., Iaquinta, P. J., and Thorner, J. (2000) *Mol Biol Cell* **11**(11), 4033-4049

57. Whitmarsh, A. J., Cavanagh, J., Tournier, C., Yasuda, J., and Davis, R. J. (1998) *Science* **281**(5383), 1671-1674

58. Dohlman, H. G. (2008) *Sci Signal* **1**(42), pe46

59. Tsunoda, S., Sierralta, J., Sun, Y., Bodner, R., Suzuki, E., Becker, A., Socolich, M., and Zuker, C. S. (1997) *Nature* **388**(6639), 243-249

60. Hardie, R. C., and Raghu, P. (2001) *Nature* **413**(6852), 186-193

61. Adamski, F. M., Zhu, M. Y., Bahiraei, F., and Shieh, B. H. (1998) *J Biol Chem* **273**(28), 17713-17719

62. Xu, X. Z., Choudhury, A., Li, X., and Montell, C. (1998) *J Cell Biol* **142**(2), 545-555

63. Shieh, B. H., and Zhu, M. Y. (1996) *Neuron* **16**(5), 991-998

64. Shieh, B. H., Zhu, M. Y., Lee, J. K., Kelly, I. M., and Bahiraei, F. (1997) *Proc Natl Acad Sci U S A* **94**(23), 12682-12687

65. Liu, M., Parker, L. L., Wadzinski, B. E., and Shieh, B. H. (2000) *J Biol Chem* **275**(16), 12194-12199

66. Hardie, R. C., Peretz, A., Suss-Toby, E., Rom-Glas, A., Bishop, S. A., Selinger, Z., and Minke, B. (1993) *Nature* **363**(6430), 634-637

67. Etienne-Manneville, S., and Hall, A. (2003) *Curr Opin Cell Biol* **15**(1), 67-72

68. Watts, J. L., Etemad-Moghadam, B., Guo, S., Boyd, L., Draper, B. W., Mello, C. C., Priess, J. R., and Kemphues, K. J. (1996) *Development* **122**(10), 3133-3140

69. Tabuse, Y., Izumi, Y., Piano, F., Kemphues, K. J., Miwa, J., and Ohno, S. (1998) *Development* **125**(18), 3607-3614

70. Hung, T. J., and Kemphues, K. J. (1999) *Development* **126**(1), 127-135

71. Joberty, G., Petersen, C., Gao, L., and Macara, I. G. (2000) *Nat Cell Biol* **2**(8), 531-539

72. Huynh, J. R., Petronczki, M., Knoblich, J. A., and St Johnston, D. (2001) *Curr Biol* **11**(11), 901-906

73. Nakaya, M., Fukui, A., Izumi, Y., Akimoto, K., Asashima, M., and Ohno, S. (2000) *Development* **127**(23), 5021-5031

74. Choi, S. C., Kim, J., and Han, J. K. (2000) *Mech Dev* **91**(1-2), 347-350

75. Ohno, S. (2001) *Curr Opin Cell Biol* **13**(5), 641-648

76. Betschinger, J., Mechtler, K., and Knoblich, J. A. (2003) *Nature* **422**(6929), 326-330

77. Yamanaka, T., Horikoshi, Y., Izumi, N., Suzuki, A., Mizuno, K., and Ohno, S. (2006) *J Cell Sci* **119**(Pt 10), 2107-2118

78. Hurov, J. B., Watkins, J. L., and Piwnica-Worms, H. (2004) *Curr Biol* **14**(8), 736-741

79. Hurd, T. W., Fan, S., Liu, C. J., Kweon, H. K., Hakansson, K., and Margolis, B. (2003) *Curr Biol* **13**(23), 2082-2090

80. Benton, R., and St Johnston, D. (2003) *Cell* **115**(6), 691-704

81. Lin, D., Edwards, A. S., Fawcett, J. P., Mbamalu, G., Scott, J. D., and Pawson, T. (2000) *Nat Cell Biol* **2**(8), 540-547

82. Qiu, R. G., Abo, A., and Steven Martin, G. (2000) *Curr Biol* **10**(12), 697-707

83. Yamanaka, T., Horikoshi, Y., Suzuki, A., Sugiyama, Y., Kitamura, K., Maniwa, R., Nagai, Y., Yamashita, A., Hirose, T., Ishikawa, H., and Ohno, S. (2001) *Genes Cells* **6**(8), 721-731

84. van Heusden, G. P. (2005) *IUBMB Life* **57**(9), 623-629

85. Saurin, A. T., Durgan, J., Cameron, A. J., Faisal, A., Marber, M. S., and Parker, P. J. (2008) *Nat Cell Biol* **10**(8), 891-901

86. Staudinger, J., Zhou, J., Burgess, R., Elledge, S. J., and Olson, E. N. (1995) *J Cell Biol* **128**(3), 263-271

87. Staudinger, J., Lu, J., and Olson, E. N. (1997) *J Biol Chem* **272**(51), 32019-32024

88. Leitges, M., Kovac, J., Plomann, M., and Linden, D. J. (2004) *Neuron* **44**(4), 585-594

89. Chung, H. J., Steinberg, J. P., Huganir, R. L., and Linden, D. J. (2003) *Science* **300**(5626), 1751-1755

90. Steinberg, J. P., Takamiya, K., Shen, Y., Xia, J., Rubio, M. E., Yu, S., Jin, W., Thomas, G. M., Linden, D. J., and Huganir, R. L. (2006) *Neuron* **49**(6), 845-860

91. Stiffler, M. A., Chen, J. R., Grantcharova, V. P., Lei, Y., Fuchs, D., Allen, J. E., Zaslavskaia, L. A., and MacBeath, G. (2007) *Science* **317**(5836), 364-369

Footnotes

*Abbreviations: DAG, Diacylglycerol; PKC, protein kinase C; PIP2, phosphoinositide-4,5-bisphosphate; PS, phosphatidylserine; C1, PKC conserved region 1; C2, PKC conserved region 2; PH, pleckstrin homology; ENTH, Epsin N-terminal homology; BAR, Bin/Amphiphysin/ Rvs; PLC, phospholipase C; cPKC, conventional PKC; nPKC, novel PKC; aPKC, atypical PKC; PDK-1, phosphoinositide-dependent kinase-1; mTORC2, mammalian target of rapamycin complex 2; PAP, phosphatidic acid phosphatase; PA, phosphatidic acid; FRET, fluorescence resonance energy transfer; DAGR, diacylglycerol reporter; CKAR, C kinase activity reporter; RACK, receptor for activated C kinase; PDZ, post-synaptic density-95/discs large/zonula occludens 1; PICK1, protein interacting with kinase 1; MAGUK, membrane-associated guanylate kinase; PB-1, phox and bem-1; CFP, cyan fluorescent protein; YFP, yellow fluorescent protein; DBD, DAG binding domain; FHA, forkhead-associated; PMCKAR, plasma membrane-targeted CKAR; PMDAGR, plasma membrane-targeted DAGR; InaD, inactivation-no afterpotential D; NORPA, no receptor potential A; TRP, transient receptor potential Ca^{2+} channel; Par1-6, partitioning-defective proteins 1-6; MAPK, mitogen-activated protein kinase; GSK3, glycogen synthase kinase 3; LTD, long-term depression; AMPA-R, α-amino-3-hydroxy-5-methyl-4-isoxazolepropionic acid receptor; DLG1, discs large homolog 1.

This Chapter is, in part, a reprint of the material as it appears in IUBMB life, 2008, Gallegos LL and Newton AC. I was the primary author for this literature review

Chapter 2

Targeting Protein Kinase C Activity Reporter to Discrete Intracellular Regions Reveals Spatiotemporal Differences in Agonist-dependent Signaling[§]

Abstract

Protein kinase C (PKC*) family members transduce an abundance of diverse intracellular signals. Here we address the role of spatial and temporal segregation in signal specificity by measuring the activity of endogenous PKC at defined intracellular locations in real time in live cells. We targeted a genetically-encoded FRET-based reporter for PKC activity, C Kinase Activity Reporter [CKAR (1)], to the plasma membrane, Golgi, cytosol, mitochondria, or nucleus by fusing appropriate targeting sequences to the N- or C- terminus of CKAR. Measuring the phosphorylation of the reporter in the presence of PKC inhibitors, activators, and/or phosphatase inhibitors shows that activity at each region is under differential control by phosphatase activity: nuclear activity is completely suppressed by phosphatases, whereas membrane-associated activity is the least suppressed by phosphatases. UTP stimulation of endogenous P2Y receptors in COS 7 cells reveals spatiotemporally divergent PKC responses. Imaging the second messengers Ca^{2+} and diacylglycerol (DAG) reveal that PKC activity at each location is driven by an initial spike in Ca^{2+}, followed by location-specific diacylglycerol generation. In response to UTP, phosphorylation of GolgiCKAR was sustained the longest, driven by persistence of DAG, while phosphorylation of CytoCKAR was of shortest duration, driven by high phosphatase activity. Our data reveal that the magnitude and duration of PKC signaling is location-specific and controlled by the level of phosphatase activity and persistence of DAG at each location.

Introduction

Cells respond dynamically to environmental cues conveyed by complex networks of signal transduction. Phosphorylation is the archetypal language that relays information from environmental stimuli throughout the cell; thus hundreds of kinases and phosphatases exist to regulate the phosphorylation status of intracellular substrates. A delicate balance of phosphorylation and dephosphorylation underlies cellular decisions ranging from controlling global functions, such as proliferation or apoptosis, to regulating specialized functions, such as secretion of hormones (2, 3). Disturbing this balance can lead to disease states, most notably cancer (4).

The protein kinase C (PKC) family of Ser/Thr kinases transduces an abundance of extracellular signals that control diverse cellular functions including differentiation, memory, and apoptosis. There are ten mammalian isozymes of the PKC family and they share a conserved C-terminal kinase core, as well as an N-terminal autoinhibitory pseudosubstrate peptide that is lodged in the active site under resting conditions. PKC isoforms are classified into three sub-categories (conventional, novel, and atypical) based on differing composition of their regulatory modules, which lie between the kinase core and inhibitory pseudosubstrate peptide (5). Conventional isoforms of PKC (cPKCs; α, βI, βII, and γ) contain a tandem C1 repeat followed by a C2 domain, which allow them to respond to second the messengers diacylglycerol (DAG) and Ca^{2+}, respectively. When extracellular signals stimulate phosphoinositide (PI) hydrolysis, DAG is produced and Ca^{2+} is released. The binding of these second messengers to the regulatory domains results in translocation of cPKCs to cellular membranes. Both second messengers must be present for high-affinity membrane binding, an event which provides the energy to

disengage the inhibitory pseudosubstrate peptide from the active site, allowing downstream signaling (6). Novel isoforms of PKC (nPKCs: δ, ε, η, and θ) are similarly activated by membrane binding; however, the novel C2 domain of the nPKCs cannot bind Ca^{2+}. For these isozymes, high affinity membrane binding is achieved exclusively by the C1 domain, which compensates by having an increased affinity for DAG (7). Consequently, this subclass is regulated by DAG production but not by Ca^{2+} release. Atypical PKCs (aPKCs; ζ andι) are unique in that they are not regulated by either DAG or Ca^{2+}: their regulatory region consists of an atypical C1 domain that does not bind DAG, and a PB1 (Phox and Bem 1) domain, recently recognized for its role in protein-protein interactions (8). Since activation of receptors can result in different profiles of Ca^{2+} release and DAG production, PKC isoforms are poised to respond to receptor activation with varying magnitude and duration of activity (9).

Previously, our lab generated a genetically-encoded fluorescence resonance energy transfer (FRET)-based reporter for PKC activity (1). C Kinase Activity Reporter (CKAR) is composed of a cyan fluorescent protein (CFP) and yellow fluorescent protein (YFP) tethered together by a substrate peptide specific for PKC and an FHA2 phosphopeptide-binding module. When CKAR is not phosphorylated, excitation at the characteristic CFP wavelength (434 nm) results in FRET, and YFP emission (528 nm) is observed. When PKC phosphorylates the substrate sequence, the FHA2 domain binds the phosphopeptide, reducing the energy transfer and increasing CFP emission (476 nm). A ratio of CFP/FRET emission provides a readout of the phosphorylation state of the population of reporters in the cell. The affinity of the phosphopeptide for the phosphopeptide-binding module is sufficiently high to trigger intramolecular binding,

but, importantly, is also in a range that allows for access of the phospho-substrate to cellular phosphatases. Thus, CKAR is sensitive to dephosphorylation and provides a reversible, real-time readout of the balance between PKC and phosphatase activity. Importantly, CKAR is an assay of endogenous PKC activity from live, intact cells, and retains any potential inputs from other key cellular partners, such as protein and lipid regulatory factors.

Although the plasma membrane has historically been considered the site of action of PKCs, several studies have demonstrated PKC translocation to the Golgi, mitochondria, and the nucleus in response to different stimuli (7, 10-12). However, mechanisms controlling the differential regulation of PKC activity, the balance between phosphatase and kinase activity, and the duration of signaling at these locations are not known.

In this study, we targeted CKAR to the plasma membrane, Golgi, mitochondria, cytosol, and nucleus and characterized activity of PKC at each region in response to stimulation. We used a specific inhibitor of conventional PKCs, Gö6976, to measure basal PKC activity; the potent DAG mimic, PdBu, to measure stimulated PKC activity; and the phosphatase inhibitor, calyculin A, to measure phosphatase-suppressed PKC activity. Stimulation of endogenous P2Y G protein- coupled receptors (GPCRs) with UTP in COS 7 cells revealed regionally- divergent PKC responses. We investigated the underlying basis for phosphorylation profiles in COS 7 cells at each intracellular localization by imaging Ca^{2+} release and localized DAG production in response to UTP. We discovered that the early phase of the PKC response is governed by Ca^{2+} release, while the later phase of the PKC response is controlled by localized DAG persistence.

Unexpectedly, in COS 7 cells, DAG production and the corresponding PKC response to UTP are highly sustained at the Golgi compared to the plasma membrane.

Materials and Methods

Construction of targeted reporters—CKAR was generated previously in the mammalian expression vector pcDNA3 (+) (Invitrogen) (1). The construct contains CFP and YFP tethered together by an FHA2 phosphopeptide binding domain followed by a PKC-specific substrate peptide. PMCKAR was created previously [MyrPalm-CKAR (1)] by the addition of sequences encoding the amino terminal 7 amino acids of Lyn kinase to the 5' end of CKAR. GolgiCKAR and MitoCKAR were generated by fusing in frame sequences encoding the amino terminal 33 amino acids of eNOS and the amino terminal 33 amino acids of TOM 20, respectively, to the immediate 5' end of CKAR (13-15). CytoCKAR was generated by fusing a region encoding the nuclear export sequence, LALKLAGLDI, to the 3' end of CKAR immediately preceding the termination codon (16). NucCKAR was generated similarly by fusing to the 3' end of CKAR sequences encoding a basic nuclear localization signal, PKKRKVEDA (17).

Construction of other plasmids—DAGR was constructed as previously described (1). PMCFP was constructed as previously described (1); the amino terminal 7 residues of Lyn kinase were attached to the 5' end of monomeric CFP. GolgiCFP was constructed similar to GolgiCKAR; sequences encoding the amino terminal 33 residues of eNOS were fused in frame to the 5' end of CFP (13). YFP-tagged DAG binding domain (YFP-DBD) was first constructed by fusion of monomeric YFP to the 5' end of the C1b domain of PKCβ. This construct was improved for DAG binding by introducing the Y123W point mutation via Quikchange (Stratagene).

Cell Culture—COS 7 cells were used in all experiments. These cells were plated and maintained in Dulbecco's modified Eagle's medium (Cellgro) containing 10% fetal bovine serum and 1% penicillin/streptomycin at 37 °C in 5% CO_2. Cells were plated in sterilized 35 mm imaging dishes at 60% confluency and transfected using FuGENE 6 (Roche Diagnostics). For DAGR imaging experiments, cells were cotransfected with PMCFP and YFP-DBD (PMDAGR) or GolgiCFP and YFP-DBD (GolgiDAGR). Cells were allowed to grow posttransfection for 12-24 h before imaging. For Ca^{2+} imaging experiments, 1.0 μM Fura-2 AM (Molecular Probes, Eugene, OR) was loaded into cells for 30 min and cells were washed twice with HBSS (Cellgro) before imaging.

Cell imaging—COS 7 cells were rinsed once with and imaged in HBSS containing 1 mM Ca^{2+}. For imaging in Ca^{2+}-free saline, cells were rinsed once with and imaged in HBSS containing 5 mM EGTA. Images were acquired on a Zeiss Axiovert microscope (Carl Zeiss Microimaging, Inc.) using a MicroMax digital camera (Roper-Princeton Instruments) controlled by MetaFluor software (Universal Imaging, Corp.). Optical filters were obtained from Chroma Technologies. Using a 10% neutral density filter, CFP and FRET images were obtained every 10-15 s through a 420/20-nm excitation filter, a 450-nm dichroic mirror, and a 475/40-nm emission filter (CFP) or 535/25-nm emission filter (FRET). YFP emission was also monitored as a control for photobleaching through a 495/10-nm excitation filter, a 505-nm dichroic mirror, and a 535/25-nm emission filter. Images of cells loaded with Fura-2 were obtained every 10 s through a 380/10-nm or 340/10-nm excitation filter, a 450-nm dichroic mirror, and a 535/45-nm emission filter. Excitation and emission filters were switched in filter wheels (Lambda 10–2, Sutter). Integration times were 200 ms for CFP, FRET, and Fura-2, and 50–100 ms for YFP.

Imaging data analysis—Images were reanalyzed using Metaflour Analyst (Universal Imaging, Corp.). One region per cell was selected such that there was no net movement of the targeted reporter in and out of the selected region, and Metafluor Analyst was used to calculate the average FRET ratio within the selected region as described previously (1). Baseline images were acquired for 15-30 min before adding ligand. In some cases, there was a baseline drift which accounted for up to a 7 % change in maximal FRET ratio per 10 min. This baseline was subtracted from traces. The corrected data traces were normalized to 1 by dividing by the average baseline FRET ratio, and data from different imaging dishes were referenced around the ligand addition time point. The normalized average FRET ratio is the average of these corrected values ± SEM.

Results

Targeted CKARs

To monitor PKC activity at defined intracellular locations, we fused short sequences to the amino or carboxyl terminus of the reporter that drive specific intracellular localization. The fluorescent images in Figure 2.1 show the subcellular localization of the targeted CKAR constructs expressed in COS 7 cells. PMCKAR (Figure 2.1A) contains the N-terminal 7 residues of Lyn kinase fused in frame before CFP, effectively targeting it to the plasma membrane via myristoylation and palmitoylation (1). GolgiCKAR (Figure 2.1B) was targeted to the cytoplasmic face of the Golgi apparatus by attaching the N-terminal 33 residues of eNOS (13, 15). CytoCKAR (Figure 2.1C) was excluded from the nucleus by C-terminal fusion of a hydrophobic sequence for nuclear export (16) and MitoCKAR (Figure 2.1D) was targeted to the outer mitochondrial membrane by fusion of the N-terminal 33 residues of TOM 20

(14). NucCKAR (Figure 2.1E) was localized to the nucleus by C-terminal fusion of a basic nuclear localization sequence (17). Figure 2.1F shows a cartoon representation of the localization of the tethered CKARs. To verify proper targeting of GolgiCKAR and MitoCKAR, we stained cells transfected with the reporters using Golgi-specific tracker dye, BODIPY TR C_5 ceramide, and with mitochondria-specific tracker dye, Deep Red–Fluorescent MitoTracker® (Invitrogen). The reporters completely co-localized with dyes specific for their respective cellular compartment (data not shown). Note that the juxtanuclear concentration of GolgiCKAR was dispersed in the presence of the Golgi-fragmenting agent, Brefeldin A; we also observed a minimal juxtanuclear concentration of PMCKAR and this was insensitive to Brefeldin A (data not shown), suggesting that the apparent juxtanuclear concentration of PMCKAR was in a region distinct from Golgi.

The specificity and reversibility of phosphorylation was tested for each targeted reporter by addressing the sensitivity to activation by phorbol esters and inhibition by a PKC-specific inhibitor. Figure 2.2 shows that PdBu treatment of COS 7 cells triggered an increase in FRET ratio of GolgiCKAR, revealing robust activity of endogenous PKC at this location. This phosphorylation was reversed with addition of the specific PKC inhibitor, Gö6983. Similar phorbol ester-dependent and inhibitor-reversed phosphorylation was noted for each targeted CKAR (data not shown).

Dynamic range of targeted CKARs

Phorbol esters, potent functional analogs of DAG, are the classic tool for activating PKC in cells (18). We first determined the kinetics and magnitude of the stimulated PKC response at each cellular region as a consequence of PdBu treatment. Figure 2.3A shows the change in FRET ratio following PdBu stimulation of COS 7 cells

expressing PMCKAR, GolgiCKAR, CytoCKAR, MitoCKAR, or NucCKAR. The fastest response was observed at the plasma membrane ($t_{1/2} \approx 0.6$ min), followed by Golgi ($t_{1/2} \approx 2.7$ min), mitochondria ($t_{1/2} \approx 4$ min), and cytosol ($t_{1/2} \approx 7$ min). These differences did not simply reflect the rate of PdBu partitioning, since the isolated C1b domain from PKCβ translocated to membranes throughout the cell within 0.5 min of PdBu addition (data not shown). No PdBu-stimulated activity was observed in the nucleus. The highest magnitude of the response was at the Golgi. While the initial FRET ratios varied, the normalized traces were highly consistent in rate and magnitude and were characteristic to each region.

Reversal of PdBu-stimulated activity by inhibition of PKC typically resulted in a decrease in reporter phosphorylation below baseline (Figure 2.2A), leading us to hypothesize that the differences in PdBu-stimulated activity might result from differing levels of basal PKC activity at each region. Thus, after acquiring baseline images, we measured the effect of treating cells with the conventional PKC inhibitor Gö6976 as a measure of the basal PKC activity (Figure 2.3B). Although Gö6983 specifically inhibits all isoforms of PKC, it could not be used to characterize the basal activity because it emits at a wavelength that is visible in the FRET channel and partitions unequally within the cell (data not shown). The highest basal activity was at the plasma membrane. GolgiCKAR and CytoCKAR were also basally phosphorylated, while NucCKAR and MitoCKAR responded minimally to inhibition of basal PKC activity with Gö6976. Thus, basal PKC activity in unstimulated cells varies dramatically depending on the cellular region.

Another component of the localized PKC response is the opposition to substrate phosphorylation by regional phosphatases. We reasoned that the basis for low basal and stimulated activity in some areas may be potent signal termination by local phosphatases. To test this hypothesis, we first stimulated PKC with PdBu and allowed phosphorylation to reach a steady state. Once the response leveled, we added the broad-spectrum phosphatase inhibitor, calyculin A, to release phosphatase suppression (Figure 2.3C). Inhibition of phosphatases resulted in a robust phosphorylation of nuclear-localized CKAR and, to a lesser extent, cytosolic CKAR. Membrane-tethered CKAR was much less sensitive to phosphatase inhibition, particularly at the plasma membrane where the prior treatment with phorbol esters had resulted in maximal CKAR phosphorylation. Interestingly, even in the absence of PdBu, inhibition of phosphatase activity with calyculin A was sufficient to induce phosphorylation of CKAR at each region (Figure 2.3D). The increase in CKAR phosphorylation upon treatment with calyculin A was a specific effect of releasing PKC inhibition, since it was blocked with Gö6983 (unpublished results, J. Violin). These data reveal that PKC activity is antagonized by phosphatases to varying degrees depending on the enzyme's cellular location.

Assembling the components of the PKC response at each region into a bar graph revealed that the sum of basal, stimulated, and phosphatase-suppressed PKC activity was similar at all intracellular regions, with the exception of MitoCKAR, which had about two-thirds the range of an untethered reporter (Figure 2.3E). Further analysis revealed that the mitochondrial reporter, unlike all the others, becomes partially cleaved within CFP when expressed in mammalian cells (data not shown). Thus, with the exception of MitoCKAR, the range of the reporters was not affected by targeting, thus allowing

accurate comparison of responses following stimulation of endogenous signaling pathways. Furthermore, this characterization reveals that the subsequent data showing phosphorylation of the targeted CKARs in response to the GPCR ligand, UTP, is not limited by reporter saturation.

Localized PKC responses to stimulation of endogenous receptors

We next addressed the profile of regional phosphorylation triggered by receptor-mediated stimulation. UTP initiates a PKC response by activating Gq-coupled P2Y receptors on the surface of epithelial cells, producing the second messengers DAG and inositol trisphosphate (IP_3), which stimulates intracellular Ca^{2+} release (19, 20). Figure 2.4 summarizes targeted CKAR phosphorylation in COS 7 cells in response to UTP. PMCKAR, GolgiCKAR, and CytoCKAR were rapidly phosphorylated, with an early crest (peaking within 1 min) followed by a late sustained plateau. Phosphorylation on CytoCKAR was most readily reversed back to baseline, consistent with higher phosphatase sensitivity of CytoCKAR. Phosphorylation on GolgiCKAR was sustained throughout the course of the experiment, while PMCKAR was dephosphorylated to baseline within 35 min. MitoCKAR and NucCKAR were not readily phosphorylated in response to UTP.

Second messenger responses

We next examined the underlying causes for the biphasic nature of the PKC response to UTP. Specifically, we asked how CKAR phosphorylation correlated with production of Ca^{2+} and DAG. First, we monitored Ca^{2+} release downstream of receptor stimulation using the Ca^{2+}-sensitive fluorescent probe, Fura-2 (21). Figure 2.5A reveals the temporal relationship between Ca^{2+} release and the early phase of the PKC response

at the Golgi and plasma membrane. Upon addition of UTP, a transient wave of Ca^{2+} was released that corresponded with the early phase of PKC activity. To confirm that this early phase of PKC activity is driven by Ca^{2+}, we monitored phosphorylation in response to UTP after pretreatment with BAPTA to chelate intracellular Ca^{2+} (22). Chelation of Ca^{2+} abolished the early peak in PKC activity both at the plasma membrane (Figure 2.5B) and at the Golgi (Figure 2.5C). These data reveal that Ca^{2+} is required for the initial peak in PKC activity following UTP stimulation.

The rate of PMCKAR phosphorylation ($t_{1/2} \approx 0.2$ min) was significantly reduced in the presence of BAPTA ($t_{1/2} \approx 1.2$ min). The rate of GolgiCKAR phosphorylation in the presence of BAPTA was also reduced, although only modestly. This reduction could arise because novel PKCs are activated at a slower rate than conventional PKCs, or because the lower level of novel PKCs compared to conventional PKCs in COS cells results in slower kinetics of CKAR phosphorylation. Alternatively, the diminished activity in the presence of BAPTA could represent partial activation of conventional PKCs, with the C1 domain participating in activation by binding DAG, but the C2 domain refraining from providing the extra energy to fully disengage the pseudosubstrate. To address whether the slower phosphorylation catalyzed by endogenous novel PKCs (i.e. in the presence of BAPTA) reflected subsaturating concentrations of these kinases, we transfected in PKCδ, a novel isoform, to attempt to rescue the fast kinetics of phosphorylation in response to UTP. To ensure the residual activity was not due to partial activation of cPKCs, we also added the conventional PKC inhibitor, Gö6976. Gö6976 did not block the response and, while the response was slightly faster with over-expressed PKCδ (as a result of higher total PKC expression) the fast phase of the PKC

response was not restored (Figure 2.5B and C). Therefore, Ca^{2+}-responsive cPKCs are responsible for the fast, early phase of the PKC response while nPKCs account for the slow, later phase of the PKC response.

Because Ca^{2+} release was necessary for the fast phase of PKC activation, we tested if calcium release alone was sufficient for activation of cPKCs. To uncouple Ca^{2+} release from DAG production, we stimulated COS 7 cells with UTP in the absence of extracellular calcium and in the presence of cell-impermeant Ca^{2+} chelator, EGTA. This allows Ca^{2+} release from intracellular stores, resulting in a sharp peak of calcium release (Figure 2.5D), but does not allow calcium-induced calcium release. Under these conditions, no overall DAG increase occurred, as monitored by the intermolecular FRET-based diacylglycerol reporter, DAGR (Figure 2.5E, gray triangles (1)). Importantly, with Ca^{2+} release alone, no phosphorylation of PMCKAR or GolgiCKAR occurred (Figure 2.5 E).

Because the Ca^{2+} release terminated well before reporter dephosphorylation, we tested whether the persistence of the PKC response correlated with the other upstream second messenger, DAG. Specifically, phosphorylation of PMCKAR was reversed within 35 minutes, but GolgiCKAR remained phosphorylated throughout the course of the experiment (Figure 2.4). In order to examine local DAG levels, we cotransfected a YFP-tagged DAG binding domain (YFP-DBD) with either PMCFP (PM DAG reporter, or PMDAGR) or GolgiCFP (Golgi DAG reporter, or GolgiDAGR) and watched a stimulated increase in the ratio of FRET/CFP emission (FRET ratio) as the DBD translocated from the cytosol to the plasma and Golgi membranes (Figure 2.6A). The DBD consists of the C1b domain from PKCβ containing a recently discovered single

point mutation (Y123W) that increases the affinity of the C1b domain for DAG (manuscript in preparation, D. Dries, L. Gallegos, and A. Newton). Figure 2.6B shows that upon addition of UTP, DAG was produced at both the plasma and Golgi membranes. However, while the FRET ratio increase from PMDAGR reversed within 40 minutes, the FRET ratio increase from GolgiDAGR was sustained throughout the course of the experiment. Thus, UTP caused differential duration of the DAG signal at the plasma membrane and Golgi, setting the duration of CKAR phosphorylation at each location.

To further examine the contribution of DAG to the late phase of the PKC response, we next tested whether excess DBD would competitively block DAG-dependent PKC activation. We cotransfected untagged DBD with PMCKAR (Figure 2.6C) or GolgiCKAR (Figure 2.6D) and monitored phosphorylation in response to UTP treatment. We found that the DBD did not completely block the fast phase of the PKC response in either region, but caused shorter duration of phosphorylation in both regions.

Discussion

We have dissected the PKC response at distinct subcellular locations by targeting CKAR, a genetically-encoded FRET-based PKC activity reporter to specific locations within the cell. Imaging the reporter following stimulation of endogenous P2Y receptors in COS 7 cells revealed biphasic responses in phosphorylation that were characteristic to each region. We show that the magnitude and duration of responses at each location are controlled by Ca^{2+} release, localized DAG production, and the level of phosphatase activity at each site.

CKAR was successfully targeted to the plasma membrane, Golgi, mitochondria, cytosol, and nucleus. Each reporter revealed different basal, stimulated, and

phosphatase-suppressed activity, while the dynamic range of responses was similar at all locations. Even taking into consideration the possibility of incomplete targeting, the reporters are undeniably enriched in the regions targeted, resulting in distinct phosphorylation profiles among the different regions.

Phosphorylation of PMCKAR was basally elevated and rapidly increased in the presence of PdBu, which highlights the responsiveness of the plasma membrane to external signaling. PdBu caused the greatest increase in phosphorylation of GolgiCKAR, indicating a high capacity for stimulated changes in PKC activity at the Golgi. Membrane-tethered reporters, in general, were much less sensitive to phosphatases than untethered reporters, allowing these substrates a fuller range of responses to stimulation. Strikingly, phosphatase suppression was both necessary and sufficient to allow phosphorylation of NucCKAR. It is possible that provoking a PKC response in the nucleus depends upon coincident inhibition of phosphatase activity rather than the presence of second messengers. Additionally, simply inhibiting phosphatase activity at any region of the cell increased CKAR phosphorylation, which underscores the importance of phosphatases in regulating PKC activity. The targeted CKARs likely serve as faithful representatives of natural PKC substrates, and can be useful tools to provide information about the cellular environment surrounding PKC substrates that are localized in different regions of the cell for any period of time.

UTP stimulates G_q-coupled P2Y receptors in epithelial cells (19, 20) which, in COS 7 cells, generates a spike of Ca^{2+} release as well as production of DAG via PLC-mediated lipid hydrolysis. We were able to detect an early peak of PKC activity on PMCKAR, GolgiCKAR and CytoCKAR that correlated temporally with Ca^{2+} release.

By buffering intracellular Ca^{2+} with BAPTA, the early peak of activity at the plasma membrane was abolished, implicating cPKCs in the early phase of the PKC response. The effect is less dramatic at the Golgi, consistent with previous data that generally localizes the Ca^{2+}-independent nPKCs at the Golgi (7, 23). When intracellular Ca^{2+} was chelated, it was impossible to rescue the fast kinetics of the response by over-expressing PKCδ, indicating a genuine difference in the rate of activation of cPKCs vs. nPKCs. Additionally, while inhibiting cPKCs reduced the rate of response, it did not block the later phase of activation, suggesting a role for the nPKCs in sustaining phosphorylation.

We determined conditions for intracellular Ca^{2+} elevation without the corresponding DAG production, and used the localized reporters to test for cPKC activity. While Ca^{2+} appears to be required for the faster kinetics of cPKCs, Ca^{2+} alone is not sufficient to drive activation of cPKCs in live cells, consistent with *in vitro* data (24). These data also underscore the importance of the feed-forward effect of Ca^{2+} on PLC-mediated DAG generation (25, 26), since DAG must be generated along with IP_3 production in response to P2Y receptor stimulation; however, this amount of DAG is clearly not sufficient to be read out using our DAG reporter and is not sufficient to activate PKC at even the most responsive region, the plasma membrane.

PKC activity persisted longer at the Golgi than at the plasma membrane, which could not be explained by differences in phosphatase activity; however, regional variations in DAG production could cause differences in sustained phosphorylation by PKC. Previous methods for detecting whole cell DAG production consisted of imaging DAGR, a probe consisting of the entire C1 domain of PKCβ flanked by CFP and YFP. Upon generation of DAG, DAGR translocates to cellular membranes, and the increased

concentration resulting from the reduction in dimensionality is read as an increase in intermolecular FRET (1). One disadvantage of DAGR is that it cannot be localized to any particular subset of cellular membranes because targeting the reporter would confine the movement of DAGR, which is the sole basis for the FRET change.

In order to visualize local production of DAG, we transfected COS 7 cells with targeted FRET-based DAG reporters: PMDAGR and GolgiDAGR. Using the targeted DAGRs, we were able to correlate persistence of the PKC response with local DAG persistence. Specifically, DAG persistence and the corresponding PKC activity were highly sustained at the Golgi, while DAG and PKC activity at the plasma membrane reversed back to baseline within 35 min. Competitively inhibiting PKC activation by over-expressing a DAG binding domain (DBD) shortens the duration of the PKC response to UTP, further supporting the idea that DAG persistence is required for sustained PKC activity. However, over-expression of the DBD does not completely block the early phase of the PKC activation, likely due to the fast kinetics of the cPKC response imparted by the C2 domain.

A major finding from our study is that the Golgi is the site of the most robust and sustained activity of endogenous PKC in response to natural agonists. Specifically, we find that although the magnitude of initial PKC activation is similar at the plasma membrane, the historical site of PKC activation, and at the Golgi, the duration of the activity persists considerably longer at the Golgi. This activity is relatively-insensitive to either Ca^{2+} chelation or inhibition by Gö6976, an inhibitor directed at cPKCs, suggesting that it is mediated by nPKCs. Consistent with this, biochemical fractionation, immunofluorescence, and GFP-fusion protein studies over the past decade have

established that the novel isozymes of PKC (δ, ε, and θ) localize to intracellular membranes, most typically Golgi, following activation (e.g. 7, 27-32). Taken together, our data show that the Golgi-localized PKC accounts for the bulk of the PKC activity following the first few minutes after GPCR stimulation. Our data also reveal that the plasma membrane is the site of the initial activation of PKC, and that this activity is Ca^{2+}-driven and inhibited by Gö6976. This is consistent with the abundant literature showing that conventional isozymes of PKC (α, β, and γ) translocate to the plasma membrane following activation (e.g. 10, 33-37).

Although DAG production at the Golgi has been demonstrated elegantly by indirect methods (38), and DAG-dependent binding of proteins at the Golgi has been established previously (39), this is the first imaging study directly visualizing stimulus-dependent DAG generation at the Golgi. We find that DAG is rapidly produced at this location and that, in striking contrast to plasma membrane DAG, the levels of this second messenger are sustained at the Golgi. DAG can be produced at the Golgi by several means, including phospholipase D-mediated hydrolysis of phosphatidylcholine to phosphatatidic acid, which is converted to DAG via phosphatidic acid phosphatase (40). Phospholipase C (PLC) activity has also been documented to generate DAG at the Golgi. Specifically, PLCε translocates to the Golgi in a Ras-proximate 1 (Rap1)-dependent manner (41). Intriguingly, in response to GPCR agonists, it has recently been shown that PLCε is responsible for sustained (60 min) PI hydrolysis, while PLCβ is responsible for acute (1 min) PI hydrolysis (42). Thus, activation of PLCε could account for the sustained DAG levels at the Golgi.

In this study, cPKCs mediated rapid, transient phosphorylation while phosphorylation mediated by nPKCs was slower and longer in duration. The fast phase was more prominent at the plasma membrane, and the slow phase was more persistent at the Golgi. Thus, in response to UTP, specific substrate phosphorylation was achieved by variation in the kinetics and duration of the PKC response resulting from recruitment of different isoforms to different regions. Because isoforms of the PKC family share a conserved kinase core and differ most in their regulatory modules (43), spatiotemporal specificity may be more important in determining PKC substrate specificity than active site specificity, underscoring the need for sensitive tools to study spatiotemporal dynamics of PKC signaling.

Acknowledgements

We thank Nathan Shaner for generating constructs targeting CKAR to the nucleus and cytosol and Roger Tsien for helpful discussions.

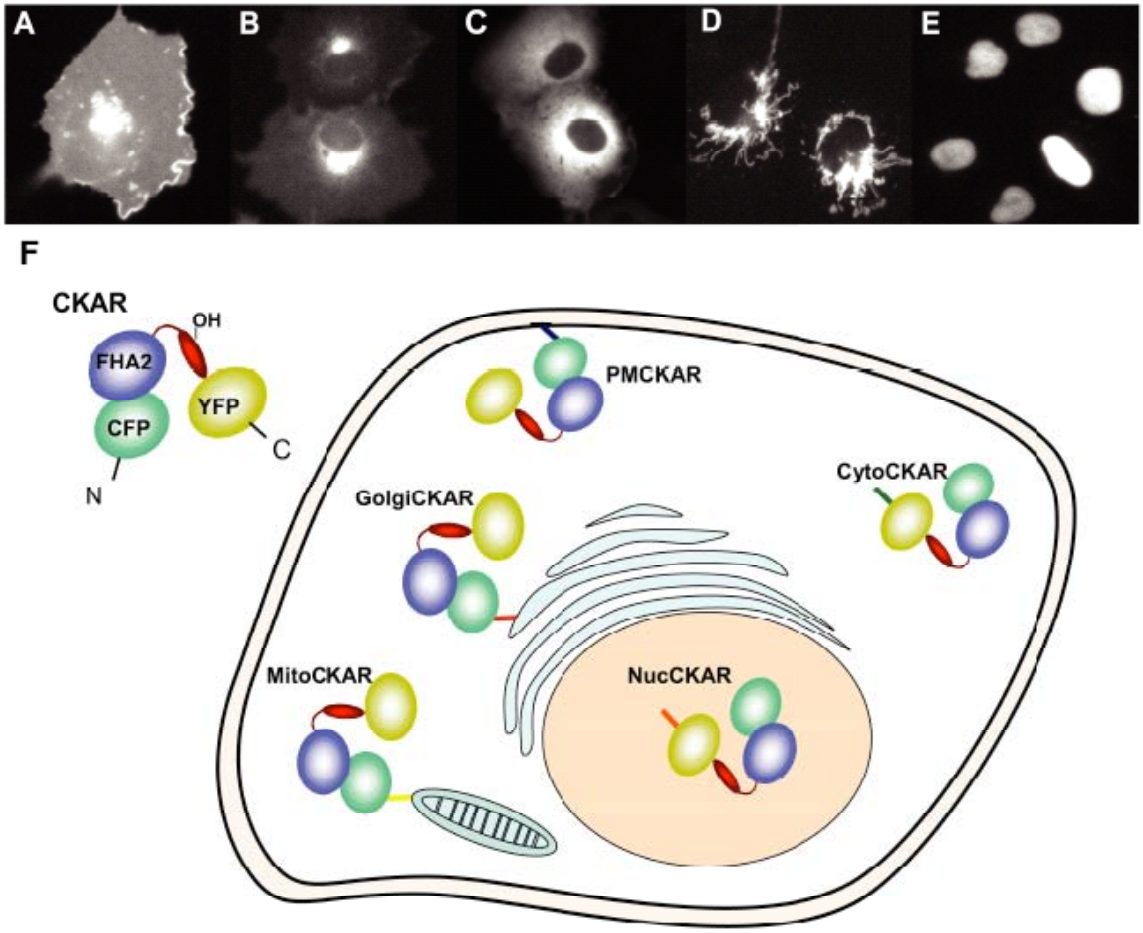

Figure 2.1. Targeting C Kinase Activity Reporter (CKAR). CKAR, composed of CFP and YFP flanking a substrate sequence specific for PKC and an FHA2 phosphopeptide binding module, can be targeted to different intracellular locations by fusing short targeting motifs to the amino or carboxyl terminus. *A*, CKAR was targeted to the plasma membrane by fusion of the amino terminal 7 residues of Lyn kinase. *B*, Golgi targeting was achieved by fusion of the amino terminal 33 residues of eNOS. *C*, CytoCKAR was generated by C-terminal fusion of a hydrophobic sequence for nuclear export. *D*, CKAR was targeted to the outer membrane of the mitochondria by fusion of the amino terminal 33 residues of TOM20. *E*, Fusion of a basic nuclear localization sequence to the C-terminus targeted CKAR to the nucleus. *F*, Schematic representation of targeted CKARs.

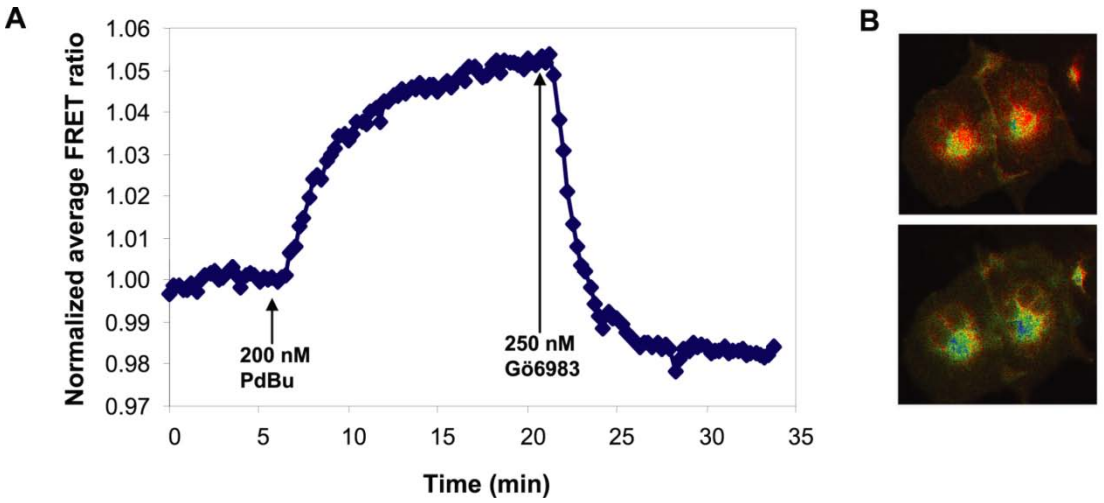

Figure 2.2. Targeted CKAR retains specificity and reversibility in monitoring PKC activity in live cells. *A*, COS 7 cells were transfected with GolgiCKAR and FRET ratio quantified following addition of PdBu (200 nM) and then the specific PKC inhibitor Gö6983 (250 nM). *B*, Images corresponding to data in Figure 2.2A show phosphorylation (red-shift of pseudocolored FRET ratio image, top) of CKAR after PdBu treatment (15 min time point) and dephosphorylation (blue-shift of pseudocolored FRET ratio image, bottom) after Gö6983 addition (30 min time point). Data are representative of three independent experiments.

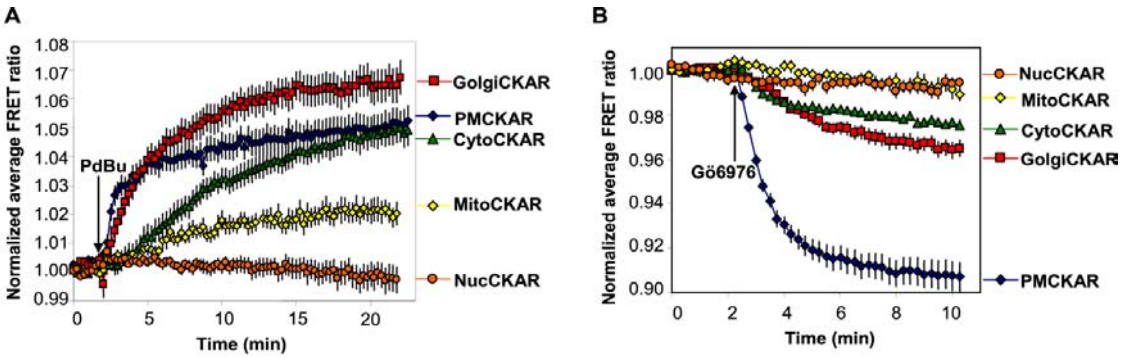

Figure 2.3. Localized PKC activity in COS 7 cells. *A*, COS 7 cells were transfected with the indicated targeted constructs of CKAR and the average FRET ratio quantified as a function of time following PdBu (200 nM) treatment: GolgiCKAR (red squares), PMCKAR (blue diamonds), CytoCKAR (green triangles), MitoCKAR (yellow diamonds), and NucCKAR (orange circles). These data reveal the magnitude of the phorbol ester-stimulated response. *B*, COS 7 cells were transfected with targeted CKAR constructs and the FRET ratio monitored following treatment with Gö6976 (500 nM), an inhibitor of conventional isoforms of PKC. These data reveal the magnitude of the basal conventional PKC activity at each location.

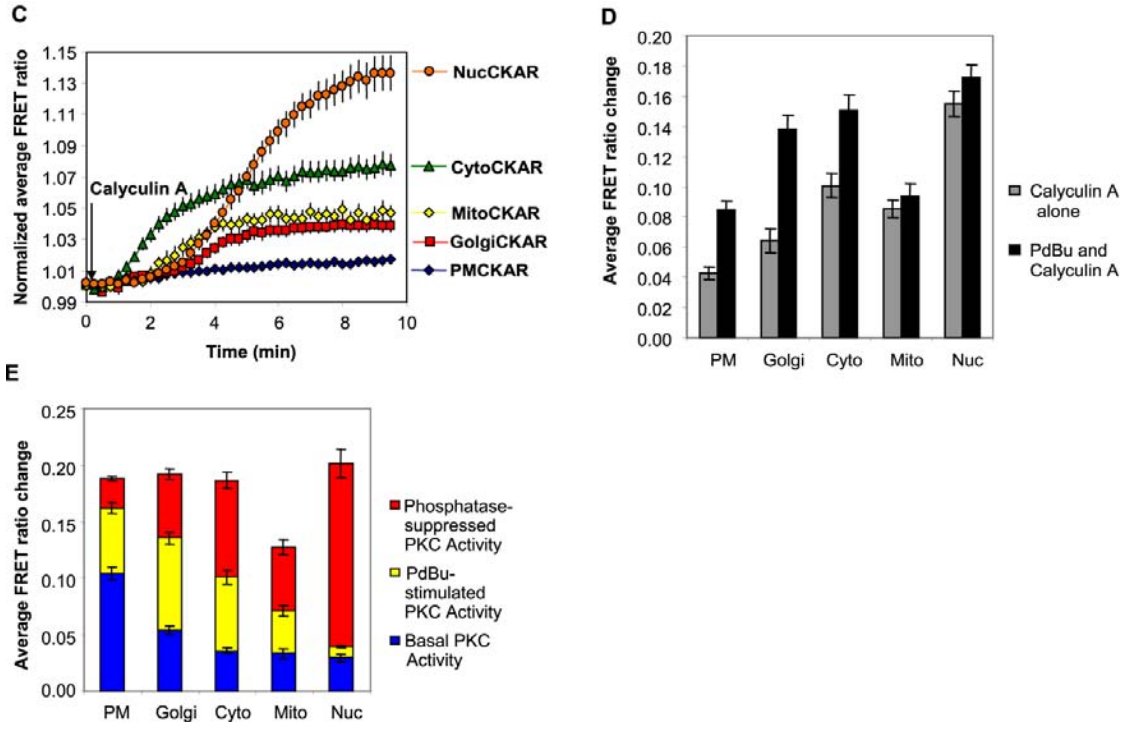

(Figure 2.3, continued) *C,* COS 7 cells transfected with various CKAR constructs were stimulated with PdBu (200 nM) for 20 min until the maximal phorbol ester stimulation was achieved. At this point, the FRET ratio was measured before and after addition of calyculin A (50 µM) to inhibit cellular phosphatases. The magnitude of the calyculin A-stimulated response reveals the phosphatase-suppressed PKC activity at each region. *D,* COS 7 cells transfected with the various CKAR constructs were stimulated with PdBu (200 nM) and calyculin A (50 µM) (black bars) or calyculin A (50 µM) alone (gray bars). *E,* Quantitation of the basal, stimulated, and phosphatase-suppressed PKC activities at specific regions, showing the range of CKAR at each cellular location. Data represent the average ± SEM of 10-25 cells from at least three independent experiments referenced around the addition time point.

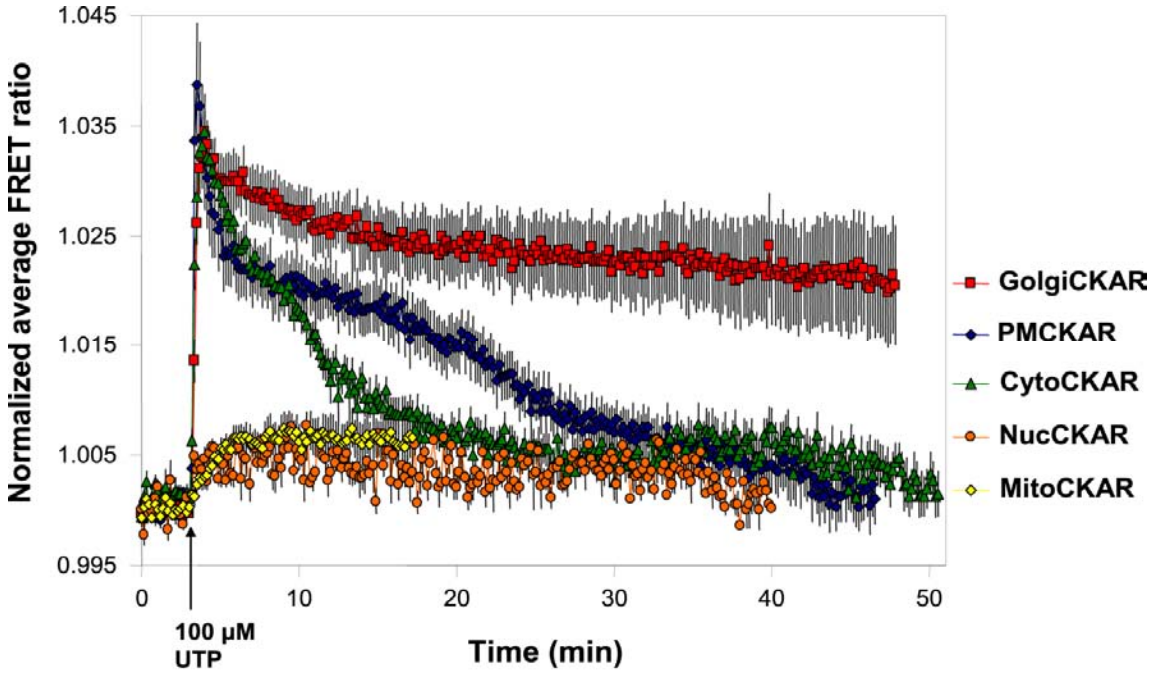

Figure 2.4. PKC response to UTP in COS 7 cells. COS7 cells transfected with the indicated targeted CKARs were treated with UTP (100 µM) and the FRET ratio visualized as a function of time. Data shown are an average + SEM of 11-16 cells from three independent experiments referenced around the ligand addition time point.

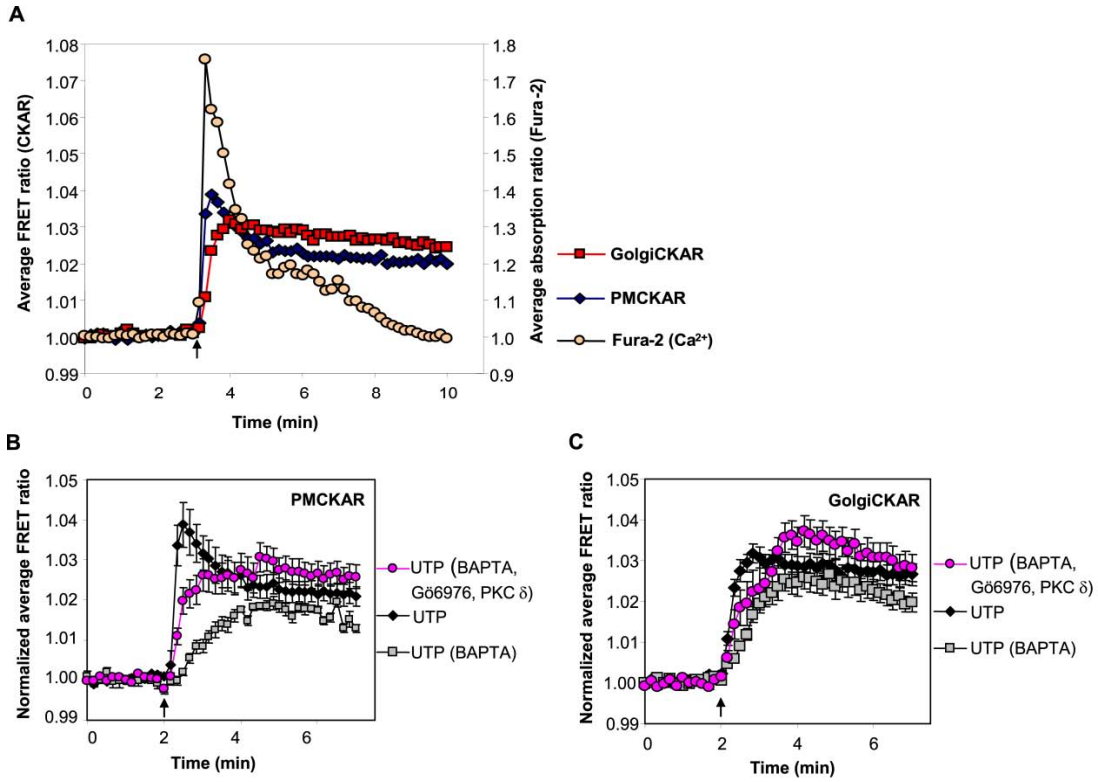

Figure 2.5. Ca^{2+} release is responsible for early phase of the UTP-stimulated PKC response. *A*, COS 7 cells loaded with Fura-2 were imaged after stimulation with UTP (100 µM) at 3 min (black arrow). Fura-2 absorption ratio (340/380 nm) monitors Ca^{2+} release (tan circle). PMCKAR (blue diamonds) and GolgiCKAR (red squares) responses to UTP (100 µM) were scaled and overlaid on the plot to show temporal correlation. *B*, COS 7 cells were transfected with PMCKAR alone (black diamonds, gray squares) or PMCKAR and PKCδ (pink circles). Cells were then stimulated with UTP (100 µM, black diamonds) or pre-treated with BAPTA (15 min, 15 µM) and then stimulated with UTP (100 µM, gray squares) or pre-treated with both BAPTA (15 µM) and Gö6976 (500 nM) and then stimulated with UTP (100 µM, pink circles). Black arrow shows UTP added at 2 min. *C*, COS 7 cells were transfected with GolgiCKAR alone (black diamonds, gray squares) or GolgiCKAR and PKCδ (pink circles). Cells were then stimulated with UTP (100 µM, black diamonds) or pre-treated with BAPTA (15 min, 15 µM) and then stimulated with UTP (100 µM, gray squares) or pre-treated with both BAPTA (15 µM) and Gö6976 (500 nM) and then stimulated with UTP (100 µM, pink circles). Black arrow shows UTP added at 2 min.

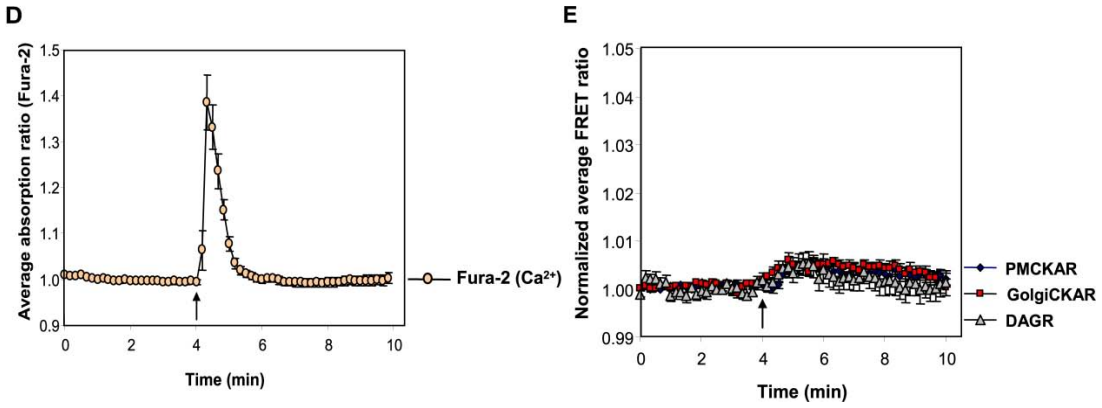

(Figure 2.5, continued) *D*, COS 7 cells were loaded with Fura-2 and imaged in Ca^{2+}-free saline and EGTA (5 mM) after stimulation with UTP (100 µM) at 4 min (black arrow). Fura-2 absorption ratio (340/380 nm) monitors Ca^{2+} release (tan circles). *E*, COS 7 cells were transfected with DAGR to monitor global DAG production (gray triangles), PMCKAR (blue diamonds), or GolgiCKAR (red squares) and imaged in Ca^{2+}-free saline and EGTA (5 mM) after stimulation with UTP (100 µM) at 4 min (black arrow). Data represent the average ± SEM of 10-25 cells from at least three independent experiments referenced around the addition time point.

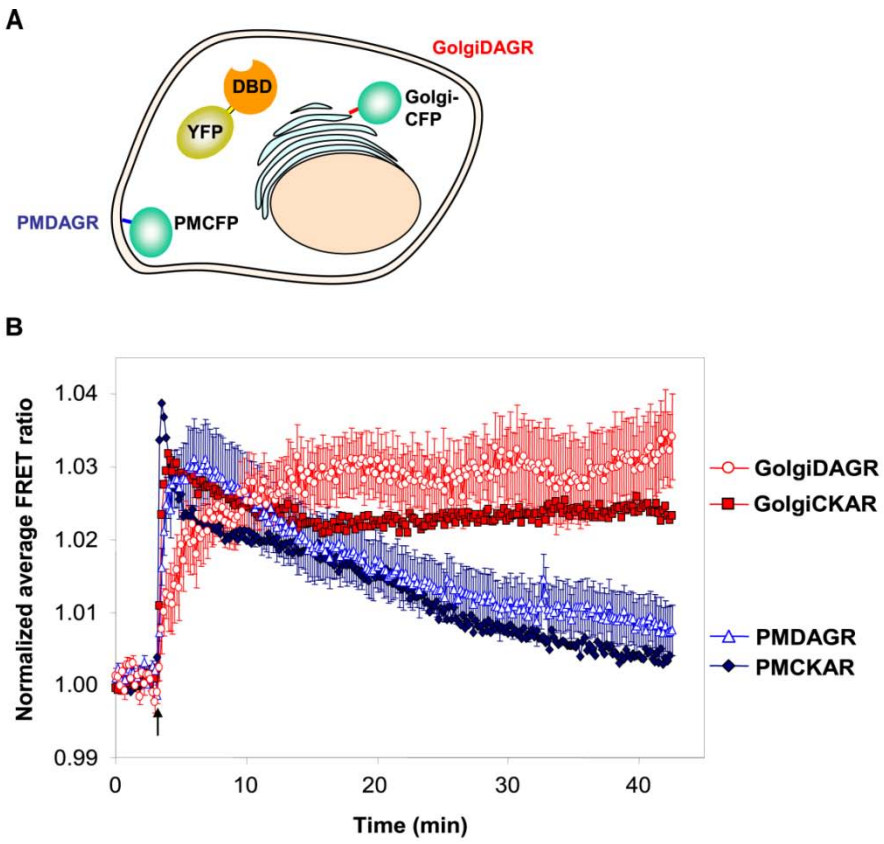

Figure 2.6. Localized persistence in PKC activity follows DAG persistence. *A*, Schematic representation of PMDAGR and GolgiDAGR system. *B*, COS 7 cells cotransfected with YFP-DBD and PM-CFP (PMDAGR, open blue triangles) or YFP-DBD and Golgi-CFP (GolgiDAGR, open red circles) were stimulated with UTP (100 μM) at 3 min (black arrow). Localized DAGR responses were plotted together with PMCKAR (closed blue diamonds) and GolgiCKAR (closed red squares) responses to UTP (100 μM) to show temporal correlation.

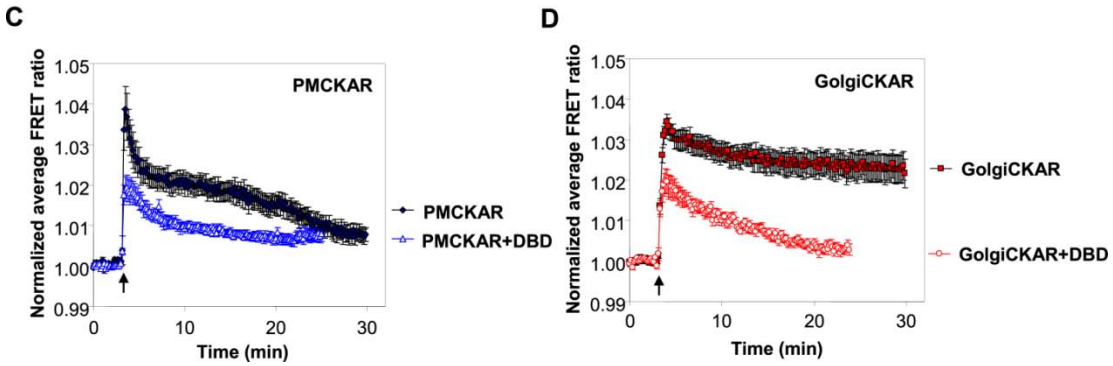

(Figure 2.6, continued) *C*, COS 7 cells transfected with PMCKAR (blue diamonds) or PMCKAR and DBD (open blue triangles) were stimulated with UTP (100 µM) at 3 min (black arrow). *D*, COS 7 cells transfected with GolgiCKAR (red squares) or GolgiCKAR and DBD (open red circles) were stimulated with UTP (100 µM) at 3 min (black arrow). CKAR and DAGR responses derive from an average of 15-25 cells from three independent experiments, referenced around the ligand addition time point.

References

1. Violin, J. D., Zhang, J., Tsien, R. Y., and Newton, A. C. (2003) *J Cell Biol* **161**, 899-909

2. Vermeulen, K., Berneman, Z. N., and Van Bockstaele, D. R. (2003) *Cell Prolif* **36**, 165-175

3. Naor, Z. (1990) *Endocr Rev* **11**, 326-353

4. Majumder, P. K., and Sellers, W. R. (2005) *Oncogene* **24**, 7465-7474

5. Newton, A. C. (2003) *Biochem J* **370**, 361-371

6. Orr, J. W., and Newton, A. C. (1992) *Biochemistry* **31**, 4661-4667

7. Giorgione, J. R., Lin, J. H., McCammon, J. A., and Newton, A. C. (2006) *J Biol Chem* **281**, 1660-1669

8. Lamark, T., Perander, M., Outzen, H., Kristiansen, K., Overvatn, A., Michaelsen, E., Bjorkoy, G., and Johansen, T. (2003) *J Biol Chem* **278**, 34568-34581

9. Oancea, E., and Meyer, T. (1998) *Cell* **95**, 307-318

10. Sakai, N., Sasaki, K., Ikegaki, N., Shirai, Y., Ono, Y., and Saito, N. (1997) *J Cell Biol* **139**, 1465-1476

11. Wang, Q. J., Bhattacharyya, D., Garfield, S., Nacro, K., Marquez, V. E., and Blumberg, P. M. (1999) *J Biol Chem* **274**, 37233-37239

12. Wang, W. L., Yeh, S. F., Chang, Y. I., Hsiao, S. F., Lian, W. N., Lin, C. H., Huang, C. Y., and Lin, W. J. (2003) *J Biol Chem* **278**, 37705-37712

13. Fulton, D., Babbitt, R., Zoellner, S., Fontana, J., Acevedo, L., McCabe, T. J., Iwakiri, Y., and Sessa, W. C. (2004) *J Biol Chem* **279**, 30349-30357

14. Kanaji, S., Iwahashi, J., Kida, Y., Sakaguchi, M., and Mihara, K. (2000) *J Cell Biol* **151**, 277-288

15. Sasaki, K., Sato, M., and Umezawa, Y. (2003) *J Biol Chem* **278**, 30945-30951

16. Wen, W., Meinkoth, J. L., Tsien, R. Y., and Taylor, S. S. (1995) *Cell* **82**, 463-473

17. Makkerh, J. P., Dingwall, C., and Laskey, R. A. (1996) *Curr Biol* **6**, 1025-1027

18. Castagna, M., Takai, Y., Kaibuchi, K., Sano, K., Kikkawa, U., and Nishizuka, Y. (1982) *J Biol Chem* **257**, 7847-7851

19. Balboa, M. A., Firestein, B. L., Godson, C., Bell, K. S., and Insel, P. A. (1994) *J Biol Chem* **269**, 10511-10516

20. Insel, P. A., Ostrom, R. S., Zambon, A. C., Hughes, R. J., Balboa, M. A., Shehnaz, D., Gregorian, C., Torres, B., Firestein, B. L., Xing, M., and Post, S. R. (2001) *Clin Exp Pharmacol Physiol* **28**, 351-354

21. Grynkiewicz, G., Poenie, M., and Tsien, R. Y. (1985) *J Biol Chem* **260**, 3440-3450

22. Harrison, S. M., and Bers, D. M. (1987) *Biochim Biophys Acta* **925**, 133-143

23. Kajimoto, T., Shirai, Y., Sakai, N., Yamamoto, T., Matsuzaki, H., Kikkawa, U., and Saito, N. (2004) *J Biol Chem* **279**, 12668-12676

24. Hannun, Y. A., Loomis, C. R., and Bell, R. M. (1985) J Biol Chem 260, 10039-10043

25. Murthy, K. S., Zhou, H., Huang, J., and Pentyala, S. N. (2004) Am J Physiol Cell Physiol 287, C1679-1687

26. Thore, S., Dyachok, O., Gylfe, E., and Tengholm, A. (2005) J Cell Sci 118, 4463-4471

27. Lehel, C., Olah, Z., Jakab, G., and Anderson, W. B. (1995) *Proc Natl Acad Sci U S A* **92**, 1406-1410

28. England, K., and Rumsby, M. G. (2000) *Biochem J* **352 Pt 1**, 19-26

29. Kajimoto, T., Shirai, Y., Sakai, N., Yamamoto, T., Matsuzaki, H., Kikkawa, U., and Saito, N. (2004) *J Biol Chem* **279**, 12668-12676

30. Kang, M., and Walker, J. W. (2005) *J Mol Cell Cardiol* **38**, 753-764

31. Kashiwagi, K., Shirai, Y., Kuriyama, M., Sakai, N., and Saito, N. (2002) *J Biol Chem* **277**, 18037-18045

32. Schultz, A., Jonsson, J. I., and Larsson, C. (2003) *Cell Death Differ* **10**, 662-675

33. Oancea, E., and Meyer, T. (1998) *Cell* **95**, 307-318

34. Ohmori, S., Sakai, N., Shirai, Y., Yamamoto, H., Miyamoto, E., Shimizu, N., and Saito, N. (2000) *J Biol Chem* **275**, 26449-26457

35. Saito, K., Ito, E., Takakuwa, Y., Tamura, M., and Kinjo, M. (2003) *FEBS Lett* **541**, 126-131

36. Abdel-Raheem, I. T., Hide, I., Yanase, Y., Shigemoto-Mogami, Y., Sakai, N., Shirai, Y., Saito, N., Hamada, F. M., El-Mahdy, N. A., Elsisy Ael, D., Sokar, S. S., and Nakata, Y. (2005) *Br J Pharmacol* **145**, 415-423

37. Dale, L. B., Babwah, A. V., Bhattacharya, M., Kelvin, D. J., and Ferguson, S. S. (2001) *J Biol Chem* **276**, 35900-35908

38. Baron, C. L., and Malhotra, V. (2002) *Science* **295**, 325-328

39. Carrasco, S., and Merida, I. (2004) *Mol Biol Cell* **15**, 2932-2942

40. Billah, M. M., and Anthes, J. C. (1990) *Biochem J* **269**, 281-291

41. Song, C., Hu, C-D., Masago, M., Kariya, K., Yamawaki-Kataoka, Y., Shibatohge, M., Wu, D., Satoh, T., and Kataoka, T. (2001) *J Biol Chem* **276**, 2752-2757

42. Kelley, G. G., Kaproth-Joslin, K. A., Reks, S. E., Smrcka, A. V., and Wojcikiewicz, R. J. H. (2006) *J Biol Chem* **281**, 2639-2648

43. Nishikawa, K., Toker, A., Johannes, F. J., Songyang, Z., and Cantley, L. C. (1997) *J Biol Chem* **272**, 952-960

Footnotes

[§]This work was supported by NIH P01 DK54441 and NIH GM-43154.

[*]Abbreviations: PKC, protein kinase C; cPKC, conventional PKC; nPKC, novel PKC; DAG, diacylglycerol; FRET, fluorescence resonance energy transfer; CKAR, C kinase activity reporter; CFP, cyan fluorescent protein; YFP, yellow fluorescent protein; PDBu, phorbol 12,13-dibutyrate; DBD, DAG binding domain; DAGR, DAG reporter; BAPTA, 1,2-bis(2-aminophenoxy) ethane-N,N,N',N'-tetraacetic acid; PLC, phospholipase C.

This Chapter is, in full, a reprint of the material as it appears in The Journal of Biological Chemistry, 2006, Gallegos LL, Kunkel MT, and Newton AC. I was the primary researcher and author; coauthors helped direct and supervise the research included in this chapter.

APPENDIX 1

This Appendix presents data primarily validating the targeting of CKAR to and specificity of CKAR at each location. Concerns with pharmacological reagents used in this study are also addressed here. Specifically, the rate of distribution of PdBu into intracellular membranes was investigated, and the compatibility of the inhibitor Gö6983 with FRET reporter imaging studies was assessed. Additionally, to maintain restrictions for publication, some data were omitted from the preceding chapter and mentioned as "data not shown;" this Appendix contains these data.

Validation of CKAR targeting

In COS7 cells, Cyto-CKAR and Nuc-CKAR were clearly excluded from or localized in the nucleus; this was validated by comparing the fluorescent signal to a DIC image (Figure A1.1A and B). Targeting of Golgi-CKAR to the Golgi was validated in two ways: first, by co-localization of Golgi-CKAR with Bodipy ceramide (Invitrogen; Figure A1.1C), a dye that is used to highlight the Golgi, and second, by disruption of the targeting by Brefeldin A, a Golgi-disrupting agent (Figure A1.2). Because a small amount of YFP signal from Golgi-CKAR appears in the RFP channel, which is used to observe Bodipy ceramide, the localization of Golgi-CFP alone was also confirmed to co-localize with the Golgi-tracking dye (Figure A1.1C). Similarly, targeting of Mito-CKAR to mitochondria was verified by co-localization of Mito-CKAR (and Mito-CFP) with Mito-tracker (Invitrogen, Figure A1.1D), a dye used to highlight the mitochondria. The PM-CKAR construct was previously published (Violin); in COS7 cells, this reporter localized to the plasma membrane of the cell. A small amount of juxta-nuclear PM-

CKAR localization was of concern; however, in COS7 cells, which adhere and spread out well for imaging, it was trivial to avoid selecting these regions. These regions were confirmed to be distinct from Golgi, since they were not disrupted with Brefeldin A (Figure A1.2), and are possibly endosomes. The ability of the selected targeting sequences to place the reporter at the desired location might vary depending on the cell type in which they are used. Thus, the success of targeting CKAR in other cell lines should be characterized before use.

Partial cleavage of Mito-CKAR

Mito-CKAR was partially cleaved in COS7 cells. Figure A1.3B shows MitoCKAR fluorescence in the CFP and YFP channels. While CFP fluorescence is clearly targeted to mitochondria, some diffuse YFP fluorescence is observed. In agreement with this, when analyzed by western blot in comparison to a reporter of exactly the same size, GolgiCKAR, a sub-population of MitoCKAR migrates at a faster mobility (Figure A1.3A). However, it is possible to find cells in which the diffuse YFP fluorescence is reduced; these cells were selected for imaging in this study. Furthermore, this partial cleavage may contribute to the slightly decreased range of MitoCKAR relative to the other targeted CKARs.

Specificity of CKAR for PKC at each location

Although CKAR has been shown to be phosphorylated by PKC with high specificity *in vitro* as well as in cells, targeting CKAR to a discrete localization might force it to encounter a high concentration of competing kinase that could potentially produce an artifactual response. To control for this possibility, the response of each targeted CKAR in COS7 cells was demonstrated to be blocked by Gö6983, a specific

inhibitor of PKC (Figure A1.4). In addition, to ensure that the sustained PKC signal at Golgi membranes was not artifactual, the response was reversed back to below baseline with Gö6983 (Figure A1.4E)

Kinetics of distribution of phorbol into intracellular membranes

Because the kinetics of the CKAR response to PdBu varied at the different locations, it was important to investigate whether this simply reflected the rate of phorbol distribution throughout the cell. To test this, we transfected cells with a YFP-tagged C1 domain that will bind to membranes in the presence of PdBu. Figure A1.5 shows that the C1 domain translocated to all cellular membranes within 0.5 min of the addition of PdBu (200 nM). Because this precedes all of the CKAR responses, distribution of PdBu to intracellular membranes is not likely to be the factor governing the differences in phosphorylation kinetics.

Bleed-through of Gö6983 and accumulation in juxtanuclear membranes

As mentioned in Chapter 2, Gö6976, which only inhibits conventional PKC isoforms, was used to assess basal PKC activity rather than Gö6983, which inhibits all PKC isoforms. Gö6983, which is red in color, produces an emission that appears in the FRET channel. Figure A1.6A shows the artifactual FRET ratio decrease from Gö6983 partitioning into juxtanuclear membranes in cells transfected with CKAR containing an Ala residue at the PKC phospho-acceptor site (CKAR T/A). It is likely that concentration of Gö6983 in intracellular membranes relative to other regions of the cell might have affected any comparison amongst the targeted reporters; even when comparing different cells using the same reporter, differences in CFP expression offsetting bleed-through of Gö6983 into the FRET channel might lead to FRET ratio

changes that are inconsistent in magnitude. However, the kinetics of this artifactual FRET ratio decrease are slower ($t_{1/2}$=2.9 ± 0.4; Figure A1.6C) than the kinetics of the FRET ratio decrease of CKAR due to dephosphorylation ($t_{1/2}$=1.7 ± 0.3; Figure A1.6B). Thus, Gö6983 is still a useful tool for validating specificity when the kinetics of the inhibition are clearly faster than those of accumulation, or when used to prevent phosphorylation.

Validation of targeted DAGR results with untargeted DAGR

To further confirm the difference in DAG kinetics at the plasma membrane vs. the Golgi, I sought to recapitulate the results from PMDAGR and GolgiDAGR using the original DAGR. COS 7 cells were transfected with DAGR and DAG production was monitored at a peripheral membrane region compared to a juxtanuclear membrane region (Figure A1.7B). In support of the results derived from PMDAGR and GolgiDAGR, there is a rapid rise in DAG at peripheral membranes that returns to baseline within 15 minutes (Figure A1.7A, blue). At the juxtanuclear region, there is a slight decrease in response (likely due to DAGR leaving the region to respond at the plasma membrane) followed by a sustained elevation of DAG (Figure A1.7B, red). These results qualitatively mirror and confirm the results from targeted DAG reporters.

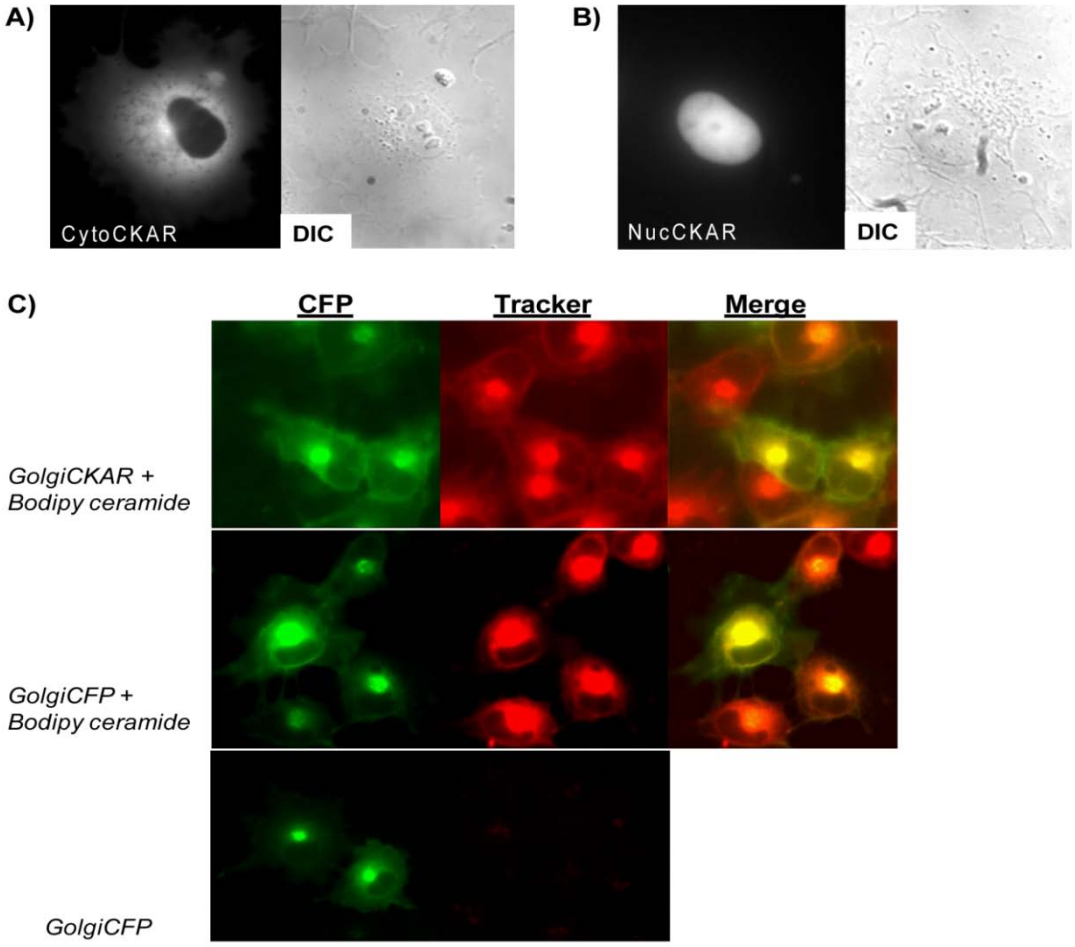

Figure A1.1. Validating targeting of CKAR to sub-cellular locations. *A*, CytoCKAR fluorescence (left panel) is excluded from the nucleus, as compared to the DIC image (right panel). *B*, NucCKAR fluorescence (left panel) is targeted to the nucleus, as compared to the DIC image (right panel). *C*, CFP fluorescence from GolgiCKAR (top left panel) and fluorescence from Bodipy ceramide (top middle panel) completely colocalize (merged image, top right panel). Golgi-CFP alone (middle left panel) also completely colocalizes with Bodipy ceramide (merged image, middle right panel). Importantly, Golgi-CFP fluorescence only appears in the CFP channel (bottom left panel) and does not bleed into the RFP channel (bottom right panel), which is used to observe Bodipy ceramide.

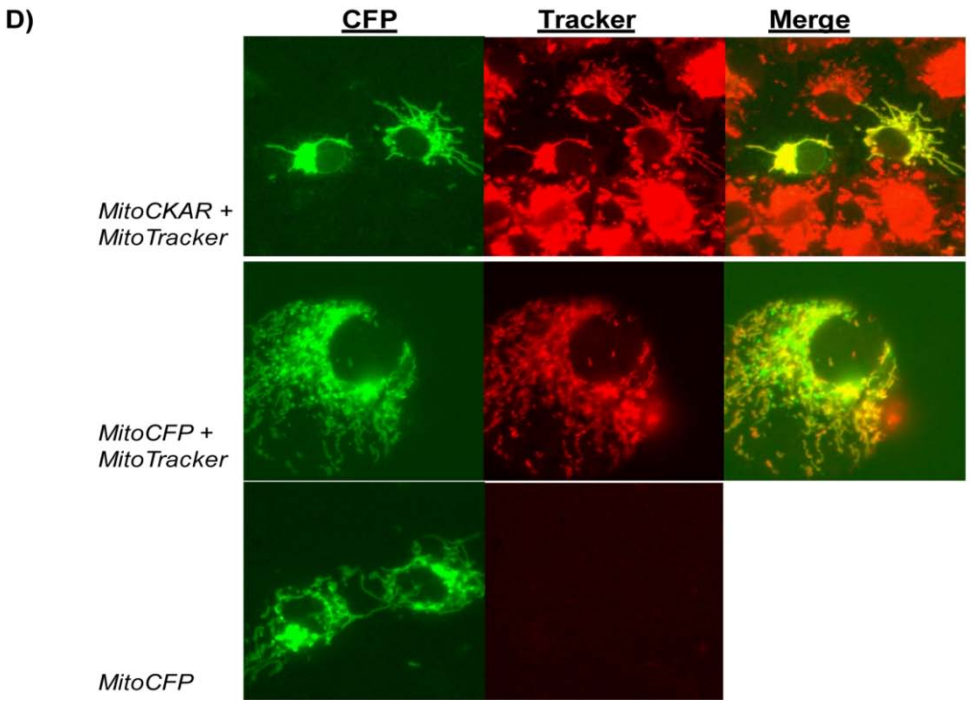

(Figure A1.1, continued) *D*, CFP fluorescence from MitoCKAR (top left panel) and fluorescence from MitoTracker (top middle panel) completely colocalize (merged image, top right panel). Mito-CFP alone (middle left panel) also completely colocalizes with MitoTracker (merged image, middle right panel). Importantly, Mito-CFP fluorescence only appears in the CFP channel (bottom left panel) and does not bleed into the RFP channel (bottom right panel), which is used to observe MitoTracker.

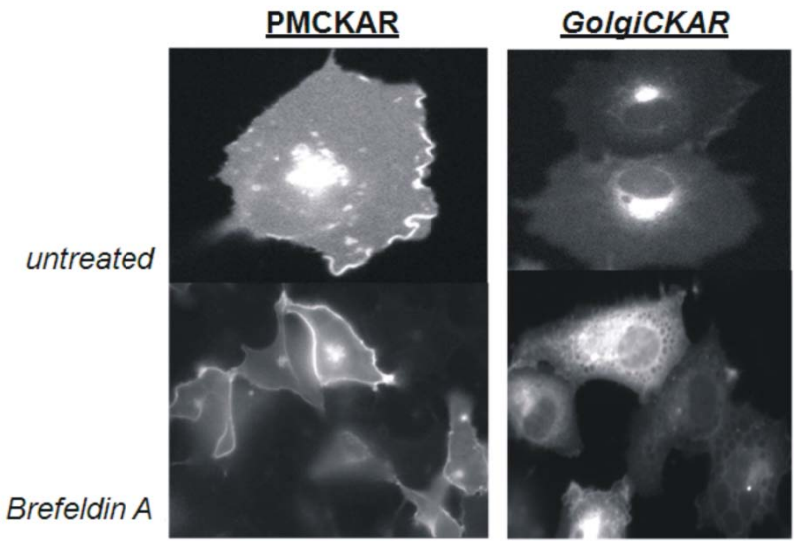

Figure A1.2. Validation of targeting of GolgiCKAR and PMCKAR using Brefeldin A. COS7 cells transfected with PMCKAR (left panels) or GolgiCKAR (right panels) were treated for 30 min with 2.5 μg/ml Brefeldin A. With Brefeldin A treatment, GolgiCKAR (bottom right panel) is dramatically dispersed from the juxtanuclear localization evident in the untreated image (top right panel). However, the juxtanuclear accumulation of PMCKAR (top left panel) is still present with Brefeldin A (bottom left panel).

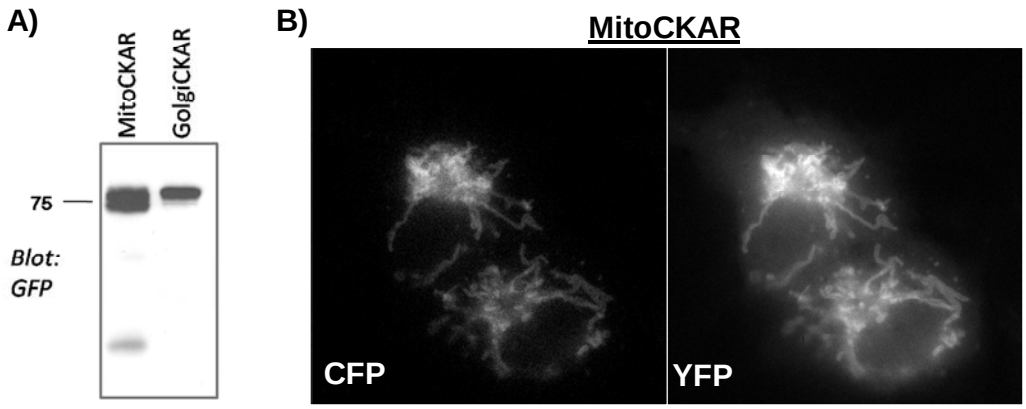

Figure A1.3. Partial cleavage of MitoCKAR. *A*, Lysates from COS 7 cells transfected with MitoCKAR (left lane) or GolgiCKAR (right lane) were analyzed by immunoblotting for GFP. For GolgiCKAR, a single band above 75 kDa is apparent, while MitoCKAR exists as two separate bands near 75 kDa and one faint band which migrates much faster. *B*, CFP fluorescence from MitoCKAR is targeted discretely to mitochondria (left panel), while YFP fluorescence from MitoCKAR is both targeted and diffuse (right panel). These results are consistent with partial cleavage of MitoCKAR, possibly within the N-terminus of CFP.

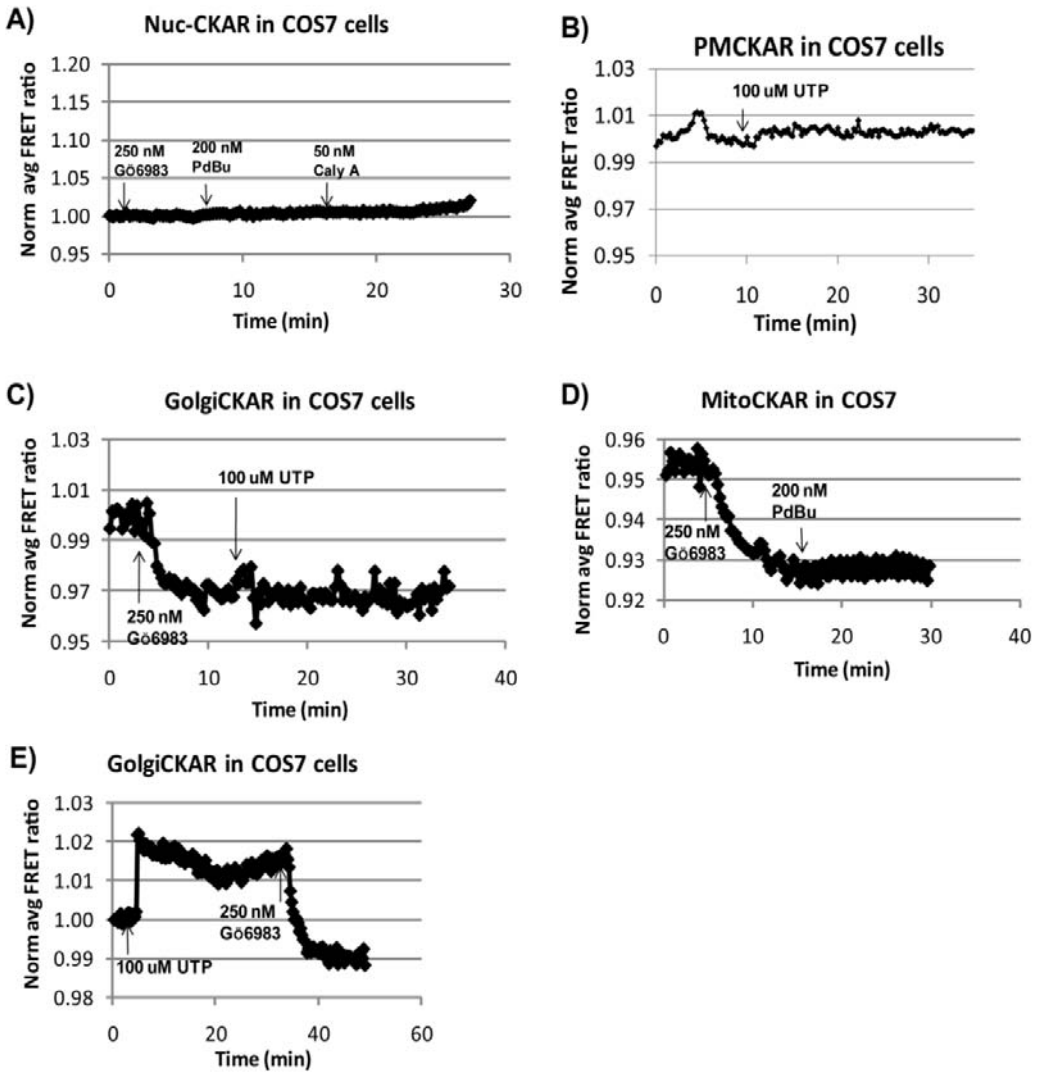

Figure A1.4. Validating specificity of targeted CKARs. *A*, COS7 cells transfected with NucCKAR were treated with Gö6983 (250 nM, 2.5 min) followed by PdBu (200 nM, 7.5 min) and Calyculin A (50 nM, 17.5 min). During 15 min of combined treatment with PdBu and Calyculin A, Gö6983 prevented phosphorylation of NucCKAR. *B*, COS7 cells transfected with PMCKAR were pre-treated with Gö6983 for 10 min, followed by stimulation with UTP (100 μM, 10 min). Pre-treatment with Gö6983 completely prevented PMCKAR phosphorylation in response to UTP. *C*, COS7 cells transfected with Golgi-CKAR were treated with Gö6983 (250 nM, 3 min), followed by UTP (100 μM, 13 min). Pre-treatment with Gö6983 completely prevented GolgiCKAR phosphorylation in response to UTP. *D*, COS7 cells transfected with Mito-CKAR were treated with Gö6983 (250 nM, 5 min), followed by PdBu (200 nM, 15 min). Pre-treatment with Gö6983 completely prevented GolgiCKAR phosphorylation in response to PdBu. *E*, COS7 cells transfected with Golgi-CKAR were treated with UTP (100 μM, 5 min), followed by Gö6983 (250 nM, 35 min). Gö6983 reversed GolgiCKAR phosphorylation in response to UTP.

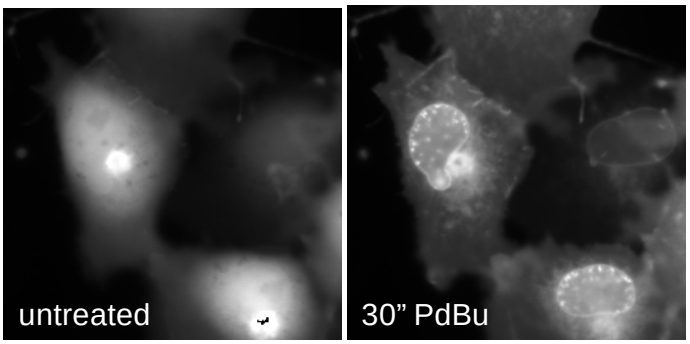

Figure A1.5. Kinetics of PdBu distribution into intracellular membranes. COS7 cells were transfected with the C1b domain from PKCβ tagged with YFP (C1b-YFP, left panel). C1b-YFP translocates to nuclear and other intracellular membranes within 30 seconds of treatment with PdBu (200 nM, right panel).

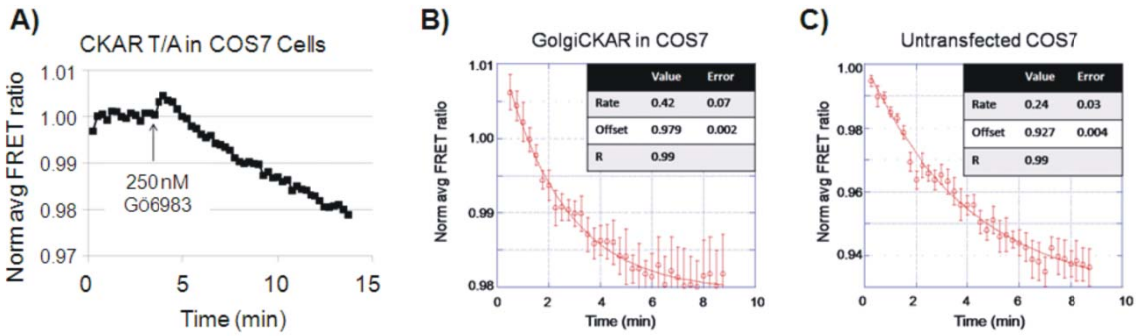

Figure A1.6. Gö6983 accumulation in intracellular membranes. *A*, A juxtanuclear region was selected from COS7 cells transfected with CKAR containing an Ala residue at the phospho-acceptor site (CKAR T/A) and the FRET ratio was monitored following treatment with Gö6983 (250 nM, 4.25 min). Even in these cells, in which CKAR cannot be phosphorylated, Gö6983 produces a gradual decrease in the FRET ratio over time. *B*, COS7 cells were transfected with GolgiCKAR and treated with Gö6983. The decrease in FRET ratio was plotted using kaleidograph, and the half-time for dephosphorylation was determined to be 1.7 ± 0.3 min. *C*, Untransfected COS7 cells were treated with Gö6983, and a juxtanuclear region was selected to determine the rate of the FRET ratio decrease attributed to bleed-through of Gö6983 into the FRET channel. The decrease in FRET ratio was plotted using kaleidograph, and the half time for accumulation of Gö6983 was determined to be 2.9 ± 0.4 min.

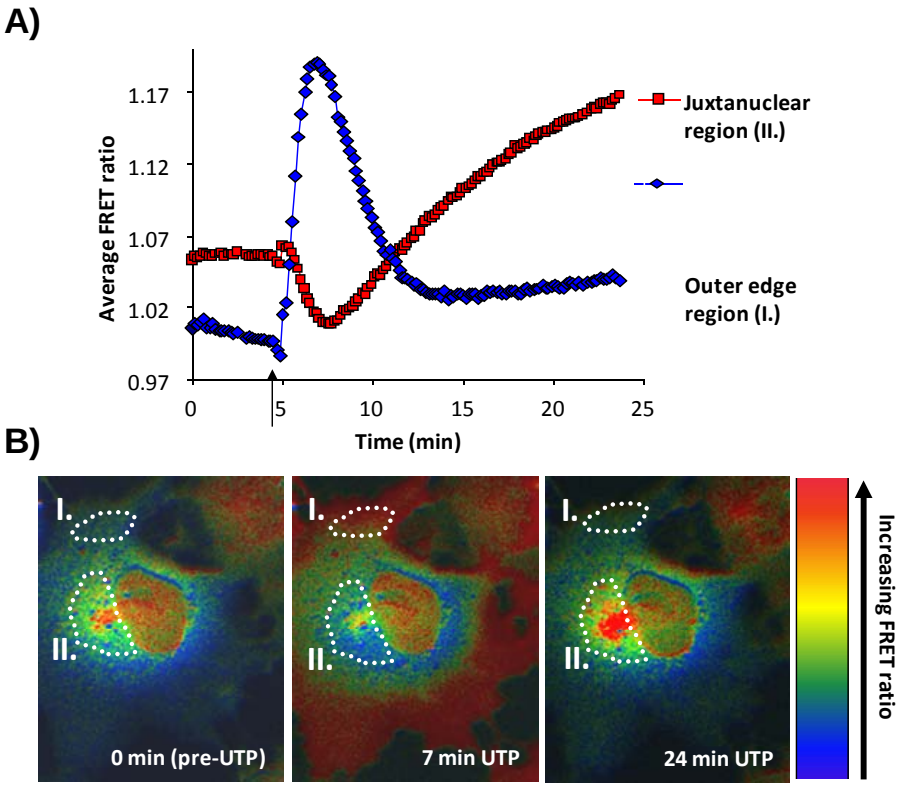

Figure A1.7. Untargeted DAGR reports differences in DAG production at peripheral membranes compared to juxtanuclear membranes. *A*, COS7 cells were transfected with DAGR and treated with UTP (100 μM, black arrow). FRET ratios averaged over an outer edge region (blue diamonds) or a juxtanuclear region (red squares) were monitored over time. The outer edge region responded within 5 min and decreased to near baseline within 10 min, while the juxtanuclear region responded more slowly, and was elevated after 20 min. *B*, Pseudocolored images of cells described in A, reflecting the FRET ratio and showing selected region I. (outer edge) and region II. (juxtanuclear).

Chapter 3

A Single Residue in the C1 Domain Sensitizes Novel Protein Kinase C Isoforms to Cellular Diacylglycerol Production[§]

Abstract

The C1 domain mediates the diacylglycerol (DAG*)-dependent translocation of conventional and novel protein kinase C (PKC) isoforms. In novel PKC isoforms (nPKCs), this domain binds membranes with sufficiently high affinity to recruit nPKCs to membranes in the absence of any other targeting mechanism. In conventional PKC (cPKC) isoforms, however, the affinity of the C1 domain for DAG is two orders of magnitude lower, necessitating the coordinated binding of the C1 domain and a Ca^{2+}-regulated C2 domain for translocation and activation. Here we identify a single residue that tunes the affinity of the C1b domain for DAG- (but not phorbol ester-) containing membranes. This residue is invariant as Tyr in the C1b domain of cPKCs and invariant as Trp in all other PKC C1 domains. Binding studies using model membranes, as well as live cell imaging studies of YFP-tagged C1 domains, reveal that Trp vs. Tyr toggles the C1 domain between a species with sufficiently high affinity to respond to agonist-produced DAG to one that is unable to respond to physiological levels of DAG. In addition, we show that while Tyr at this switch position causes cytosolic localization of the C1 domain under unstimulated conditions, Trp targets these domains to the Golgi, likely due to basal levels of DAG at this region. Thus, Trp vs. Tyr at this key position in the C1 domain controls both the membrane affinity and localization of PKC. The finding that a single residue controls the affinity of the C1 domain for DAG-containing membranes provides a molecular explanation for why 1) DAG alone is sufficient to activate nPKCs but not cPKCs and 2) nPKCs target to the Golgi.

Introduction

Protein kinase C (PKC) is a critical transducer of intracellular signaling pathways, with a variety of outputs, most notably tumor promotion (1,2). The hallmark of PKC activation is its translocation to membranes (3). This translocation is mediated through the ligand-dependent engagement of two membrane-targeting modules: the C1 (ligand: diacylglycerol, or DAG) and C2 (ligand: Ca^{2+}) domains. The regulatory domains vary within the PKC family, which is subdivided into three groups based on regulation. The conventional PKC isoforms (cPKCs: α, βI/II, γ) contain two tandem C1 domains and one conventional C2 domain; consequently, cPKCs are regulated both by DAG and Ca^{2+}. The novel isoforms (nPKCs: δ, θ, ε, and η) contain two tandem C1 domains and a non-Ca^{2+}/membrane binding novel C2 domain; consequently, nPKCs are regulated only by DAG. Atypical PKCs (aPKCs: ζ and ι) contain a single non-DAG binding ("atypical") C1 domain and no C2 domain; as a result, aPKCs are regulated by neither DAG nor Ca^{2+} (4).

The C1 domain is an ~8 kDa domain that binds DAG or the potent DAG-mimicking phorbol esters, such as *p*horbol-12-*m*yristate-13-*a*cetate (PMA) and *p*horbol *di**bu*tyrate (PDBu) (5). Structural studies have established that all C1 domains have a similar fold (6-11). An "unzipped" β sheet forms a groove lined by hydrophobic residues in which membrane-embedded diacylglycerol or phorbol esters bind (7). Membrane interaction is also facilitated by a ring of positive charges around the middle of the domain that potentially interacts with phosphatidylserine (PS) and other anionic lipids (12).

Nearly all C1 domains have been shown to bind PS (13), but their affinity for

ligand (DAG/phorbol esters) varies substantially (14). The C1 domain of nPKCs has an intrinsic affinity for DAG-containing membranes two-orders of magnitude higher than that of the C1 domain of cPKCs, allowing nPKCs to respond to agonists that trigger diacylglycerol production alone (15). In contrast, cPKCs must be pre-targeted to membranes by their C2 domain in response to an elevation of intracellular Ca^{2+} in order to respond to DAG (16). The molecular basis by which nPKC C1 domains bind to DAG membranes with two orders of magnitude higher affinity than those of cPKC C1 domains has not been elucidated.

In this report, we identify a single conserved residue at position 22 in the C1 domain that tunes its affinity for DAG-containing membranes. Our findings provide a molecular basis for why nPKCs respond to DAG alone, whereas cPKCs require the coordinated elevation of Ca^{2+}.

Materials and Methods

Materials—1-palmitoyl-2-oleoyl-*sn*-glycero-3-phosphocholine (POPC), 1-palmitoyl-2-oleoyl-*sn*-glycero-3-phosphoserine, 1-palmitoyl-2-oleoyl-*sn*-glycero-3-phosphoglycerol, and 1,2-*sn*-dioleoylglycerol in chloroform were purchased from Avanti Polar Lipids, Inc. Tritiated POPC was purchased from American Radiochemical Co. γ-^{32}P-ATP was purchased from PerkinElmer, Inc. PMA, PDBu, and BAPTA/AM were purchased from CalBiochem. Glutathione-Sepharose 4B and PreScission Protease were purchased from Amersham Biosciences. Electrophoresis reagents were from Bio-Rad Laboratories, Inc. Oligonucleotides used in PCR were purchased from GenBase, Inc. Restriction enzymes were from New England Biolabs, Inc. All other reagents and chemicals were reagent-grade.

Sequence Alignments—The sequences of the C1 domains of PKC isoforms were aligned using CLUSTALW from the LaserGene 6 software package (DNASTAR, Inc.). Sequences were taken from Ref. (13). The residues that contact ligand in the structure of C1bγ with phorbol were taken from the LIGPLOT file provided through the PDB repository (PDB ID: 1PTR).

Construction of plasmids and protein purification— For bacterial expression, C1bβ was cloned into pGEX-KG as described (17). C1bδ (Gln221 to Ala290) and C1bβ were subcloned into pGEX-6P3, in which the Tyr22Trp mutation was introduced. For mammalian expression, all constructs were cloned into pcDNA3. PM-CFP was cloned as described (MyrPalm-CFP, 18). YFP was fused to the 3' end of C1bβ (Pro93 to Gly152) and C1bδ (Phe225 to Gly281) to make C1bβ-YFP and C1bδ-YFP. These constructs were used to produce the mutants Tyr22Trp (C1bβ) and Trp22Tyr (C1bδ). YFP was fused to the 3' end of PKCβII or δ, and Tyr123Trp or Trp252Tyr mutations were introduced, respectively. Rat PKCβII and murine PKCδ isoforms were used in these studies. All mutations were made using QuikChange (Stratagene). Wild-type C1bβ was expressed in bacteria and purified as described previously (17). The C1bβII-Y123W and C1bδ domains were purified similarly (17), with the substitution of PreScission Protease for thrombin.

Sucrose-Loaded Vesicle Preparation and Binding Assay—Lipid vesicles were prepared and PMA was incorporated into these vesicles as described (15). The final concentration of lipid was determined by phosphate analysis as described (19). The binding of the C1b domain to sucrose-loaded large unilamellar vesicles was measured as described (20). To

normalize data between 0 and 100% bound, curves were fitted to the equation

$$\text{fraction bound} = (n*[L]^H)/([L]^H + K_d{}^H) + \text{int} \quad \text{(Eq. 1)}$$

where K_d is the apparent equilibrium constant, *[L]* is the lipid concentration, *H* is the Hill coefficient, *n* is the range of apparent % bound, and *int* is the *y*-intercept. Experiments were performed in triplicate. Measurements at each lipid concentration were averaged, and data were fitted to one master standard error of the mean (SEM)-weighted plot of the form

$$\text{fraction bound} = [L]^H/([L]^H + K_d{}^H) \quad \text{(Eq. 2)}$$

where the terms represent the same parameters as in *Eq. 1*. All curve fitting was done using Kaleidagraph v5.32.

Cell Culture—COS7 cells were plated in Dulbecco's modified Eagle's medium (Cellgro) containing 10% fetal bovine serum and 1% penicillin/streptomycin at 37 °C in 5% CO_2. Cells were plated in 35-mm imaging dishes at 60% confluency and transfected using FuGENE 6 (Roche Diagnostics). Cells were cotransfected with PM-CFP and C1b-YFP constructs for translocation studies. For localization experiments, the YFP-tagged constructs were transfected alone. Cells were allowed to grow for 12-24 h post-transfection before imaging. For kinase activity assays, cells were transfected with full-length YFP-tagged constructs (to monitor expression) and allowed to grow for 48 h post-transfection before harvesting.

Cell imaging—Cells were imaged as previously described (18,21). Because of cell-to-cell variability in CFP and YFP expression, the dynamic range varied from cell to cell. However, treatment with phorbol esters caused maximal membrane binding of each domain (Figure 3.1C and Ref. (22)). Therefore, the responses to DAG generation via

UTP were calibrated to the dynamic range of the cell by dividing each point by the maximal response elicited by PDBu. Thus, the data are presented in relative translocation units.

Kinase assay—Lysates from untransfected COS7 cells or COS7 cells transfected with PKCβII, PKCβII-Y123W or PKCδ were assayed for PKC activity by monitoring phosphorylation of a synthetic peptide as described (23). Non-activating conditions contained 20 mM HEPES (pH 7.5) and 2 mM EGTA. Activating conditions contained 140 μM PS, 3.8 μM DAG, and either 2 mM $CaCl_2$ (total PKC activity) or 2 mM EGTA (Ca^{2+}-independent PKC activity).

Molecular modeling—The structure of the C1 domain was visualized and manipulated using Swiss-PdbViewer, v3.7. Coordinates for C1-Raf (1FAR), C1b-PKCγ (1TBN) and C1b-PKCδ (1PTQ) were taken from the PDB repository (PDB IDs in parentheses). The C1 domain of human PKCζ was modeled on the C1 domains of DGKδ (1R79), Ksr (1KBE), β2-chimaerin (1XA6), munc-13 (1Y8F), PKCδ, PKCγ, and Raf, using Swiss-PdbViewer (24-26).

Results and Discussion

The C1 domains of nPKCs bind DAG-containing membranes with two orders of magnitude higher affinity than those of cPKCs (15). Alignment of the sequences of the C1 domains of cPKCs and nPKCs revealed that the residue at position 22 is invariant as Trp in all C1 domains except the C1b domains of cPKCs, where it is invariant as Tyr (Figure 1A). This residue lies along one of the two loops that bind ligand and is on a surface that interacts with the membrane (12), suggesting that this is a likely candidate to modulate ligand-dependent membrane affinity.

To test the hypothesis that position 22 controls the affinity of the C1b domain for lipid membranes, we first mutated Tyr22 to Trp in the C1b domain of the cPKC βI/II (C1bβ-Y22W) and measured the binding of the bacterially-purified wild-type and mutant domains to lipid vesicles containing 30 mol% PS and 5 mol% DAG (Fig. 1B, *filled symbols*). Wild-type C1bβ (C1bβ-WT) bound to vesicles containing 5 mol% DAG with a K_d of 780 ± 50 μM (*filled diamonds*). On the other hand, the mutant C1bβ-Y22W bound with 31-fold higher affinity to vesicles of the same composition (K_d = 24 ± 1 μM, *filled squares*). Binding was dependent on the presence of DAG, as the domain did not bind to 500 μM lipid vesicles containing 30 mol% PS and 0 mol% DAG (data not shown). We next measured the binding of these two domains to vesicles containing 30 mol% PS and 1 mol% PMA (Fig. 1B, *open symbols*). C1bβ-WT and -Y22W bound with the same affinity to vesicles containing 1 mol% PMA (K_d's of 35 ± 3 and 35 ± 2 μM, *open diamonds and squares*, respectively). These data reveal that mutation of Tyr22 to Trp in the C1 domain of PKCβ converts the domain from a low-affinity to a high-affinity DAG binding module.

We next tested whether the isolated C1b domain of the nPKC δ (C1bδ, which has a Trp at position 22, also has higher intrinsic affinity for DAG-containing membranes than C1bβ. We used a GST-tagged construct for C1bδ, as removal of the GST tag greatly reduced the stability of the protein. GST-C1bδ bound to vesicles containing 5 mol% DAG and 1 mol% PMA with K_d's of 35 ± 3 and 56 ± 6 μM, respectively (Fig. 1B, *triangles*). Low, but pure, amounts of untagged C1bδ showed that the GST tag had no effect on the affinity of the C1bδ for DAG- or PMA-containing membranes (data not

shown). Moreover, while C1bβ-WT showed a 110-fold preference for PMA over DAG on an equimolar basis (Fig. 1B, *open vs. closed diamonds*), C1bβ-Y22W and GST-C1bδ showed modest 3.6- and 3.1-fold selectivities for PMA over DAG, respectively (Fig. 1B, *open vs. closed squares* for C1bβ-Y22W and *triangles* for GST-C1bδ).

We previously observed that the C1 domain exhibits selectivity amongst anionic lipids only in the presence of DAG, with preference for PS over phosphatidylglycerol (PG) (17,27). Since residue 22 is important for sensitizing the C1b domain to DAG, this position should also allow the domain to discriminate between PS and PG. Consistent with this observation, measurement of the affinities of the C1bβ-WT, C1bβ-Y22W and GST-C1bδ domains for membranes containing 30 mol% PS or PG and 5 mol% DG or PMA revealed that wild-type C1bβ showed 2-fold selectivity for PS over PG, regardless of whether the ligand was DAG or PMA. Trp-containing C1 domains, however, showed selectivity for PS only in the context of DAG membranes (5- and 20-fold selectivity for C1bβ-Y22W and GST-C1bδ, respectively) but showed no or 3-fold selectivity for PS for C1bβ-Y22W and GST-C1bδ, respectively, in the context of PMA-containing membranes (data not shown). Taken together, these data reveal that Trp at position 22 increases the affinity of C1bβ for DAG-containing membranes, reduces selectivity between PMA and DAG, and increases DAG-dependent PS selectivity.

To monitor the real-time membrane translocation of isolated C1b domains in live cells, we fused YFP to the C-terminus of C1bβ and C1bδ. We also generated YFP fusion constructs for these two C1b domains containing point mutations reversing the identity of residue 22: C1bβ-Y22W and C1bδ-W22Y. We co-transfected COS7 cells with CFP that

had been targeted to the plasma membrane (PM-CFP) and the indicated YFP-tagged C1b construct; translocation to the plasma membrane was monitored as an increase in the ratio of FRET-based YFP emission: CFP emission (FRET ratio) (21).

UTP, acting through endogenous P2Y receptors, stimulates the production of DAG at the plasma membrane via phospholipase C-mediated lipid hydrolysis (28). Figure 3.1C shows that stimulation of COS7 cells with UTP (100 μM) resulted in an increase in FRET ratio, which was further increased to maximal translocation following addition of PDBu (200 nM). Upon stimulation of COS7 cells with UTP, C1bβ did not significantly translocate to membranes (Figure 3.1C, *blue diamonds*). In contrast, UTP stimulation caused robust translocation of C1bδ (Figure 3.1C, *green triangles*). Consistent with *in vitro* binding data (Figure 3.1B), C1bβ-Y22W responded to UTP (Figure 3.1C, *red squares*), resulting in a 10-fold increase in DAG binding at the plasma membrane relative to C1bβ-WT (Figure 3.1C, *blue diamonds*). Conversely, mutating Trp22 to Tyr in C1bδ (C1bδ-W22Y) reduced the translocation in response to UTP 10-fold relative to C1bδ without altering the maximal translocation driven by PdBu (Figure 3.1C, *yellow circles*). These data reveal that Trp vs. Tyr at position 22 in the C1b domain renders the domain responsive to DAG generated by receptor-mediated phospholipid hydrolysis.

In order to determine whether binding differences arising from changes in the C1b domain affected the cofactor dependence of the full-length kinase, we generated a full-length PKCβII construct in which Tyr123 (position 22 of the C1b domain) was mutated to Trp (PKCβII-Y123W). We transfected COS7 cells with either this mutant construct,

wild-type PKCβII, or PKCδ and assayed kinase activity from the detergent-soluble lysates compared to untransfected control cells. We assayed PKC activity in the presence of PS, DAG, and either Ca^{2+} (for total PKC activity) or EGTA (for Ca^{2+}-independent activity), and Ca^{2+}-independent activity was calculated as a percent of total PKC activity. Figure 3.1D shows the Ca^{2+}-independent activity of PKCβII, PKCβII-Y123W, and PKCδ. Consistent with the standard model where Ca^{2+}, DAG, and PS are required for full activation of cPKCs (29,30), PKCβII had minimal (6%) activity in the absence of Ca^{2+}. In contrast, PKCδ was activated to near maximal levels in the absence of Ca^{2+}, consistent with the Ca^{2+} independence of novel PKC isoforms (29,30). Strikingly, the single point mutation of Y123W in PKCβII was sufficient to confer significant Ca^{2+}-independent activity (28% of maximal activity). These results are consistent with the tighter membrane affinity conferred by Trp vs. Tyr in the C1b domain, which results in reduced dependence on the C2 domain (and hence Ca^{2+}) for activation, and is consistent with our previous studies which showed that activation of PKC depends upon the affinity by which PKC binds to membranes (17). This provides a molecular explanation for why novel PKC isoforms are able to respond to DAG alone, while conventional PKC isoforms require pre-targeting by Ca^{2+} via their C2 domains for translocation and activation (15,16).

Translocation of different PKC isoforms to discrete subcellular regions is an important mechanism for achieving specificity in PKC signaling. While the typical site of signaling for cPKCs is the plasma membrane (31), localization at endomembranes – particularly the Golgi – has been shown to be critical for PKCδ activity (32). We

observed striking differences in the localization of the isolated, YFP-tagged C1bβ and C1bδ: C1bβ was localized diffusely throughout the cell (Fig. 2A, upper left panel), while C1bδ was concentrated at a juxtanuclear region resembling Golgi membranes (Fig. 2A, lower left panel). Localization at the Golgi was confirmed by treatment with brefeldin A, which abolished the juxtanuclear concentration of C1bδ (data not shown). Moreover, the reversion mutants C1bβ-Y22W and C1bδ-W22Y showed a complete reversal of the subcellular localization of their wild-type counterparts (Fig. 2A, right panels). A previous study reported constitutive Golgi localization of the C1b domain of the nPKCθ in unstimulated cells; this localization was redistributed to the cytosol upon inhibition of phospholipase C or phosphatidic acid phosphatase (35). Thus, the targeting effects of position 22 are likely due to DAG-dependent membrane binding.

Next, we tested whether having a Tyr or Trp at position 22 also affected the localization of either full-length PKCβII or PKCδ. PKCδ pre-localized to juxtanuclear membranes, while PKCβII was basally cytosolic (Fig. 2B, left panels). Consistent with data from the isolated C1b domains, basal Golgi localization of the full-length PKCδ was greatly diminished upon mutation of Trp252 (position 22 of the C1b domain) to Tyr (Fig. 2B, lower right panel). However, mutation of Tyr123 to Trp in PKCβII did not cause any change in its localization, as PKCβII remained cytosolic (Fig. 2B, upper panels). Thus, merely increasing the C1b domain's affinity for DAG is not sufficient to determine the subcellular distribution of PKC. This suggests that other determinants control cPKC localization. For example, the Ca^{2+}-binding C2 domain of cPKCs – a feature absent from nPKCs – may override targeting to the Golgi (33,34). Thus, in addition to affecting PKC

function by regulating activation in response to DAG, position 22 of the C1b domain may also regulate DAG-dependent pre-localization of novel PKC isoforms. Taken together, these data suggest a model of activation in which low DAG levels allow pre-targeting of PKCδ to the Golgi through the C1b domain, while an additional agonist-stimulated increase in DAG shifts the equilibrium to full binding and full activation.

To gain insight into how Trp vs. Tyr at position 22 controls the affinity of the C1 domain for DAG-containing membranes, we compared the backbone structures and molecular surfaces of several C1 domains (Figure 3.3). We chose representatives of three C1 groups for modeling studies: those that bind DAG membranes with relatively high affinity (C1bδ), those that bind DAG membranes with relatively low affinity (C1bγ - a surrogate for C1bβ, with which C1bγ shares 80% identity and 92% similarity), and those that do not bind DAG (C1ζ). As shown in Figure 3.3, comparison of the C1b domains of PKCγ, δ, and ζ reveals large movements within the β3/4 loop (upper left panel). The β1/2 and β3/4 loops form the phorbol/DAG-binding pocket and contain the ligand- and membrane-binding determinants (7,13). Residue 22 lies at the apex of this highly mobile β3/4 loop, in keeping with its role as a critical regulator for the C1 domain's ability to bind DAG.

Numerous elegant studies delineating the residues in the C1 domain involved in ligand binding have identified residue 22 as participating in DAG-dependent membrane binding (8,14,36,37); yet the mechanism by which this position controls binding to membranes has not been clear. Our modeling studies suggest that position 22 may regulate the size of the ligand-binding pocket (Figure 3.3). The phenol ring of Tyr22 in

C1bγ lies in a very different orientation relative to the membrane compared to the indole ring of Trp22 in C1bδ. Moreover, these two amino acids are known to be positioned very differently at the water/lipid bilayer interface (38,39), suggesting that mobility in the β3/4 loop may dictate the width and depth of the ligand-binding pocket. Indeed, several studies have shown flexibility within this loop, whereas the rest of the structure tends to remain static (7,8,40). The presence of two highly conserved Gly residues within the β3/4 loop (Gly23 and 28) suggests that such flexibility is not only possible, but may also be required for function. Particularly relevant to our study, the ligand-binding cavity in C1bδ is narrow and deep, while that of the non-DAG responsive C1bγ is wide and shallow. Thus, whereas the smaller DAG can bind well to C1bδ, only the larger phorbol esters can make hydrophobic contacts across the wide gorge of C1bγ.

Curiously, the C1 domain of PKCζ has Trp at position 22, yet it still does not bind DAG. Rather, C1ζ appears to lose the ability to bind DAG by sterically and electrostatically occluding the ligand-binding pocket through substitution of hydrophobic residues (*grey*) for large basic amino acids (*blue*) (Figure 3.3). Consistent with this, Blumberg and coworkers have recently shown that mutation of Asn7, Ser10, Pro11, and Leu20 in the β1/2 and β3/4 loops to arginine in C1bδ results in almost complete loss of binding to phorbol ester-containing membranes, while the reverse mutations in C1ζ confer phorbol ester responsiveness (41).

Conclusion

In this study, we identify Trp vs. Tyr at residue 22 of the C1b domain as a molecular switch that controls whether PKC isoforms can respond to DAG alone, or

whether the coordinated binding of a second membrane-targeting module (i.e., the C2 domain of cPKCs) is required to confer responsiveness to agonist stimulation. Our findings provide a molecular basis for why nPKCs respond to DAG alone, whereas cPKCs require the coordinated elevation of Ca^{2+}. This cautions against drawing physiological conclusions when substituting phorbol esters for DAG in the context of cellular signaling, an idea that has also been suggested by other groups (36). Taken further, our results also suggest that therapeutic compounds designed to target the C1 domain of a specific isoform should more closely resemble DAG than phorbol, an approach taken by Blumberg and coworkers (42).

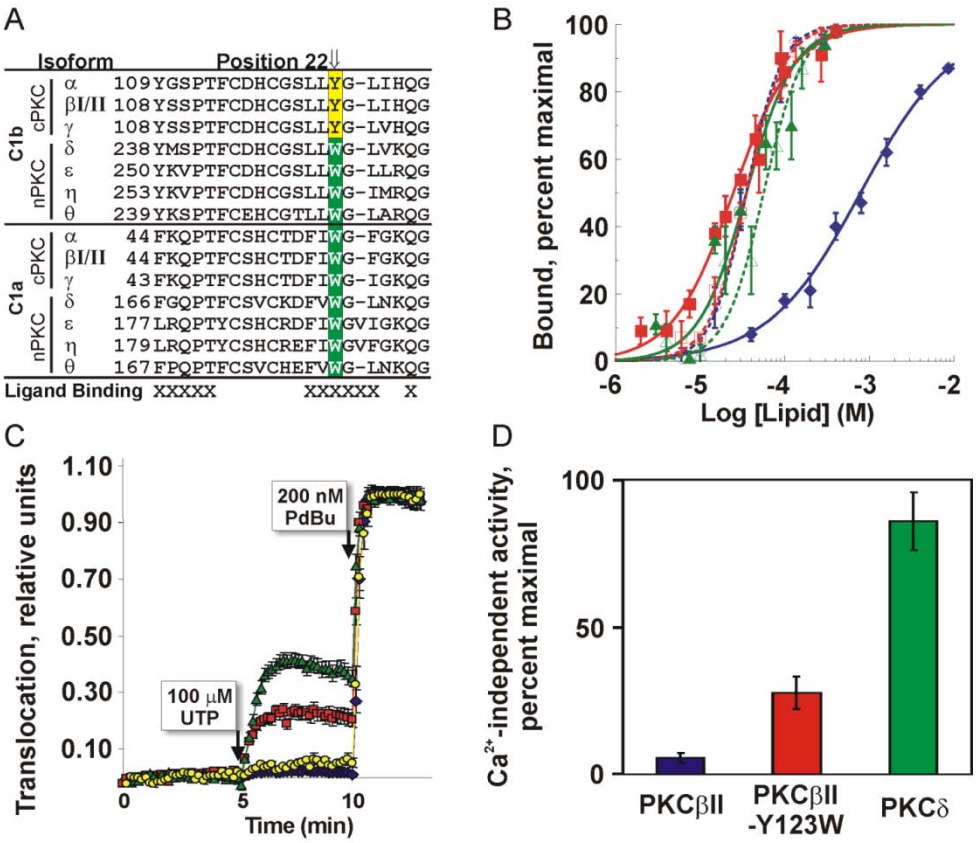

Figure 3.1. Residue 22 tunes binding of the C1b domain to DAG membranes *in vitro* and *in vivo* and affects kinase activity. *A*, Sequence alignment of the C1 domains of cPKC and nPKC isoforms. Position 22 is boxed in *yellow* for Tyr and *green* for Trp. Residues that contact phorbol and/or form the hydrophobic wall of the groove in which DAG or phorbol binds are marked below with an "*X*". *B*, Binding of C1bβ-WT (*blue diamonds*) and -Y22W (*red squares*) and GST-C1bδ (*green triangles*) to lipid vesicles containing 30mol% PS and either 5mol% DAG (*filled symbols*) or 1mol% PMA (*open symbols*). Each data point represents the mean of triplicate experiments ± SEM. *C*, *In vivo* translocation of C1b domains to membranes. COS7 cells were co-transfected with PM-CFP and the indicated YFP-tagged C1b domain constructs: C1bβ (*blue diamonds*), C1bβ-Y22W (*red squares*), C1bδ (*green triangles*), and C1bδ-W22Y (*yellow circles*). The relative translocation in response to UTP (100 μM) and PDBu (200 nM) treatment was calculated and plotted as a function of time. Data represent the average ± SEM of 10-15 cells from three independent experiments. *D*, Lysates from COS7 cells transfected with PKCβII, PKCβII-Y123W, or PKCδ were assayed for PKC activity in the presence of PS, DAG, and either Ca^{2+} (total PKC activity) or EGTA (calcium-independent PKC activity). Ca^{2+}-independent PKC activity was calculated as a percent of total activity; total activity was comparable for both PKCβII constructs and typically slightly lower for the PKCδ construct. These data represent the relative activity of the over-expressed kinases in response to lipid cofactors in the absence of Ca^{2+}. Data represent the average ± S.D. from three experiments.

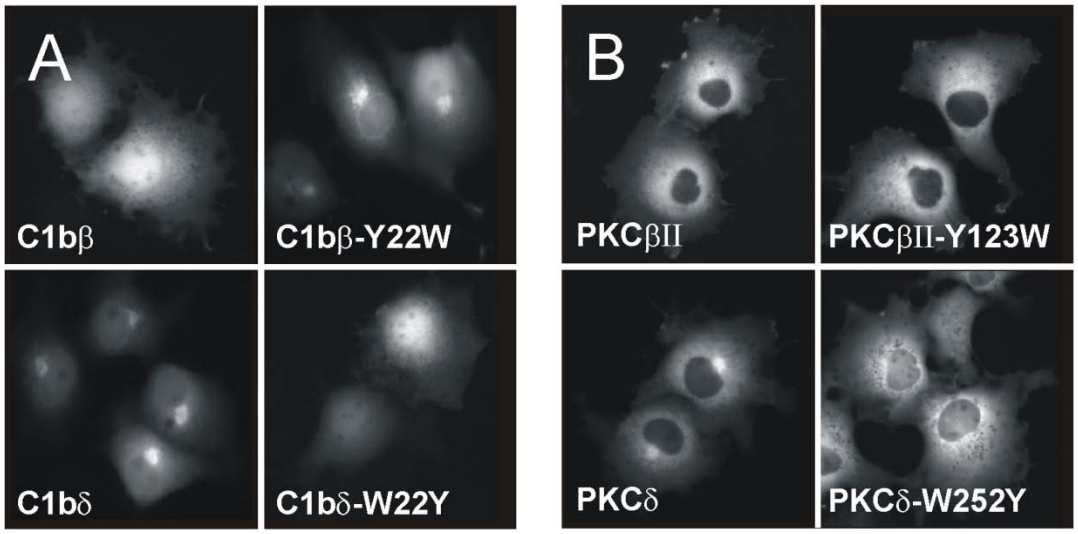

Figure 3.2. Residue 22 affects localization of the C1b domain (*A*) and full-length PKC (*B*). *A*, Representative images of COS7 cells transfected with YFP-tagged C1b domains: C1bβ (top left), C1bβ-Y22W (top right), C1bδ (lower left), and C1bδ-W22Y (lower right). *B*, Representative images of COS7 cells transfected with YFP-tagged full-length PKC: PKCβII (top left), PKCβII-Y123W (top right), PKCδ (lower left), and PKCδ-W252Y (lower right). Mutated residues correspond to position 22 of the C1b domain in the full-length protein. Data are representative of at least three independent experiments.

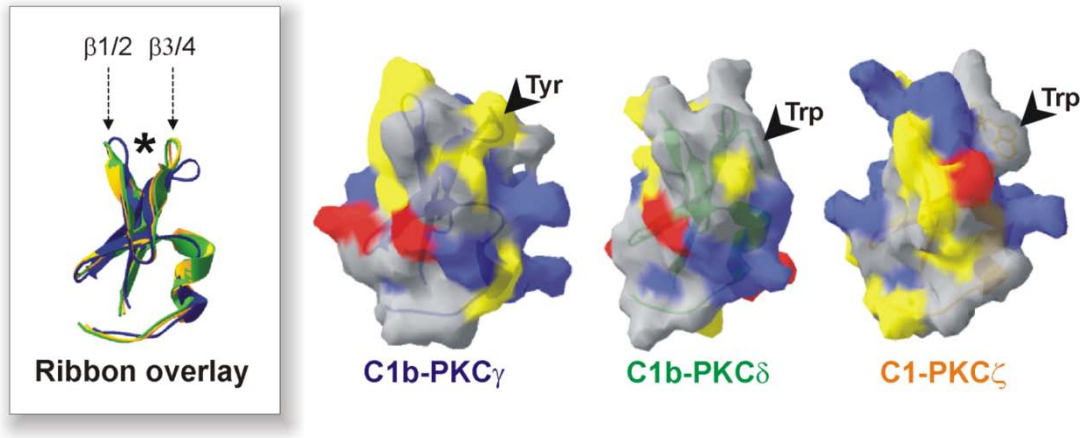

Figure 3.3. The C1 domain's ability to bind DAG arises from modulation of the width and surface properties of the loops surrounding the hydrophobic DAG-binding cleft. Shown are a ribbon diagram overlay and molecular surfaces of C1b-PKCδ (*green*), C1b-PKCγ (*blue*), and C1-PKCζ (*orange*). Phorbol binds between the two loops at the top of the domain as indicated with an asterisk (*). The identity of residue 22 is marked with an arrowhead. Surface coloring scheme is as follows: basic – *blue*; acidic – *red*; polar – *yellow*; nonpolar – *grey*.

Table 3.1. Binding constants (K_d) for the interaction of the C1b domain with membranes. K_d values were calculated from binding curves as described in Materials & Methods. Data shown here are for lipid vesicles consisting of 5 mol% DAG or PMA and 30 mol% PS or PG. K_d (in μM) is represented as the average of three experiments ± *SEM*. Errors for the ratio of PG:PS were propagated from the errors associated with the tabulated K_d values.

	K_d (μM)					
	C1bβ		C1bβ-Y22W		C1bδ	
Ligand:	DAG	PMA	DAG	PMA	DAG	PMA
PS	780 ± 50	11.5 ± 0.5	24 ± 1	5.3 ± 0.5	35 ± 3	8.5 ± 0.6
PG	1690 ± 60	22 ± 1	130 ± 10	6.0 ± 0.9	700 ± 200	25 ± 3
PG:PS	2.2 ± 0.2	1.9 ± 0.1	5.4 ± 0.5	1.1 ± 0.2	20 ± 6	2.9 ± 0.4

References

1. Koivunen, J., Aaltonen, V., and Peltonen, J. (2005) *Cancer Lett*

2. Mellor, H., and Parker, P. J. (1998) *Biochem J* **332 (Pt 2)**, 281-292

3. Nishizuka, Y. (1995) *Faseb J* **9**, 484-496

4. Newton, A. C. (2001) *Chem Rev* **101**, 2353-2364

5. Colon-Gonzalez, F., and Kazanietz, M. G. (2006) *Biochim Biophys Acta*

6. Zhou, M., Horita, D. A., Waugh, D. S., Byrd, R. A., and Morrison, D. K. (2002) *J Mol Biol* **315**, 435-446

7. Zhang, G., Kazanietz, M. G., Blumberg, P. M., and Hurley, J. H. (1995) *Cell* **81**, 917-924

8. Xu, R. X., Pawelczyk, T., Xia, T. H., and Brown, S. C. (1997) *Biochemistry* **36**, 10709-10717

9. Mott, H. R., Carpenter, J. W., Zhong, S., Ghosh, S., Bell, R. M., and Campbell, S. L. (1996) *Proc Natl Acad Sci U S A* **93**, 8312-8317

10. Canagarajah, B., Leskow, F. C., Ho, J. Y., Mischak, H., Saidi, L. F., Kazanietz, M. G., and Hurley, J. H. (2004) *Cell* **119**, 407-418

11. Shen, N., Guryev, O., and Rizo, J. (2005) *Biochemistry* **44**, 1089-1096

12. Hurley, J. H., and Meyer, T. (2001) *Curr Opin Cell Biol* **13**, 146-152

13. Hurley, J. H., Newton, A. C., Parker, P. J., Blumberg, P. M., and Nishizuka, Y. (1997) *Protein Sci* **6**, 477-480

14. Stahelin, R. V., Digman, M. A., Medkova, M., Ananthanarayanan, B., Rafter, J. D., Melowic, H. R., and Cho, W. (2004) *J Biol Chem* **279**, 29501-29512

15. Giorgione, J. R., Lin, J. H., McCammon, J. A., and Newton, A. C. (2006) *J Biol Chem* **281**, 1660-1669

16. Nalefski, E. A., and Newton, A. C. (2001) *Biochemistry* **40**, 13216-13229

17. Johnson, J. E., Giorgione, J., and Newton, A. C. (2000) *Biochemistry* **39**, 11360-11369

18. Violin, J. D., Zhang, J., Tsien, R. Y., and Newton, A. C. (2003) *J Cell Biol* **161**, 899-909

19. Bartlett, G. R. (1959) *J Biol Chem* **234**, 466-468

20. Mosior, M., and Newton, A. C. (1995) *J Biol Chem* **270**, 25526-25533

21. Gallegos, L. L., Kunkel, M. T., and Newton, A. C. (2006) *J Biol Chem*

22. Takuwa, N., Fukui, Y., and Takuwa, Y. (1999) *Mol Cell Biol* **19**, 1346-1358

23. Edwards, A. S., Faux, M. C., Scott, J. D., and Newton, A. C. (1999) *J Biol Chem* **274**, 6461-6468

24. Peitsch, M. (1995) *Bio/Technology* **13**, 658-660

25. Schwede, T., Kopp, J., Guex, N., and Peitsch, M. C. (2003) *Nucleic Acids Res* **31**, 3381-3385

26. Guex, N., and Peitsch, M. C. (1997) *Electrophoresis* **18**, 2714-2723

27. Newton, A. C., and Keranen, L. M. (1994) *Biochemistry* **33**, 6651-6658

28. Insel, P. A., Ostrom, R. S., Zambon, A. C., Hughes, R. J., Balboa, M. A., Shehnaz, D., Gregorian, C., Torres, B., Firestein, B. L., Xing, M., and Post, S. R. (2001) *Clin Exp Pharmacol Physiol* **28**, 351-354

29. Newton, A. C. (2003) *Biochem J* **370**, 361-371

30. Adams, R. A., Liu, X., Williams, D. S., and Newton, A. C. (2003) *Biochem J* **374**, 537-543

31. Saito, N. (2003) *Methods Mol Biol* **233**, 93-103

32. Brodie, C., and Blumberg, P. M. (2003) *Apoptosis* **8**, 19-27

33. Rodriguez-Alfaro, J. A., Gomez-Fernandez, J. C., and Corbalan-Garcia, S. (2004) *J Mol Biol* **335**, 1117-1129

34. Feng, X., Becker, K. P., Stribling, S. D., Peters, K. G., and Hannun, Y. A. (2000) *J Biol Chem* **275**, 17024-17034

35. Carrasco, S., and Merida, I. (2004) *Mol Biol Cell* **15**, 2932-2942

36. Ananthanarayanan, B., Stahelin, R. V., Digman, M. A., and Cho, W. (2003) *J Biol Chem* **278**, 46886-46894

37. Wang, Q. J., Fang, T. W., Nacro, K., Marquez, V. E., Wang, S., and Blumberg, P. M. (2001) *J Biol Chem* **276**, 19580-19587

38. Killian, J. A., and von Heijne, G. (2000) *Trends Biochem Sci* **25**, 429-434

39. Khandwala, A. S., and Kasper, C. B. (1971) *Biochim Biophys Acta* **233**, 348-357

40. Pak, Y., Enyedy, I. J., Varady, J., Kung, J. W., Lorenzo, P. S., Blumberg, P. M., and Wang, S. (2001) *J Med Chem* **44**, 1690-1701

41. Pu, Y., Peach, M. L., Garfield, S. H., Wincovitch, S., Marquez, V. E., and Blumberg, P. M. (2006) *J Biol Chem* **In Press**

42. Marquez, V. E., and Blumberg, P. M. (2003) *Acc Chem Res* **36**, 434-443

Footnotes

[§]This work was supported by NIH GM-43154, 2T32 GM-07752, and 2T32 GM-08326.

[*]The abbreviations used are as follows: CFP, cyan fluorescent protein; cPKCs, conventional PKCs; DAG, diacylglycerol; nPKCs, novel PKCs; PdBu, phorbol-12,13-dibutyrate; PKC, protein kinase C; PMA, phorbol-12-myristate-13-acetate; PM-CFP, plasma membrane-targeted CFP; PG, phosphatidylglycerol; PS, phosphatidylserine; YFP, yellow fluorescent protein.

This Chapter is, in full, a reprint of the material as it appears in The Journal of Biological Chemistry, 2007, Dries DR, Gallegos LL, and Newton AC. I was co-primary researcher and author; coauthors performed specific experiments and helped direct and supervise the research included in this chapter.

APPENDIX 2

This Appendix contains data explaining the rationale for adjusting the FRET responses from C1b translocation studies to account for differences in relative CFP and YFP expression. Also, to satisfy space restrictions for publication, validation of Golgi localization of the C1b domains was not shown in the preceding chapter; it is shown here. This Appendix also contains data showing that increasing the affinity of PKCβII for DAG-containing membranes does not affect activity in the presence of Ca^{2+}.

FRET ratios from C1b domain translocation in individual cells

In many FRET reporters, the FRET donor (CFP) and FRET acceptor (YFP) are encoded in the same polypeptide. Because of this, the FRET ratio changes (i.e. "responses") will have a consistent range, even when the reporter is expressed to different levels in cells. Because C1b domains tagged with YFP are encoded on a different polypeptide than the plasma membrane-tethered CFP, each individual cell will have a different capacity to respond, and thus, a different range of responses. In fact, the range can be made larger by expressing more acceptor than donor. So, while it is always possible to tell whether there is a response, and the rate of the response, quantifying the magnitude of the FRET change is a challenge when CFP and YFP are encoded on different polypeptides. However, in this instance, *in vitro* measurements determined that all of the C1b domains in this study bind with equal affinity to phorbol esters, even though they show differences in the ability to bind membranes in the presence of DAG. Furthermore, we noticed that translocation of the C1b domains in response to DAG

production and phorbol ester treatment was proportional (Fig A2.1A), with cells having a higher-in-magnitude response to DAG also showing a higher response to phorbol. We reasoned we could range-adjust responses from individual cells by assuming that the initial FRET was close to zero and the maximal FRET possible for an individual cell was the value reached after stimulation with phorbol esters. When this range adjustment is done, the responses to receptor-mediated DAG are strikingly consistent from cell to cell (Fig A2.1B).

Validation of Golgi localization of the C1b domain

Although other studies have determined that the C1b domain from novel PKCθ localizes to the Golgi in a DAG-dependent manner, we wanted to ensure that, in COS7 cells, the juxtanuclear concentration of the high-affinity DAG-binding C1b domains was truly Golgi. Figure A2.2 shows YFP-C1bβ (Y22W) before and after treatment for 30 min with 2.5 μg/ml Brefeldin A, a compound which disrupts Golgi membranes. This compound completely disperses the juxtanuclear concentration of C1b domain, verifying that this is, in fact, Golgi.

Total PKC activity is equivalent for PKCβII and PKCβII-Y123W

In an *in vitro* kinase activity assay, we sought to determine whether increasing the affinity of full-length PKCβII for DAG-containing membranes restored activity in the absence of Ca^{2+}. In Figure A2.3, we show that the raw counts for PKCβII and PKCβII (Y123W) are equivalent in the presence of Ca^{2+} and DAG, and that the difference in

activity is only found in the absence of Ca^{2+}. Thus, increasing the affinity for DAG in the presence of Ca^{2+} does not result in hyper-activation of the kinase.

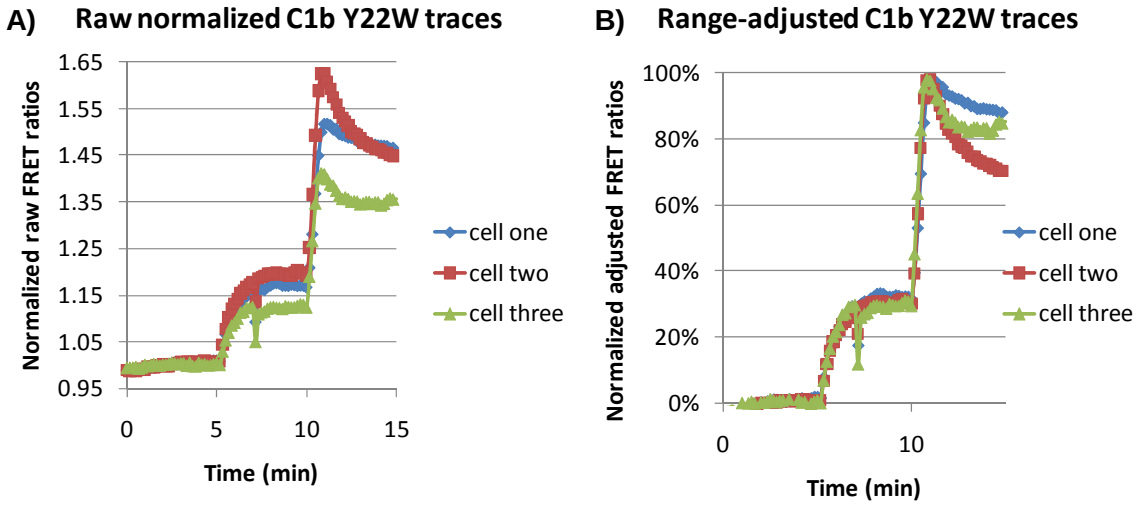

Figure A2.1. FRET ratios reflecting C1b translocation can be adjusted to accurately account for differences in the ranges of individual cells. *A*, COS7 cells transfected with PM-CFP and YFP-C1b (Y22W) were treated with UTP (100 μM, 5 min) followed by PdBu (200 nM, 10 min). Raw FRET ratios from individual cells were normalized by dividing each data point by the initial FRET ratio. *B*, Traces from A, adjusted for the range of the individual cell. This is done by subtracting the initial FRET ratio (1, for normalized traces) and dividing each trace by the maximal response to PdBu.

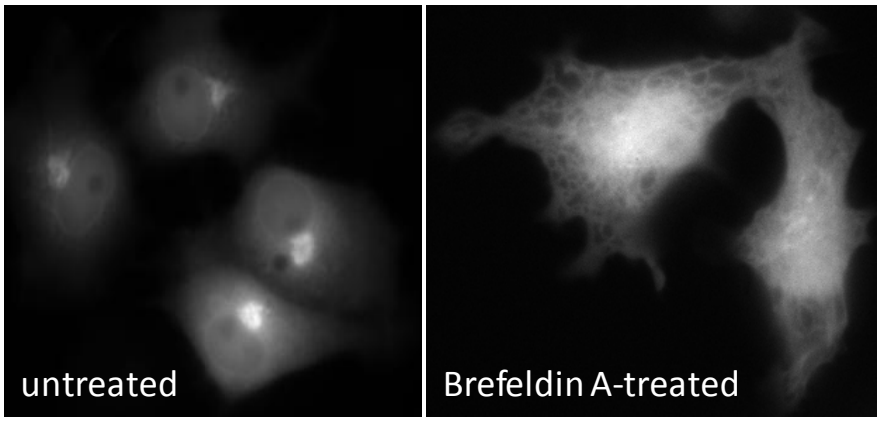

Figure A2.2. Brefeldin A treatment disperses Golgi-localized C1b domains. COS7 cells transfected with C1bβ (Y22W)-YFP (left panel) localizes to juxtanuclear membranes, resembling Golgi. When these cells are treated for 30 min with 2.5 μg/ml Brefeldin A (right panel), C1bβ (Y22W)-YFP is dramatically dispersed.

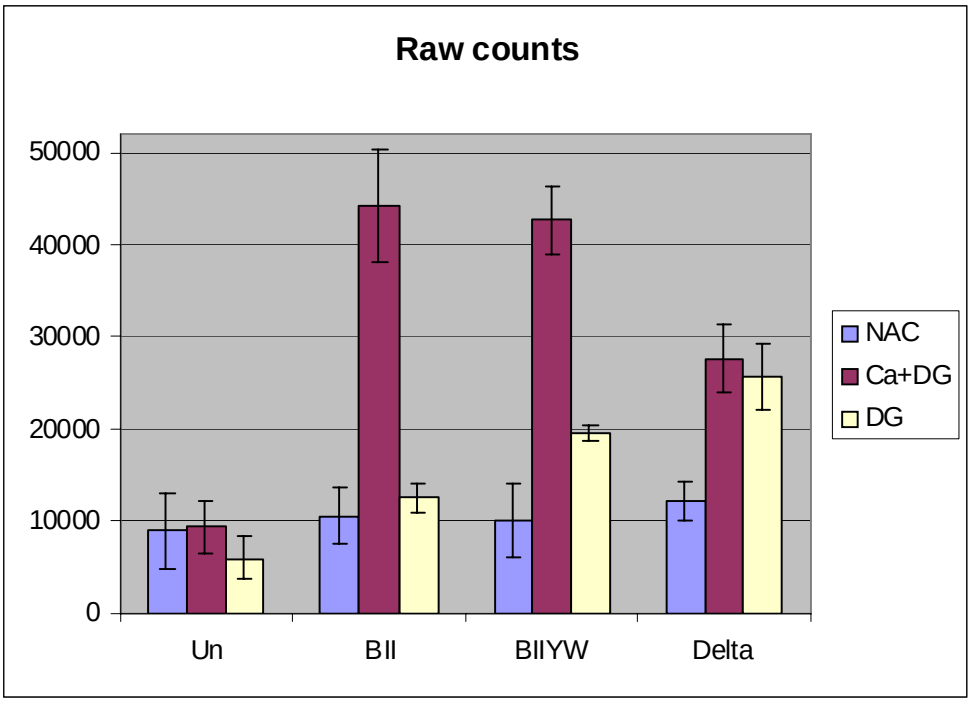

Figure A2.3. Raw counts from kinase assay demonstrate that the DAG-sensitizing mutation does not affect PKC activity in the presence of Ca^{2+}. Lysates from untransfected COS7 cells (first series of bars, Un), or cells transfected with YFP-PKCβII (second series of bars, BII), YFP-PKCβII-Y123W (third series of bars, BIIYW), or YFP-PKCδ (fourth series of bars, Delta) were prepared for use in an *in vitro* kinase assay. These lysates were incubated with substrate under non-activating conditions (NAC, periwinkle bars), or under activating conditions with Ca^{2+} and DAG (Ca+DG, magenta bars), or with DAG alone (DG, cream bars). For PKCβII and PKCβII-Y123W, activating conditions with Ca^{2+} and DAG produce nearly identical raw counts, while PKCβII-Y123W has increased raw counts in the presence of DAG alone.

Chapter 4

A Putative Cancer Driver Mutation in Protein Kinase C βII Decreases Diacylglycerol-dependent Signaling and Prevents Apoptosis in the Context of Oncogenic K-Ras[§]

Abstract

Protein kinase C (PKC*) is a family of ten signal-transducing enzymes that has been extensively studied in the context of cancer. Recently, large-scale efforts to systematically sequence candidate genes in cancer genomes in search of "cancer driver" mutations have uncovered a number of somatic mutations throughout the PKC family that occur in tumors and, thus, may have contributed to the progression of cancer in human patients. Here we characterize one mutation occurring in a tumor from a patient with colorectal adenocarcinoma, a Val to Met change at position 144 (V144M) in the C1b domain of PKCβII, and show that it results in impaired activation of PKC. In this tumor, the only other identified somatic mutation occurred in K-Ras, a well-characterized activating mutation at Gly 12. K-Ras and PKC have been extensively linked in the literature; specifically, K-Ras signaling induces PKC expression, while PKC phosphorylates K-Ras to alter its sub-cellular targeting and promote apoptosis. In this study, we determined that the putative cancer driver mutation in PKCβII, V144M, decreases the ability of the C1 domain to bind diacylglycerol-containing membranes. Using live cell imaging, we show this has the predicted effect of desensitizing PKCβII to receptor-mediated signaling in cells. Interestingly, when PKCβII is expressed in colon cancer cell lines containing oncogenic K-Ras mutations, the V144M mutation protects cells from apoptosis but does not hinder the ability of PKC to promote proliferation. In addition, somatic mutations occurring across the PKC family are also found in other colon tumors harboring K-Ras mutations. These data are consistent with a model in which a slight decrease in PKC activity in colon tumors prevents pro-apoptotic phosphorylation of K-Ras, but still permits phosphorylation of pro-proliferative

substrates. This is the first study to propose a molecular basis of how a mutation in PKCβII occurring in a human tumor can promote the survival of colon cancer cells harboring an oncogenic K-Ras mutation.

Introduction

Cancer results from a process of Darwinian evolution whereby individual cells acquiring random mutations are acted upon by natural selection for the ability to proliferate and survive in a tissue microenvironment. This process produces heterogeneous mechanisms for achieving tumorigenesis (1). Nonetheless, alterations in several pro-proliferative, pro-survival genes, such as *KRAS* and *PI3KCA*, are often prevalently mutated in many cancers and implicated in both tumor initiation and progression (reviewed in (2)). Recently, large-scale efforts have been made to systematically sequence candidate genes in cancer genomes, including sequences encoding the 518 kinases, in search of genes in which non-synonymous somatic mutations in tumor tissues are enriched relative to synonymous mutations (3,4). Non-synonymous mutations in "cancer genes" that occur more frequently than would be expected from random chance, based on the size of the gene are termed "cancer driver" mutations. These sequencing efforts have uncovered a number of putative cancer driver mutations throughout the protein kinase C (PKC) family, and statistical analysis from these studies supports that many PKC isoforms pass the threshold for being characterized as cancer genes (3,4).

The protein kinase C (PKC) family, which consists of ten signal-transducing enzymes, has been intensely investigated in cancer studies. Historically, this arises from the discovery of PKC as the first receptor for the tumor-promoting phorbol esters (5).

Activity of PKC is regulated by phosphorylation and membrane binding. First, the signaling-competent species of PKC must be 'matured' through a series of ordered phosphorylation events at specific carboxy-terminal sites: the activation loop, turn motif, and hydrophobic motif (reviewed in (6)). This phosphorylated, signaling-competent species of PKC is maintained in an inactive conformation by a pseudosubstrate peptide that blocks access to the substrate-binding cavity. In order to become acutely activated, PKC isoforms engage membranes using their lipid-targeting modules, the C1 and C2 domains, which bind anionic phospholipids in cellular membranes in response to diacylglycerol (DAG) and Ca^{2+}, respectively. Phorbol esters are highly potent DAG analogs which also activate PKC via C1 domain binding. Membrane binding activates PKC allosterically by providing the energy required to release the pseudosubstrate peptide, which grants active-site access to cellular substrates (reviewed in (7)). Within the PKC family, there are three subcategories based on the mode of regulation in response to lipid signaling (reviewed in (8)). Conventional PKC isoforms (α, βI/II, and γ) contain a Ca^{2+}-sensitive C2 domain and tandem DAG-sensitive C1a-C1b domains. Novel PKC isoforms (δ, θ, ε and η) contain tandem DAG-sensitive C1a-C1b domains and a C2 domain that does not sense Ca^{2+}. Atypical PKC isoforms (ζ and ι) contain a single C1 domain that is insensitive to DAG; these isoforms have been shown to be regulated predominantly by interactions with scaffolding proteins.

While cancer genome sequencing efforts implicate specific genes in the progression of cancer, in many cases, the mechanism by which mutated cancer genes cooperate to initiate or enhance tumorigenesis has yet to be determined. We chose to focus on characterizing the effects of a point mutation in the C1b domain of PKCβII, Val

144 to Met, which occurred as one of two identified somatic mutations in the cancer genome of a patient with colorectal adenocarcinoma; the other somatic mutation found was a well-characterized activating mutation in K-Ras at Gly 12 (3,9). Interestingly, while mutation of Gly 12 in K-Ras is found in a large percentage of human colorectal adenocarcinomas, this alone is insufficient to promote tumorigenesis in mouse models; however, when combined with mutation of other proteins, such as APC, tumorigenesis is promoted (10). Furthermore, K-Ras and PKCβII have been linked in many studies. Specifically, expression of oncogenic K-Ras in mouse colonic epithelium induces PKCβII expression in proximal colon (11). In addition, PKC phosphorylates K-Ras at Ser 181, sending it to mitochondria to promote apoptosis (12). Thus, because of the low number of somatic mutations in this particular tumor and substantial literature linking the two mutated proteins, there is a strong indication that the V144M somatic mutation in PKCβII, occurring together with an activating G12D mutation in K-Ras, contributed to this adenocarcinoma.

In this chapter, we demonstrate that the V144M putative cancer driver mutation in the C1b domain of PKCβII decreases the ability of this domain to bind membranes in response to receptor-mediated signaling. In keeping with the role of membrane binding in acute activation of PKC, this mutation desensitizes PKCβII to receptor-mediated signaling in cells. Expression of either wild-type PKCβII or PKCβII-V144M promoted proliferation of colon cancer cell lines. Interestingly, while expression of wild-type PKCβII caused apoptosis in colon cancer cell lines with activating K-Ras mutations, PKCβII-V144M did not cause apoptosis. Furthermore, mutations in other PKC isoforms

are also present in other human colon tumor samples, and a colon cancer cell line, all of which contain activating K-Ras mutations. Thus, it is likely that reducing PKC activity promotes tumors by reducing apoptosis in the context of oncogenic K-Ras mutations. This is the first study proposing a molecular mechanism of how an identified somatic mutation in PKCβII in a human colon tumor cooperates with oncogenic K-Ras to promote survival.

Materials and Methods

Materials—Phorbol-12,13-dibutyrate (PDBu), and UTP were purchased from CalBiochem. Electrophoresis reagents were from Bio-Rad Laboratories, Inc. Oligonucleotides used in PCR were purchased from IDT. LR clonase and vector conversion kit were purchased from Invitrogen. Restriction endonucleases were purchased from New England Biolabs. All other reagents and chemicals were reagent-grade.

Construction of plasmids—All mutagenesis was conducted using QuikChange site-directed mutagenesis according to the manufacturer's protocol (Stratagene, Inc.). PM-CFP (MyrPalm-CFP) was constructed as previously described (13). YFP-tagged C1b domain of PKCβ was made as described (14). YFP-C1b-V144M was generated by using the primers 5'-CAAGCGCTGCATGATGAACGTC -3' and its complete antisense oligonucleotide. DAGR was made as previously described (13); DAGR-V144M was generated using the above-mentioned primers. A Gateway destination vector for N-terminal fusion of mCherry was constructed via a three-part ligation of (1) pCDNA3 digested with HindIII and EcoRV, (2) the RFA Gateway insert, and (3) mCherry PCR product containing a digested HindIII site at the 5' end and a blunt 3' end; this produced

the destination vector pDESTmCherry-N. pDESTmCherry-N was recombined with the pENTR-PKCβII entry clone (Invitrogen) or pENTR-PKCβII-V144M (generated with the above-mentioned primers) using LR Clonase (Invitrogen) to produce mCherry-PKCβII and mCherry-PKCβII-V144M. A Gateway destination vector for N-terminal fusion of HA was constructed by digesting pCDNA3-HA (15) with EcoRV and ligating with RFC.1 Gateway insert. HA-PKCβII and HA-PKCβII-V144M were constructed using an LR Clonase reaction as described above.

Cell culture and immunoblotting—All cell lines were plated and maintained in Dulbecco's modified Eagle's medium (Cellgro) containing 5% fetal bovine serum and 1% penicillin/streptomycin at 37 °C in 5% CO_2. For imaging, cells were plated in sterilized 35-mm imaging dishes at 60% confluency and transfected using FuGENE 6 (Roche Diagnostics). Transient transfections for all colon cancer cell lines were carried out using Effectene reagents (Qiagen), and transfection efficiency ranged from 50% to 85%. For immunoblotting, transfected cells were lysed in 50 mM Na_2HPO_4 [pH 7.5], 1 mM sodium pyrophosphate, 20 mM NaF, 2 mM EDTA, 2 mM EGTA, 1% SDS, 1 mM DTT, 200 μM benzamidine, 40 μg/ml leupeptin, and 1 mM PMSF and sonicated for 5 s. Lysates containing equal protein were analyzed on SDSPAGE gels, and individual blots were probed using the indicated antibody.

Cell imaging—Cells were rinsed once with, and imaged in, Hanks Balanced Saline Solution (Cellgro) containing 1 mM $CaCl_2$. Images were acquired on a Zeiss Axiovert microscope (Carl Zeiss Microimaging, Inc.) using a MicroMax digital camera (Roper-Princeton Instruments) controlled by MetaFluor software (Universal Imaging, Corp.). Optical filters were obtained from Chroma Technologies. Using a 10% neutral density

filter, CFP and FRET images were obtained every 10-15 s through a 420/20-nm excitation filter, a 450-nm dichroic mirror, and a 475/40-nm emission filter (CFP) or 535/25-nm emission filter (FRET). YFP emission was also monitored as a control for photobleaching through a 495/10-nm excitation filter, a 505-nm dichroic mirror, and a 535/25-nm emission filter. mCherry emission was monitored during the CKAR imaging experiments as a control for PKC expression levels. Excitation and emission filters were switched in filter wheels (Lambda 10–2, Sutter). Integration times were 200 ms for CFP and FRET, 50–100 ms for YFP, and 100 ms for mCherry.

C1 domain translocation data analysis—For C1 domain translocation experiments, the responses to DAG generation via UTP were calibrated to the dynamic range of the cell by dividing each point by the maximal response elicited by PDBu as previously described (14). Thus, the data are presented in relative translocation units.

CKAR data analysis—For CKAR experiments, the responses to UTP were referenced around the ligand addition time-point and the baseline FRET ratios were normalized to 1. If necessary, linear baseline drift was subtracted. For each concentration of UTP, the average response (which reaches a maximum within the first two minutes (16)) from at least 8 individual cells and at least three separate dishes was fitted to the following equation for mono-exponential rise:

$$y=m1 + m2*(1-e^{(-m3x)})$$

In which the variable, m1, represents the initial FRET ratio; the variable, m2, represents the maximum FRET ratio; and the variable, m3, represents the rate constant. The rate was within error for all concentrations of UTP within the same experimental conditions. The maximum FRET ratio change (m2-m1, and calculated error) at increasing

concentrations of UTP was plotted on a semi-log scale, and the data were fitted to the following michaelis-menten equation:

$$y=n1*x/(n2+x)$$

In which the variable n2 represents the concentration of UTP that produces a half-maximal response, and the variable n1 represents the maximal cellular response to saturating UTP. All data were analyzed using Kaleidograph 4.0, and curves were weighted using SEM.

Apoptosis assays and FACS analysis—Floating cells were collected, and adherent cells were harvested by trypsinization. Floating cells and harvested cells were pooled and centrifuged at 1000 *g* for 5 min. Cells were fixed in ice-cold 70% methanol, added dropwise, and then incubated at -20°C for 30 min. Cells were centrifuged and incubated with propidium iodide (25 μg/ml) supplemented with RNase A (30 μg/ml) for 30 min at room temperature. Quantification of sub-2N DNA was determined by flow cytometry analysis using a Becton Dickinson FACSort and by manual gating using CellQuest software.

Results

A mutation of Val at position 144 to Met in PKCβII was one of two mutations found in tumor tissue from a patient with colorectal adenocarcinoma (4); the other mutation is a well-characterized oncogenic mutation in K-Ras at Gly 12 (9). Valine 144 is conserved in the C1b domains of all conventional isoforms of PKC (Figure 4.1A). C1 domains have a fold in which an unzipped β sheet forms a groove lined by hydrophobic residues; this groove forms a pocket for DAG or the potent DAG-mimicking phorbol esters (such as phorbol dibutyrate (PdBu)) to bind (17). When mapped on to the structure

of the C1b domain of conventional PKCγ (Figure 4.1B), Val 144 is not located along the ligand-binding pocket. However, it is spatially located between two other conserved Val residues that form a hydrophobic core in the center of the C1b domain. Thus, mutation of this residue from Val to Met might alter the structure of the C1b domain, and might impact the ability of this domain to contribute to membrane binding and activation of the kinase. With this in mind, we sought to determine the effect of the V144M mutation on the ability of the C1b domain to bind membranes.

The C1b domain of conventional PKC isoforms binds the ligand DAG with low affinity, yet responds robustly to phorbol esters (14). To assess the impact of the V144M mutation on binding to cellular membranes, we co-transfected COS7 cells with plasma membrane-tethered CFP (PMCFP) and either YFP-tagged C1b domain from PKCβ (YFP-C1b) or YFP-tagged C1b domain in which the Val at position 144 is mutated to Met (YFP-C1bV144M). Translocation of the C1b domains to the plasma membrane is measured as an increase in the ratio of FRET-based YFP emission: CFP emission upon excitation of CFP (FRET ratio). We stimulated the cells with UTP (100 μM, 5 min) followed by treatment with PdBu (200 nM, 5 min) (Figure 4.2A). UTP stimulates DAG production in COS7 cells via endogenous P2Y G_q-coupled receptors, while PdBu maximally translocates C1b domains to cellular membranes (14). Consistent with the low affinity of the isolated C1b domain for DAG-containing membranes (14), neither domain translocates to the plasma membrane in response to UTP-stimulated DAG production. However, both domains respond to treatment with the potent ligand, PdBu. Interestingly, the rate of translocation is markedly reduced for the C1b-V144M compared to the un-mutated C1b domain. This indicates that the ability of the C1b domain to bind

cellular membranes may be compromised by the V144M mutation.

Next, we determined the effect of the V144M mutation on the ability of the tandem C1a-C1b domain to respond to UTP-mediated DAG production. We transfected COS7 cells with the C1a-C1b domain of PKCβ flanked by CFP and YFP; this construct has previously been described as DAGR, for Diacylglycerol Reporter (13). As DAGR translocates to cellular membranes, the reduction in dimensionality results in FRET; thus, an increase in the ratio of FRET-based YFP:CFP emission upon excitation of CFP (FRET ratio) also indicates membrane binding in this system. In addition, we transfected cells with DAGR in which Val at position 144 is mutated to Met (DAGR-V144M). Cells transfected with DAGR or DAGR-V144M were treated with UTP (100 μM) followed by PdBu (200 nM) as before (Figure 4.2B). Interestingly, DAGR was retained at the membrane much longer than DAGR-V144M. These data suggest that, although the C1b domain alone is insufficient to respond to cellular DAG production, the C1b domain is involved in retaining the tandem C1a-C1b domain at the membrane. Both DAGR and DAGR-V144M respond similarly to PdBu treatment; PdBu likely overcomes the deficit in C1b domain binding by utilizing the fully-functional C1a domain (18). Importantly, the V144M mutation clearly decreases the ability of the C1 domain to be retained at the membrane in response to receptor-mediated DAG production.

Because the V144M mutation reduced the ability of both the isolated C1b domain and tandem C1a-C1b domain to bind cellular membranes, and membrane affinity determines the ability of conventional PKC isoforms to be activated in response to DAG production, we tested how the V144M mutation impacts PKCβII activity in cells. C Kinase Activity Reporter, CKAR, is a tool to measure PKC activation in live cells (13).

CKAR is composed of CFP and YFP flanking a substrate peptide that is specifically phosphorylated by PKC and an FHA phospho-peptide binding module. For CKAR, basal FRET from CFP to YFP is reduced when the FHA domain binds to the phosphorylated substrate peptide; thus, for CKAR, the ratio of CFP:FRET-based YFP emission (FRET ratio) indicates increasing phosphorylation of the reporter by PKC. To first characterize the response of the endogenous PKC, COS7 cells were transfected with CKAR and stimulated with increasing concentrations of UTP. Plotting the maximal FRET ratio change of CKAR against increasing UTP concentrations yields a classical dose-response curve with Michaelis-Menten kinetics; K_{app} for the endogenous PKC in COS7 cells is 23 ± 4 μM (Figure 4.3A, open circles). Expression of exogenous mCherry-tagged PKCβII with CKAR shifts the dose-response curve leftward, sensitizing the cells to phosphorylation triggered by UTP with a K_{app} of 0.54 ± .07 μM (Figure 4.3A, closed blue circles). This increase in sensitivity is likely due to increasing the concentration of cellular PKC by overexpression, but it may also be that CKAR is an intrinsically better substrate for PKCβII than for the endogenous isoforms present in COS7 cells. Regardless, the large difference in the response of the exogenous PKCβII vs. the endogenous PKC isoforms provides a sufficient window for monitoring the effects of the V144M mutation on PKCβII activity. Indeed, when mCherry-tagged PKCβII-V144M is co-transfected with CKAR, the dose-response curve is shifted right of the wild-type PKCβII, with a K_{app} of 1.4 ± 0.5 μM (Figure 4.3A, closed red circles). Additionally, the maximal CKAR response in the presence of mCherry-PKCβII is ~38% higher than in the presence of mCherry-PKCβII-V144M or without exogenous PKC. Figure 4.3B shows

equivalent expression of mCherry-WT PKCβII and mCherry-PKCβII-V144M. These data indicate that mutation of Val 144 to Met desensitizes PKCβII to receptor-mediated stimulation in cells.

Next, we tested whether expression of PKCβII-V144M in colon cancer cell lines with oncogenic K-Ras mutations would affect proliferation and survival. Figure 4.4 shows the G1/S ratio of HCT116 cells (K-Ras mutation: G13D, (19)) transfected with empty vector, HA-WT PKCβII, or HA-PKCβII-V144M. Both HA-WT PKCβII and HA-PKCβII-V144M were capable of lowering the G1/S ratio in HCT116 cells, indicating an increase in cell cycle entry upon expression of either PKC. Interestingly, transfection of colon cancer cell lines harboring activating K-Ras mutations (HCT116, DLD1, (19) Figure 4.5) with HA-WT PKCβII causes a two-fold increase in the amount of apoptosis, while expression of HA-PKCβII-V144M causes no increase in apoptosis in DLD-1 cells, and significantly less apoptosis in HCT116 cells. As a control, Caco-2 cells are derived from an adenocarcinoma that contains wild-type K-Ras (20); these cells show no induction of apoptosis upon expression of either HA-WT PKCβII or HA-PKCβII-V144M. In addition, Figure 4.5B shows equivalent expression of HA-WT PKCβII and HA-PKCβII-V144M. Interestingly, expression of either PKC induces phosphorylation of many of the downstream substrates recognized by a pSer PKC substrate antibody (Figure 4.5B, lower panels). These data collectively indicate that PKCβII-V144M is still capable of carrying out pro-proliferative signaling, but has decreased ability to induce apoptosis in colon cancer cell lines harboring oncogenic K-Ras.

Discussion

These data support the conclusion that the V144M cancer driver mutation in PKCβII desensitizes it to receptor-mediated stimulation by G_q/phospholipase C pathways. This result is somewhat surprising because classical studies have established that overexpression of PKCβ isoforms is tumor-promoting, and genetic abrogation of PKCβ isoforms is tumor-suppressive, in an AOM-induced mouse model of colon cancer (21,22) and in a rat intestinal epithelial cell line (23). Our study has focused on a human tumor from a patient with colorectal adenocarcinoma in which the only other somatic mutation occurred in K-Ras. While the pathways mutated in AOM-induced tumors in animals do vary, oncogenic K-Ras mutations are frequent (24). However, recent studies have shown that PKC phosphorylates K-Ras to promote its association with mitochondria, inducing apoptosis; this effect is mediated by ligands that activate PKC via C1 domain binding, such as bryostatin (12). Consistent with this report, the mutation we have characterized has the effect of desensitizing PKC and protecting from apoptosis. On the other hand, our study is also consistent with reports showing a requirement for PKCβII in colon cancer, since PKC activity is not completely abolished by the cancer driver mutation, and over-expression of the mutated PKCβII is still capable of promoting proliferation.

Introduction of oncogenic K-Ras into mouse colonic epithelium drives expression of PKCβII (11), but its effects on the expression of other PKC isoforms have not been described. However, in other human colon tumors whose cancer genomes have been

sequenced, and in one colon cancer cell line, LS1034, mutations in critical functional domains in other PKC isoforms occur with activating mutations of K-Ras (Table 1, (4,25)). One plausible model for the interplay between K-Ras and PKC in colon cancer is that the first "hit" activates K-Ras, which leads to upregulation of PKC expression. PKC and K-Ras together promote tumorigenesis through a number of pro-proliferative targets (26-28); however, phosphorylation of K-Ras by PKC suppresses tumor growth by promoting apoptosis (12). A second "hit" serves to down-regulate PKC activity to a level that reduces this tumor-suppressive feedback to K-Ras but still allows PKC to carry out its tumor-promoting functions. Thus, lower (but not absent) PKC activity selectively interferes with the tumor-suppressive function of PKC on K-Ras, and now both proteins can fulfill their tumorigenic roles (Figure 4.6). In support of this, studies in human cancers have found reduced expression of PKCβ isoforms in glioma, lymphoma, leukemia, melanoma, bladder, prostate, and colon cancers (29-37). Clinical efforts to inhibit or activate PKCβII in the treatment of cancer have had varying degrees of success (38-40). Our study suggests pharmacological inhibition of PKC in colon cancers harboring oncogenic K-Ras mutations might lead to a bell-shaped curve of efficacy, with higher concentrations of PKC inhibitor being effective in antagonizing tumors and lower concentrations being potentially tumor promoting. Further investigation into how somatic mutations of PKC isoforms in tumor tissues affect activity will undoubtedly inform efforts to more effectively target this kinase family in the treatment of cancer.

Acknowledgements

I thank John Brognard for carrying out all FACS analysis experiments and Western blots. I also gratefully acknowledge both John Brognard and Tony Hunter for helpful discussions directing this research.

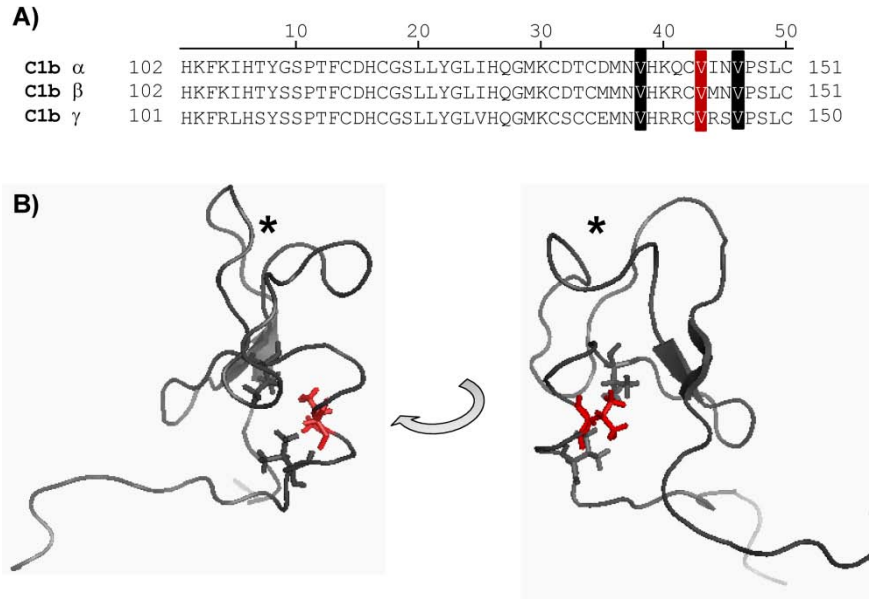

Figure 4.1. Val 144 is conserved amongst C1b domains of conventional PKC isoforms. *A*, Sequence alignment of the C1b domains of conventional PKC isoforms: α, β, and γ. Val 144 (PKCβ numbering) is boxed in *red*. Other conserved Val residues, Val 139 and Val 147 (PKCβ numbering), are boxed in *black*. *B*, Ribbon diagram of C1b-PKCγ The left view displays two loops at the top of the domain which have been demonstrated to coordinate phorbol ester (17); the site of phorbol binding is indicated with an asterisk (*). Valine 144 is presented as a red stick; other conserved Val residues are presented as black sticks. The rotated right view demonstrates the spatial organization of the three conserved Val residues at the hydrophobic core of the domain. Coordinates for C1b-PKCγ were taken from PDB ID 1TBN.

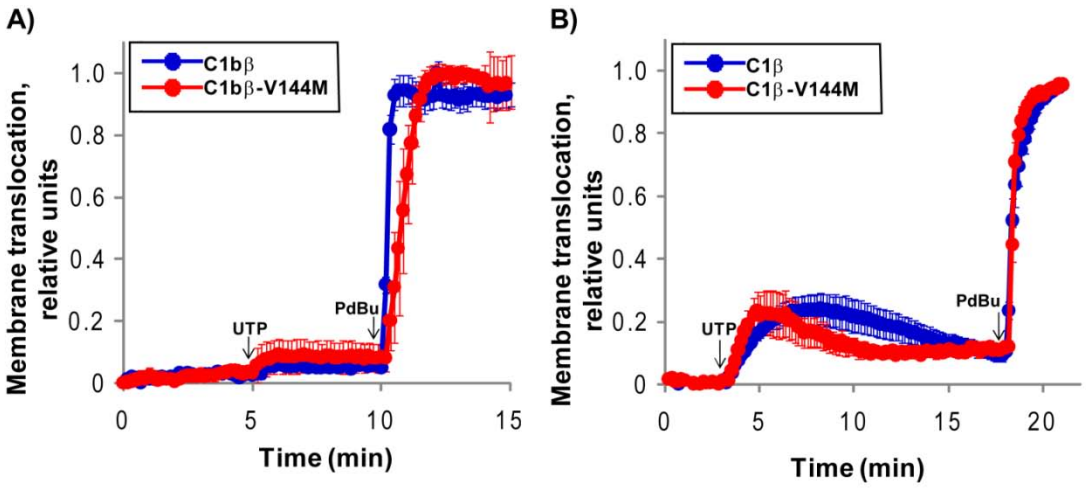

Figure 4.2. Mutation of Val 144 to Met in the C1b domain of PKCβ decreases the affinity for PdBu- and DAG-containing membranes. COS7 cells were co-transfected with *A*, PM-CFP and indicated YFP-tagged C1b domain constructs: C1bβ (closed blue circles), C1bβ-V144M (closed red circles) or *B*, DAGR (closed blue circles) and DAGR-V144M (closed red circles). The average FRET ratio change following UTP (100 μM, added at 5 min) and PDBu (200 nM, added at 10 min) treatment was plotted over time. Data were calibrated for the dynamic range of the individual cell by dividing each response by the maximum response to PDBu. These data reveal the relative translocation of each isolated domain in response to UTP (100 μM) compared to PDBu (200 nM) treatment. Data represent the average ± SEM of 10-15 cells from at least three independent experiments referenced around the addition time point.

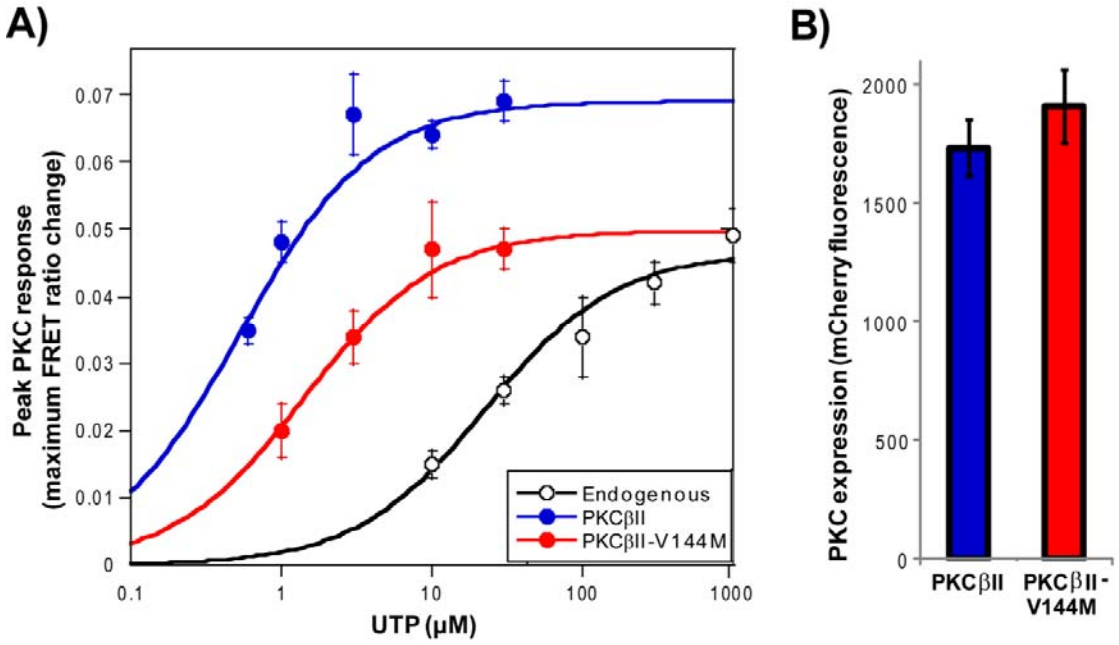

Figure 4.3. Mutation of Val 144 to Met in full-length PKCβII increases the concentration of UTP required to promote phosphorylation of CKAR, a PKC activity reporter. *A*, COS7 cells were transfected with CKAR alone (to monitor endogenous PKC activity, open circles), CKAR and mCherry-WT PKCβII (closed blue circles), or CKAR and m-Cherry PKCβII-V144M (closed red circles). The maximal FRET ratio change in response to increasing concentrations of UTP was determined in separate experiments for each concentration of UTP. Each data point represents the maximum response determined by curve-fitting the average FRET ratio change within the first two minutes from at least 8 cells from at least 3 independent experiments referenced around the addition time point and weighted using the SEM. *B*, Graph of mCherry intensity values demonstrates equivalent expression of mCherry-tagged PKC constructs. Data represent average mCherry intensity ± SEM from all CKAR imaging experiments.

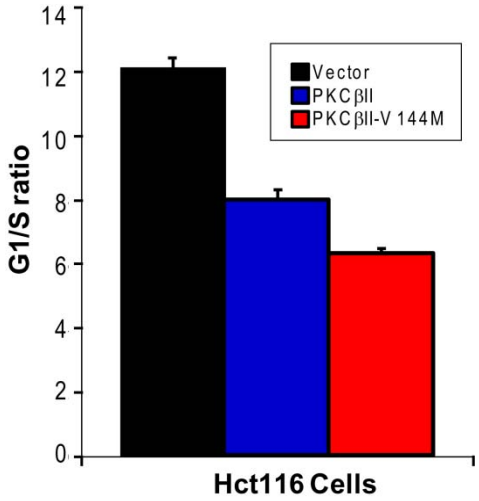

Figure 4.4. Both PKCβII and PKCβII-V144M promote cell cycle progression in cells containing oncogenic K-Ras. HCT116 cells, which harbor a G13D K-Ras mutation, were transfected with HA-WT PKCβII or HA-PKCβII-V144M. Compared to cells transfected with control vector (black bars), cells transfected with both WT-PKCβII (blue bars) and HA-PKCβII-V144M (red bars) had a lower G1/S ratio, indicating increased cell cycle progression. Data are representative of three independent experiments performed in triplicate ± S.D. These data appear courtesy of John Brognard.

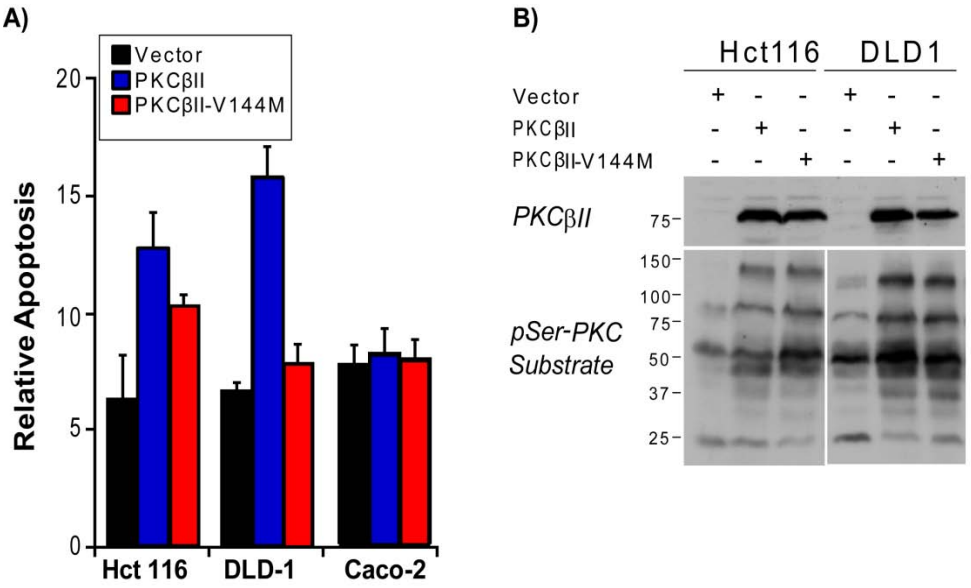

Figure 4.5. PKCβII V144M promotes survival in colon cancer cell lines containing oncogenic K-Ras mutations, but has no effect in a colon cancer cell line containing wild-type K-Ras. *A,* HCT116 cells, DLD-1 cells, and Caco-2 cells were transfected with control vector (black bars), HA-WT-PKCβII (blue bars), or HA-PKCβII-V144M (red bars) and analyzed for sub-2N DNA. Transfection of HCT116 or DLD1 cells, which harbor oncogenic K-Ras mutations, with WT PKCβII induces apoptosis. Transfection of these cells with PKCβII-V144M dramatically reduces (HCT116) or eliminates (DLD-1) the induction of apoptosis. In Caco-2 cells, which contain normal K-Ras, no apoptosis is induced. Data are representative of three independent experiments performed in triplicate ± S. D. *B,* Immunoblot analysis of HCT116 and DLD-1 cells transfected with control vector, HA-WT-PKCβII, or HA-PKCβII-V144M. Top panels show equivalent expression of HA-WT-PKCβII and HA-PKCβII-V144M. Bottom panels show increased phosphorylation of PKC substrates upon expression of either PKC construct. These data appear courtesy of John Brognard.

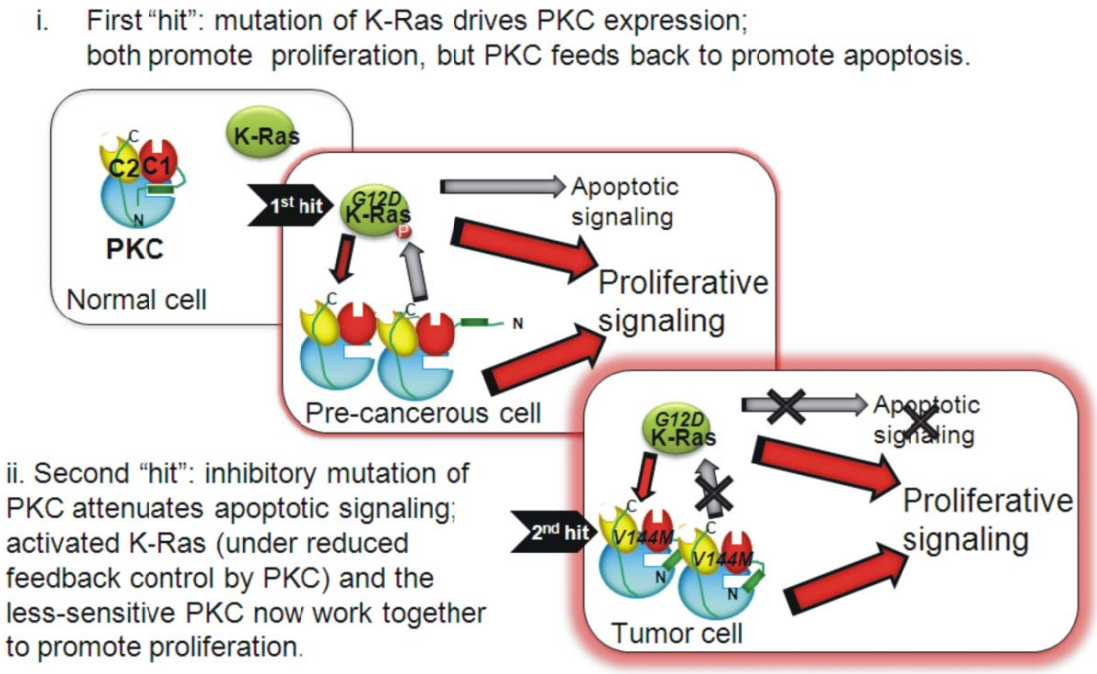

Figure 4.6. Model describing potential mechanism whereby inactivating PKC mutations contribute to tumor progression. In normal cells, PKCβII and K-Ras carry out cellular signaling functions. The first mutational event to trigger neoplastic transformation (i) is activation of K-Ras, which drives pro-proliferative signaling and up-regulates expression of PKCβII. PKCβII cooperates in pro-proliferative signaling, but also phosphorylates K-Ras to promote pro-apoptotic signaling by re-localizing K-Ras to mitochondria. A second mutational event (ii) desensitizes PKC to lipid-dependent signaling and diminishes phosphorylation of K-Ras. This event attenuates apoptotic signaling and allows both proteins to carry out pro-proliferative signaling.

Table 4.1. Mutations in PKC family members present in colon tumor samples or colon cancer cell lines harboring oncogenic K-Ras mutations. Mutations found across members of the PKC family are present in functional domains, thus may impact activity. Notably, many of these mutations occur in the C1 domain. All of the PKC mutations found in colon tumors or cell lines occurred with activating mutations in K-Ras.

Isoform	Mutation	Functional domain	K-Ras mutation	Reference
PKCα	P98S	C1 domain	G13D	(4)
PKCβII	V144M	C1b domain	G12D	(4)
PKCε	E143K	pseudosubstrate region	G13D	(25)
PKCθ	K240N	C1b domain	A146T	(4)
PKCη	T594I	kinase core	G13D	(4)
PKCζ	S514F	kinase core	G12A	(25)

References

1. Stratton, M. R., Campbell, P. J., and Futreal, P. A. (2009) *Nature* **458**(7239), 719-724

2. Vogelstein, B., and Kinzler, K. W. (2004) *Nat Med* **10**(8), 789-799

3. (2008) *Nature* **455**(7216), 1061-1068

4. Greenman, C., Stephens, P., Smith, R., Dalgliesh, G. L., Hunter, C., Bignell, G., Davies, H., Teague, J., Butler, A., Stevens, C., Edkins, S., O'Meara, S., Vastrik, I., Schmidt, E. E., Avis, T., Barthorpe, S., Bhamra, G., Buck, G., Choudhury, B., Clements, J., Cole, J., Dicks, E., Forbes, S., Gray, K., Halliday, K., Harrison, R., Hills, K., Hinton, J., Jenkinson, A., Jones, D., Menzies, A., Mironenko, T., Perry, J., Raine, K., Richardson, D., Shepherd, R., Small, A., Tofts, C., Varian, J., Webb, T., West, S., Widaa, S., Yates, A., Cahill, D. P., Louis, D. N., Goldstraw, P., Nicholson, A. G., Brasseur, F., Looijenga, L., Weber, B. L., Chiew, Y. E., DeFazio, A., Greaves, M. F., Green, A. R., Campbell, P., Birney, E., Easton, D. F., Chenevix-Trench, G., Tan, M. H., Khoo, S. K., Teh, B. T., Yuen, S. T., Leung, S. Y., Wooster, R., Futreal, P. A., and Stratton, M. R. (2007) *Nature* **446**(7132), 153-158

5. Castagna, M., Takai, Y., Kaibuchi, K., Sano, K., Kikkawa, U., and Nishizuka, Y. (1982) *J Biol Chem* **257**(13), 7847-7851

6. Newton, A. C. (2003) *Biochem J* **370**(Pt 2), 361-371

7. Gallegos, L. L., and Newton, A. C. (2008) *IUBMB Life* **60**(12), 782-789

8. Gould, C. M., and Newton, A. C. (2008) *Curr Drug Targets* **9**(8), 614-625

9. Tabin, C. J., Bradley, S. M., Bargmann, C. I., Weinberg, R. A., Papageorge, A. G., Scolnick, E. M., Dhar, R., Lowy, D. R., and Chang, E. H. (1982) *Nature* **300**(5888), 143-149

10. Sansom, O. J., Meniel, V., Wilkins, J. A., Cole, A. M., Oien, K. A., Marsh, V., Jamieson, T. J., Guerra, C., Ashton, G. H., Barbacid, M., and Clarke, A. R. (2006) *Proc Natl Acad Sci U S A* **103**(38), 14122-14127

11. Calcagno, S. R., Li, S., Colon, M., Kreinest, P. A., Thompson, E. A., Fields, A. P., and Murray, N. R. (2008) *Int J Cancer* **122**(11), 2462-2470

12. Bivona, T. G., Quatela, S. E., Bodemann, B. O., Ahearn, I. M., Soskis, M. J., Mor, A., Miura, J., Wiener, H. H., Wright, L., Saba, S. G., Yim, D., Fein, A., Perez de Castro, I., Li, C., Thompson, C. B., Cox, A. D., and Philips, M. R. (2006) *Mol Cell* **21**(4), 481-493

13. Violin, J. D., Zhang, J., Tsien, R. Y., and Newton, A. C. (2003) *J Cell Biol* **161**(5), 899-909

14. Dries, D. R., Gallegos, L. L., and Newton, A. C. (2007) *J Biol Chem* **282**(2), 826-830

15. Gao, T., Furnari, F., and Newton, A. C. (2005) *Mol Cell* **18**(1), 13-24

16. Gallegos, L. L., Kunkel, M. T., and Newton, A. C. (2006) *J Biol Chem* **281**(41), 30947-30956

17. Zhang, G., Kazanietz, M. G., Blumberg, P. M., and Hurley, J. H. (1995) *Cell* **81**(6), 917-924

18. Giorgione, J., Hysell, M., Harvey, D. F., and Newton, A. C. (2003) *Biochemistry* **42**(38), 11194-11202

19. Shirasawa, S., Furuse, M., Yokoyama, N., and Sasazuki, T. (1993) *Science* **260**(5104), 85-88

20. Lawson, K. R., Ignatenko, N. A., Piazza, G. A., Cui, H., and Gerner, E. W. (2000) *Cancer Epidemiol Biomarkers Prev* **9**(11), 1155-1162

21. Murray, N. R., Davidson, L. A., Chapkin, R. S., Clay Gustafson, W., Schattenberg, D. G., and Fields, A. P. (1999) *J Cell Biol* **145**(4), 699-711

22. Liu, Y., Su, W., Thompson, E. A., Leitges, M., Murray, N. R., and Fields, A. P. (2004) *J Biol Chem* **279**(44), 45556-45563

23. Zhang, J., Anastasiadis, P. Z., Liu, Y., Thompson, E. A., and Fields, A. P. (2004) *J Biol Chem* **279**(21), 22118-22123

24. Takahashi, M., and Wakabayashi, K. (2004) *Cancer Sci* **95**(6), 475-480

25. Sjoblom, T., Jones, S., Wood, L. D., Parsons, D. W., Lin, J., Barber, T. D., Mandelker, D., Leary, R. J., Ptak, J., Silliman, N., Szabo, S., Buckhaults, P., Farrell, C., Meeh, P., Markowitz, S. D., Willis, J., Dawson, D., Willson, J. K., Gazdar, A. F., Hartigan, J., Wu, L., Liu, C., Parmigiani, G., Park, B. H., Bachman, K. E., Papadopoulos, N., Vogelstein, B., Kinzler, K. W., and Velculescu, V. E. (2006) *Science* **314**(5797), 268-274

26. Sauma, S., and Friedman, E. (1996) *J Biol Chem* **271**(19), 11422-11426

27. Murray, N. R., Burns, D. J., and Fields, A. P. (1994) *J Biol Chem* **269**(33), 21385-21390

28. Campbell, P. M., Groehler, A. L., Lee, K. M., Ouellette, M. M., Khazak, V., and Der, C. J. (2007) *Cancer Res* **67**(5), 2098-2106

29. Doi, S., Goldstein, D., Hug, H., and Weinstein, I. B. (1994) *Mol Carcinog* **11**(4), 197-203

30. Levy, M. F., Pocsidio, J., Guillem, J. G., Forde, K., LoGerfo, P., and Weinstein, I. B. (1993) *Dis Colon Rectum* **36**(10), 913-921

31. Ki, D. H., Jeung, H. C., Park, C. H., Kang, S. H., Lee, G. Y., Lee, W. S., Kim, N. K., Chung, H. C., and Rha, S. Y. (2007) *Int J Cancer* **121**(9), 2005-2012

32. Sun, L., Hui, A. M., Su, Q., Vortmeyer, A., Kotliarov, Y., Pastorino, S., Passaniti, A., Menon, J., Walling, J., Bailey, R., Rosenblum, M., Mikkelsen, T., and Fine, H. A. (2006) *Cancer Cell* **9**(4), 287-300

33. Sanchez-Carbayo, M., Socci, N. D., Lozano, J., Saint, F., and Cordon-Cardo, C. (2006) *J Clin Oncol* **24**(5), 778-789

34. Basso, K., Margolin, A. A., Stolovitzky, G., Klein, U., Dalla-Favera, R., and Califano, A. (2005) *Nat Genet* **37**(4), 382-390

35. Durig, J., Bug, S., Klein-Hitpass, L., Boes, T., Jons, T., Martin-Subero, J. I., Harder, L., Baudis, M., Duhrsen, U., and Siebert, R. (2007) *Leukemia* **21**(10), 2153-2163

36. Welsh, J. B., Sapinoso, L. M., Su, A. I., Kern, S. G., Wang-Rodriguez, J., Moskaluk, C. A., Frierson, H. F., Jr., and Hampton, G. M. (2001) *Cancer Res* **61**(16), 5974-5978

37. Hoek, K. S., Schlegel, N. C., Brafford, P., Sucker, A., Ugurel, S., Kumar, R., Weber, B. L., Nathanson, K. L., Phillips, D. J., Herlyn, M., Schadendorf, D., and Dummer, R. (2006) *Pigment Cell Res* **19**(4), 290-302

38. Mackay, H. J., and Twelves, C. J. (2007) *Nat Rev Cancer* **7**(7), 554-562

39. Griner, E. M., and Kazanietz, M. G. (2007) *Nat Rev Cancer* **7**(4), 281-294

40. Fields, A. P., Calcagno, S. R., Krishna, M., Rak, S., Leitges, M., and Murray, N. R. (2009) *Cancer Res* **69**(4), 1643-1650

Footnotes

[§]This work was supported by NIH GM43154, NIH 1F31GM083628, and ACS PF-09-085-01-TBE.

[*]The abbreviations used are as follows: CFP, cyan fluorescent protein; CKAR, C Kinase Activity Reporter; cPKCs, conventional PKCs; DAG, diacylglycerol; DAGR, diacylglycerol reporter; PdBu, phorbol-12,13-dibutyrate; PKC, protein kinase C; PM-CFP, plasma membrane-targeted CFP; YFP, yellow fluorescent protein.

Chapter 5

Protein Kinase Cα Interacts With and Phosphorylates SAP97/DLG1 to Promote Cytoskeletal Rearrangements §

Abstract

Signaling complexes promote cytoskeletal rearrangements during critical cellular processes such as migration and cytokinesis, and are co-opted in cancer for invasion and metastasis. The protein kinase C (PKC*) family of Ser/Thr kinases has often been implicated in directing cytoskeletal rearrangements. In this Chapter, we identify a novel cytoskeletal signaling module consisting of PKCα, the scaffold protein SAP97/DLG1, and the RhoGEF Ect2 and show that it is important for the formation of podosomes in Src-transformed fibroblasts. Specifically, the C-terminal PDZ ligand of PKCα binds the third PDZ domain of the SAP97/DLG1 scaffold and phosphorylates it at a highly-conserved Thr residue, Thr656. This phosphorylation site creates a consensus for binding the BRCT domains of Ect2, a GEF for the Rho family of GTPases, an event which relieves autoinhibitory constraints on the GEF domain to activate Rho GTPases. PKCα and DLG1 co-localize at podosomes, and phospho-Thr656 staining is also found at podosomes. Phosphorylation of DLG and formation of podosomes are reversed by inhibition of PKC. Evidence for this signaling module is also found in astrocyte migration and cell division. Specifically, PKCα and DLG1 co-localize at the leading edge of migrating astrocytes, and migration is delayed by inhibition of PKC. Additionally, phosphorylated DLG is found at the midbody of cells undergoing cytokinesis. Thus, we have identified a novel PKCα-DLG1-Ect2 signaling module that activates the Rho family to promote cytoskeletal rearrangements in cells.

Introduction

Cytoskeletal rearrangements underlie many biological processes, including cell migration and cytokinesis (1,2). Signaling pathways modulating the activation of the Rho family of small GTPases, Rho, Rac and CDC42, very often mediate cytoskeletal reorganization (recently reviewed in (3)). Rho GTPases are activated by the binding of GTP and inactivated when GTP is hydrolyzed to GDP. Thus proteins that exchange GDP for GTP (guanine nucleotide exchange factors, GEFs) activate Rho GTPases and proteins that stimulate the hydrolysis of GTP into GDP (GTPase activating proteins, GAPs) inactivate them. Seminal studies by Ridley and Hall have shown that there is a very characteristic cellular cytoskeletal phenotype observed when specific Rho GTPases are activated in cells (4,5). Specifically, RhoA activation produces stress fibers and stimulates retraction, Rac activation stimulates cell spreading and lamellopodia formation, and CDC42 activation stimulates fillopodia formation (3). Signaling pathways controlling activation of these proteins have been demonstrated to be subverted not only in cancer (reviewed in (6,7)) but also rather dramatically by human pathogens (8).

The protein kinase C (PKC) family has been implicated on numerous occasions both upstream and downstream of Rho family activation (9,10), and is also implicated in control of cytoskeletal remodeling (11). This family of enzymes is composed of conventional isoforms (cPKCs: α, βI, βII, γ), novel isoforms (nPKCs: δ, ε, θ, η) and atypical isoforms (aPKCs: ζ, ι). Activation of PKC isoforms involves removal of an N–terminal autoinhibitory pseudosubstrate sequence from the substrate binding cavity of the kinase core, allowing cellular substrates access to the active site. Removal of the

pseudosubstrate typically results from the interaction of intervening regulatory domains with anionic phospholipids, which is achieved in the presence of second messengers generated downstream from phospholipid hydrolysis. Activation is mediated by C1 and C2 domains of cPKCs (ligands: DAG and Ca^{2+} respectively) and the C1 domains alone of nPKCs (ligand: DAG) (reviewed in (12)). Less understood is activation of aPKCs, whose regulatory domains, PB-1 and atypical C1, respond to neither DAG nor Ca^{2+}. In addition to receptor-mediated generation of second messengers, phorbol esters, such as PMA and PdBu, are useful pharmacological DAG analogs which activate cPKC and nPKC isoforms (13,14). Also, activation of PKC isoforms by alternative mechanisms, including stabilization of the un-inhibited conformation by protein-protein interactions, has been documented (15), and is a plausible mode of activation for atypical PKC isoforms. Protein complexes involving specific PKC isoforms have been described, including a Par6-aPKC-Par3 polarity complex (reviewed in (16)), a PKCβII-pericentrin centrosomal complex (17), a PKCε-14-3-3 cytokinesis complex (15), and a PKCα-PICK1 complex involved in cerebellar long term depression (18,19); these are often associated with structures rich in cytoskeletal components, such as the leading edge of migrating cells, the midbody of dividing cells, or the post-synaptic density of neurons. Amongst the PKC isoforms, PKCα is unique in that it contains an identified C-terminal PDZ (PSD-95/DLG/ZO-1) ligand, which mediates its interaction with the PDZ domain of PICK-1(18); other scaffolds interacting with this PDZ ligand have yet to be characterized.

The membrane-associated guanylate kinase (MAGUK) family is composed of 21 protein scaffolds sharing a core domain structure consisting of a guanylate kinase (GK)

homology region, Src-homology 3 (SH3) or WW domain, and one or more PDZ domains (reviewed in (20)). Among these, the discs large (DLG) MAGUKs, SAP97/DLG1, PSD-93/DLG2, SAP102/DLG3, PSD-95/DLG4, have close homology with the *D. melanogaster* DLG tumor suppressor, and share a nearly identical domain structure of three PDZ domains followed by an SH3 domain and GK domain separated by a region referred to as the hinge or HOOK. While expression of most of these isoforms is restricted to the brain, SAP97/DLG1 (herein referred to as DLG1) expression is nearly ubiquitous, and is often found at actin-rich structures such as the adherens junction (21), the leading edge of migrating astrocytes (10), dendritic spines (22,23), and the midbody of cells undergoing cytokinesis (24). PDZ domains of DLG1 have been demonstrated to interact with many signaling proteins via C-terminal PDZ ligands found on specific channels, receptors, and kinases, such as the Kv4 potassium channels (23), β1-adrenergic receptors (25), and p38 MAPK (26). Other proteins, such as calmodulin (27), GKAP (28), and GAKIN (29), interact in more unique ways with the SH3, HOOK, or GK domains. Additionally, DLG1 homo-oligomerizes via an N-terminal L27 domain, and also can form hetero-oligomers with other L27 domain-containing proteins (30). While DLG1 clearly coordinates local signaling events, it is also a target for phosphorylation by its associated kinases (26,31,32).

In this chapter, we identify a new PDZ domain-containing protein scaffold for PKCα, DLG1, and show that PKCα controls cytoskeletal rearrangements by phosphorylating this scaffold. Specifically, in an array of 96 purified PDZ domains, the PDZ ligand of PKCα interacts with the third PDZ domain of PSD-95 and SAP97/DLG1. This PDZ ligand-PDZ domain interaction is critical for the physical interaction of PKCα

and the scaffold proteins. In addition, DLG1 and PKCα interact functionally when expressed in COS7 cells, forming ring-shaped, actin-rich clusters resembling podosomes in a cPKC activity-dependent manner. Endogenous PKCα and DLG1 are enriched at podosomes in Src-transformed fibroblasts, and at the leading edge of migrating astrocytes. Consistent with a role for PKCα activity in promoting the architecture of these structures, inhibition of cPKC activity disrupts the formation of podosomes in Src-transformed fibroblasts, and slows the migration of primary astrocytes. We generated a phospho-specific antibody to a highly-conserved PKC phosphorylation site on DLG1, Thr656, located in the hinge/HOOK region, and show that, in primary astrocytes and other cell types, it is phosphorylated specifically by cPKC isoforms. Phospho-Thr656 staining overlaps with endogenous DLG staining at podosomes, as well as at the midbody of cells undergoing cytokinesis. By probing a peptide array with pure protein, we demonstrate that this phosphorylated Thr residue creates a binding site for the BRCT domain of Ect2, a GEF for Rho family GTPases. Collectively, these data support that a PKC-DLG-Ect2 signaling module may be fundamental in diverse cellular processes requiring cytoskeletal remodeling, including cytokinesis, migration, and invasion. Thus, our study identifies a new role for PKCα in controlling cytoskeletal remodeling by phosphorylation of a ubiquitous actin-associated scaffold, DLG1.

Materials and Methods

Materials—Phorbol-12,13-dibutyrate (PDBu), phorbol myristate acetate (PMA), Gö6976, and Gö6983 were purchased from CalBiochem. Electrophoresis reagents were from Bio-Rad Laboratories, Inc. Oligonucleotides used in PCR were purchased from IDT. LR clonase and vector conversion kit were purchased from Invitrogen. Restriction

endonucleases were purchased from New England Biolabs. Src-transformed fibroblasts were a generous gift from S. Courtneidge. All other reagents and chemicals were reagent-grade.

Antibodies—Antibodies and dilutions used were: mouse anti-Myc (1:1,000, 9E10; Covance), rat anti-HA (1:2,000; Roche Diagnostics), rabbit anti-GST (1:1,000; Sigma), mouse anti-SAP97/DLG1 (1:500 for western blot, 1:200 for immunofluorescence (IF) staining; Stressgen), rabbit anti-PKCα (1:1000 for western blot, 1:200 for IF staining; Santa Cruz), mouse anti-PKCα (1:1,000; BD transduction) rabbit anti-Tks5 (1:1,000; a generous gift of Sara Courtneidge), rabbit anti-GFP (1:1,000; Cell signaling), mouse anti-actin (1:1,000; Sigma). Secondary antibodies for immunofluorescence were: goat anti-mouse-Alexa 568, goat anti-rabbit-Alexa 488, goat anti-mouse-Alexa 488, and goat anti-rabbit-Alexa 568, all from Invitrogen. Actin was stained in fixed cells using phalloidin-Alexa 647 (1:500 for Src-transformed fibroblasts, 1:100 for COS7 cells; Invitrogen). An antibody to phospho-Thr656 was raised in rabbits immunized with the peptide, Ac-CKERARLK-T(PO_3H_2)-VKFN-NH_2 conjugated to KLH and was affinity purified (NeoMPS); this antibody, rabbit anti-pThr656, was used at 1:10,000 for western blot and 1:1,000 for IF staining.

Construction of plasmids—All mutagenesis was conducted using QuikChange site-directed mutagenesis according to the manufacturer's protocol (Stratagene, Inc.). Sequences encoding the carboxy-terminal 25 amino acids of PKCα (PDZα) were ligated into the pGEX-6P-3 vector (Amersham Biosciences) to create in-frame fusion to GST. Bovine PKCα and PKCα missing the last three amino acids were cloned by PCR into pcDNA3HA to generate an HA fusion to the N-terminus of the PKC constructs to form

HA-PKCα and HA-PKCαΔPDZ. Human PKCα was cloned from RNA isolated from LN444 cells and fused in frame to the C-terminus of mRFP in pCDNA3 to make RFP-PKCα. Human PKCα missing the C-terminal three amino acids was amplified using PCR and RFP was similarly fused to the N-terminus in pCDNA3 (RFP-PKCαΔPDZ). An entry clone encoding the BRCT domains of ECT2 (residues 1-333) was constructed using pDONR to produce pENTR-BRCT. A Gateway destination vector for N-terminal fusion of GST (pDEST-GST-N) for expression in bacteria was constructed by digesting pGEX6P3 vector with *SmaI* and ligating with RFC.1 Gateway insert. pDEST-GST-N was recombined with pENTR-BRCT using LR clonase (Invitrogen) to produce GST-BRCT. CFP-tagged SAP97/DLG1 (i3) was a generous gift from M. Dell'Acqua, Myc-SAP97/DLG1 was a generous gift from C. Garner, and Myc-PSD95 was a generous gift from M. Sheng.

Purification of GST-tagged proteins—BL21 (DE3) cells were transformed with GST-PDZα or GST-BRCT constructs described above. Cells were grown until Abs_{600}=0.6 at 37^{o} and then induced with 1 mM IPTG for 4 hours at room temperature. Pelleted cells were homogenized in 50 mM Tris, pH 7.5, 200 mM NaCl, 1 mM EDTA, 1 mM DTT, containing 300 nM PMSF, 500 nM benzamidine, 500 ng/ml leupeptin, and 1 mg/ml lysozyme and rocked for 30 minutes at 4^{o}C followed by brief sonication. The lysate was treated with 100 μg/m1 DNAase and cleared by centrifugation at 14,000 X g for 30 minutes at 4^{o}C. GST fusion proteins were purified from the filtered lysate using the Profinia Protein Purification System according to the manufacturer's specifications (BioRad). The eluted pure protein was dialyzed against 20 mM HEPES, pH 7.5, 50 mM NaCl.

Peptide overlay experiments—For dot blot analysis of phospho-Thr656 antibody, the peptides Ac-CKERARLK-T(PO_3H_2)-VKFN-NH_2 and Ac-CKERARLKTVKFN-NH_2 were synthesized (NeoMPS) and spotted onto nitrocellulose. Blots were incubated with increasing concentrations of rabbit anti-pThr656 antibody to determine phospho-specificity and appropriate antibody dilutions. Membranes containing 96 putative PDZ domains were prepared as described (35). 0.5 mg/ml of purified GST-PDZα fusion protein was overlaid onto the array and detected by far Western blotting as described previously (33). For the overlay of GST-BRCT on DLG1, DLG1 was divided into 18-amino-acid peptides, with a 2-amino-acid shift, and synthesized using the INTAVIS MultiPep peptide synthesizer (INTAVIS Bioanalytical Instruments AG), which spotted the peptides onto an AC-S01 type amino-PEGylated membrane (INTAVIS AG). After activation of the membrane with ethanol, the membrane was blocked with 5% milk, washed, and then incubated overnight with GST-BRCT at 0.75 μg/ml in 2.5% milk. After incubation with GST-BRCT protein, the peptide array was analyzed by far Western blot with an antibody to GST.

Cell culture and immunoblotting—All cell lines were plated and maintained in Dulbecco's modified Eagle's medium (Cellgro) containing 5-10% fetal bovine serum and 1% penicillin/streptomycin at 37 °C in 5% CO_2. For imaging, cells were plated in sterilized 35-mm imaging dishes at 60% confluency and on glass coverslips for immunofluorescence. Transient transfections for COS7 cells were carried out using Fugene6 (Roche Diagnostics) or Jetprime reagents (Polyplus Transfection); for HEK 293T cells, Effectene was used (Qiagen). For immunoblotting, transfected cells were lysed in Buffer A (50 mM Tris [pH 7.5], 10 mM sodium pyrophosphate, 50 mM NaF, 5

mM EDTA, 1% Triton, 1 mM DTT, 200 mM benzamidine, 40 mg/ml leupeptin, and 1 mM PMSF) or in 1X Laemelli sample buffer, where indicated. Lysates were analyzed by Western blot; individual blots were probed using the indicated antibody, and, where indicated, stripped using 0.3 M NaOH and reprobed.

Immunoprecipitation and GST pull-down experiments—To examine the interaction of PKCα with MAGUK scaffolds, HEK 293T cells were transfected with Myc-PSD95 or Myc-SAP97/DLG1 alone or together with either HA-PKCα or HA-PKCαΔPDZ. Approximately 24 h after transfection, the cells were lysed in Buffer A and centrifuged at 16,000 x g for 5 min at 22 °C, and the detergent-solubilized supernatants were incubated with monoclonal antibody against HA (Covance, 1:450) overnight at 4 °C. The immune complexes were collected with Ultra-Link protein A/G beads for 1 hour, washed with Buffer A, followed by a version of Buffer A containing 50 mM total NaCl, and analyzed by SDS-PAGE and Western blotting. To examine the interaction between phosphorylated DLG1 and the purified GST-tagged BRCT domains, COS7 cells were transfected with CFP-DLG1 and either left untreated or treated with PMA (200 nM, 20 min) and Calyculin A (50 nM, 10 min) to maximize phosphorylation of soluble DLG1. Cells were lysed in Buffer A and lysates were incubated with buffer or purified GST-BRCT overnight; complexes were collected using GST beads (GE healthcare biosciences), and analyzed by Western blot.

Immunofluorescence staining and live cell imaging—For immunofluorescence staining, cells were plated on glass coverslips, treated as indicated, and fixed with 3% paraformaldehyde, 2% sucrose in PBS pH 8.0 for 20 min before quenching in 50 mM NH_4Cl in 10 mM PIPES pH6.8, 150 mM NaCl, 5 mM EGTA, 5 mM Glucose, and 5 mM

$MgCl_2$ for 15 min. Fixed cells were incubated in blocking buffer (10% goat serum in PBS, 0.1% Tween) for 1 hour prior to incubating overnight with primary antibodies diluted in blocking buffer. After washing, indicated secondary antibodies were added at a dilution of 1:600 in PBS, 0.1% Tween for 2.5 hours. At this time, phalloidin-647 was also added to visualize F-actin. Washed slides were mounted using vectashield. For live cell imaging, cells were rinsed once with, and imaged in, Hanks Balanced Saline Solution (Cellgro) containing 1 mM $CaCl_2$. Images were acquired on a Zeiss Axiovert microscope (Carl Zeiss Microimaging, Inc.) using a MicroMax digital camera (Roper-Princeton Instruments) controlled by MetaFluor software (Universal Imaging, Corp.). Optical filters were obtained from Chroma Technologies. For live cell imaging, using a 10% neutral density filter, CFP and RFP images were obtained every 10-15 s through a 420/20-nm excitation filter, a 450-nm dichroic mirror, and a 475/40-nm emission filter (CFP) or through a 560/25-nm excitation filter, a 593-nm dichroic mirror, and a 629/53-nm emission filter (RFP). Excitation and emission filters were switched in filter wheels (Lambda 10–2, Sutter). For acquisition of immunofluorescence images, using a 10% neutral density filter, Alexa 488 images were obtained through a 480/30-nm excitation filter, a 505-nm dichroic mirror, and a 535/45-nm emission filter; Alexa 568 images were obtained in the same manner as RFP images above; and Alexa 647 images were obtained through a 635/20-nm excitation filter, a 660-nm dichroic mirror, and a 680/30-nm emission filter. Integration times were 200 ms for CFP and Alexa 647, and 100 ms for RFP, Alexa 568, and Alexa 488.

Tallying podosomes in live cells—RFP-PKCα and CFP-DLG1 or CFP-DLG1-T656A were transfected into COS7 cells; cells were treated with PMA (200 nM) for 20 min to

initiate clustering of the two proteins into podosome-like structures. For 10 min, total cells and cells containing 3 or more podosome-like structures were tallied. Over 100 cells total on 5 separate dishes were counted for each experimental setup.

Astrocyte preparation and migration assay—Primary astrocyte cultures were prepared from postnatal day 2 mouse pups similar to previously described methods (34). Briefly, cerebral hemispheres were separated from whole brain and the meninges removed. Hemispheres were homogenized by physical dissociation with scissors and incubation with 0.25% trypsin (Gibco) and 0.5 g/L pancreatin (Sigma) in HBSS for 30 minutes at 37°C. Cell suspensions were spun down at 1,200 rpm for three minutes and resuspended in DMEM with 10% FBS. Cells were plated at approximately one brain per 75 cm^2 tissue culture flask and incubated for 11 days at 37°C/5% CO_2., with new culture media added every third day. Flasks were agitated at 150 rpm for 30 minutes to remove microglia and then at 240 rpm for 16-20 hours to remove oligodendrocytes. The remaining adherent astrocytes were re-plated at approximately 3 X 10^5 cells per ml on poly-L-lysine-coated six-well dishes. Preparations were checked for GFAP expression using immunofluorescence; all cultures subjected to scratch analysis had at least 80% GFAP-positive cells. For migration assays, 48 hours after plating, confluent monolayers were treated with mitomycin C (10 μg/ml, Calbiochem) in DMEM with no serum for one hour to inhibit cell proliferation, then washed three times with PBS. Fresh DMEM containing 10% FBS and either DMSO or Gö6976 (500 nM, Calbiochem) was added to the cells. After 20 minutes of pretreatment, monolayers were scratched once with a 10 μl pipet tip, and pictures of the central region of the scratch were taken immediately and 12, 24, and 42 hours after scratch with a 5X objective. Areas left uncovered were quantified

using ImageJ (NIH) and averaged over three different astrocyte preparations. For immunofluorescence staining, cells were plated on poly-L-lysine-coated coverslips and media was replaced on cells 24 hours prior to scratch. Gö6976 was added at the time of the scratch where indicated. Cells were fixed 4 hours post-scratch, and stained as described above.

Results

The C-terminus of PKCα encodes a functional PDZ ligand. Previous studies have demonstrated that this PDZ ligand is critical for PKCα's role in cerebellar long term depression via interactions with the scaffold PICK-1(19). In order to find additional interacting partners for PDZ ligand of PKCα, we expressed and purified from bacteria the 25 C-terminal residues of PKCα with GST fused to the N-terminus. This fusion protein was overlaid on a membrane containing 96 His-tagged PDZ domains from mammalian protein scaffolds purified from bacteria. Figure 5.1 shows that the GST-tagged C-terminus of PKCα interacts with the third PDZ domain from two protein scaffolds in the membrane-associated guanylate kinase (MAGUK) family: post-synaptic density protein 95 (PSD95) and synapse-associated protein 97 (SAP97), also called discs large homolog 1 (DLG1). Purified GST alone showed no interaction with the array (35).

Previous studies have determined that endogenous PSD95 and SAP97/DLG1 co-immunoprecipitate with PKCα from rat brain lysates; however, these studies attributed the interaction to a common interacting partner, AKAP79/150 (36). Thus, it is important to determine whether the direct PDZ interaction contributes to the interaction between full-length PKCα and the MAGUK protein scaffolds in the cellular context. HEK 293T

cells were transfected with Myc-tagged PSD95 (Myc-PSD95), Myc-PSD95 and HA-tagged PKCα (HA-PKCα), or Myc-PSD95 and HA-PKCα with the C-terminal three amino acids deleted, which destroys the PDZ ligand (HA-PKCαΔPDZ). From cellular lysates, PKCα constructs were immunoprecipitated using HA antibodies, and associated Myc-PSD95 was assessed by immunoblot. Figure 5.2A shows that Myc-PSD95 interacts with HA-PKCα; this interaction is greatly reduced upon deletion of the C-terminal three amino acids. Similarly, Myc-tagged DLG1 (Myc-DLG1) interacts with HA-PKCα but not with HA PKCαΔPDZ (Figure 5.2B). These data show that the PDZ ligand constitutes a critical contact between these MAGUK scaffolds and PKCα.

Since DLG1 has the same nearly-ubiquitous tissue distribution as PKCα, we sought to determine whether PKCα and DLG1 interact functionally in cells. First, COS-7 cells were transfected with RFP-PKCα and CFP-DLG1; the proteins appear diffusely distributed in the cytosol, although DLG1 does show some pre-localization to the plasma membrane. Treatment with the PKC activator PMA (200 nM) consistently recruits the two proteins to form ring-shaped clusters in COS7 cells (Figure 5.3A, white arrow). Furthermore, upon addition of cPKC inhibitor, Gö6976 (500 nM), the ring-shaped clusters disperse, and PKCα redistributes to amorphous clusters at the bulk plasma membrane (due to high-affinity phorbol binding via its C1 domain, Figure 5.3A, white asterisk). After inhibition of cPKC, DLG1 also remains associated with amorphous membrane-bound PKCα. This PKC activity-dependent ring-shaped clustering does not depend on the presence of the PDZ ligand, but cells expressing RFP-PKCαΔPDZ appeared to contain fewer amorphous clusters (compare images in Figure 5.3B to those in

Figure 5.3A). Figure 5.3C shows that these ring-shaped clusters of PKCα and DLG1 contain actin, and this, combined with the shape of the clusters, strongly suggests these are podosome-like structures.

Src-transformed fibroblasts spontaneously form podosomes (37), so we examined the distribution of endogenous PKCα and DLG1 in these cells. Figure 5.4A shows prominent, ring-shaped DLG1 staining in these cells that co-localizes with actin and a marker for podosomes, Tks5 (37). Similarly, PKCα staining co-localizes with Tks5 and actin at podosomes in these cells (Figure 5.4B). To determine whether cPKC activity was also required for the formation of podosomes in Src-transformed fibroblasts, we added the cPKC inhibitor Gö6976 and monitored podosome formation by staining for DLG1, Tks5, and actin. Figure 5.5 shows that the ring-shaped clustering of DLG1, Tks5, and actin (left panels) is markedly disrupted after treatment of Src-transformed fibroblasts with 500 nM Gö6976 for 30 min (right panels). In particular, although Tks5 remains associated with small punctate clusters of actin, DLG1 appears to be completely redistributed away from these proteins to the membrane. These results suggest that the activity of PKCα and recruitment of the DLG1 scaffold to actin or actin-associated proteins contributes to the maintenance of podosome architecture.

The recruitment of DLG1 into podosomes in a cPKC activity-dependent manner prompted us to question whether DLG1 is a direct substrate of PKCα. Indeed, a Thr residue at position 656 (rat DLG1 numbering) in the hinge/hook region of DLG1 just N-terminal to the GK domain is predicted with high confidence (Scansite (38)) to be a phosphorylation site for either cPKCs or nPKCδ. In addition, the phosphorylatable Thr

and eight residues immediately surrounding the site, which are included in all splice variants of DLG1, are conserved in two other brain-specific DLG homologs, SAP102 and PSD93, and is conserved in DLG1 in all vertebrate species examined (Fig 6A). However, in PSD-95, the residue at this position is Ala. This phosphorylation site is also loosely conserved in a member of the MAGI scaffold family, MAGI-3; despite the inverted domain structure of the MAGI scaffold family relative to the PSD-95 family, the phosphorylatable Thr is also located just N-terminal to the GK domain. Interestingly, in a concurrent, larger-scale screen for mammalian PDZ interactions, PKCα's PDZ ligand was also found to interact with MAGI-3, SAP102, and PSD93 in addition to PSD-95 and DLG1 (39). Thus, we sought to determine whether DLG1 was phosphorylated at this highly-conserved site by PKCα in cells. To study this, we generated an antibody that recognizes phospho-Thr656. Figure 5.6B shows this antibody recognizes phospho-T656 over the dephosphorylated peptide with more than an order-of-magnitude selectivity for the phosphorylated peptide. Furthermore, in primary astrocytes (Figure 5.6C) and in other cells (COS7, Hela, Caco-2, HEK 293T; data not shown), phosphorylation of endogenous DLG1 at Thr656 is induced by PMA and prevented (or reversed, not shown) by Gö6983, a nPKC and cPKC inhibitor, or Gö7976, a specific inhibitor for cPKC isoforms. In some of these cell lines (COS7, 293T, other cells not yet determined), PKCα is the only cPKC isoform expressed; thus, in these cells, endogenous DLG1 is phosphorylated specifically by PKCα in response to PMA.

Because the PDZ ligand serves as an important contact in mediating the interaction between DLG1 and PKCα, we tested whether this interaction was critical for

phosphorylation of DLG1 by PKCα. First, we expressed CFP-DLG1 alone, CFP-DLG1 with HA-PKCα, or CFP-DLG1 with HA-PKCαΔPDZ and tested whether exogenous DLG1 is phosphorylated in response to PdBu (200 nM, Figure 5.7). Interestingly, CFP-DLG1 alone is not phosphorylated by endogenous PKC isoforms in response to PdBu. When PKCα is co-expressed, Thr656 is phosphorylated in response to PdBu. However, deletion of the PDZ ligand does not interfere with the ability of expressed PKCα to phosphorylate expressed DLG1. These results imply that the PDZ interaction may not be important for phosphorylation of DLG1 by PKCα; alternatively, overexpression may overcome the requirement for this contact for phosphorylation of Thr656 by PKCα. Attempts to disrupt phosphorylation of the endogenous DLG1 by transfecting in a GST-fusion of the C-terminus of PKCα did not consistently block phosphorylation (not shown), and it is possible that, in isolation, this low-affinity sequence is not sufficient to disrupt the interaction of endogenous PKCα with the protein complex.

Next, since stimulation of PKC activity promotes the recruitment of PKCα and DLG1 into podosomes, we tested whether Thr656 is phosphorylated at podosomes. Figure 5.8A shows COS7 cells transfected with CFP-DLG1 and HA-PKCα, stimulated with PMA as before to promote formation of podosome-like structures. PMA-stimulated phospho-Thr656 staining (top row) overlaps with total DLG1 (second row) and actin staining (third row); the phospho-specific staining, normalized to the same window and level for each set of conditions, is reversed with Gö6976. Similarly, in Src-transformed fibroblasts, phospho-Thr656 staining co-localizes with total DLG1 and actin staining (Figure 5.8B). Staining of phospho-Thr656 in Src-transformed fibroblasts is reversed by

Gö6976 treatment (Figure 5.8C). Analysis of Src-transformed fibroblasts by immunoblot reveals that phosphorylation of Thr656 is not dramatically stimulated with PMA treatment, but is reversed by Gö6976 (Figure 5.8D). Collectively, these data demonstrate that phosphorylation of DLG1 at Thr656 occurs at podosomes, and may be constitutively stimulated in Src-transformed fibroblasts.

We also tested whether mutation of Thr656 to Ala alters the ability of PKC and DLG1 to perform the cytoskeletal rearrangements necessary to promote podosome formation. However, cells expressing CFP-DLG1-T656A only showed a modest reduction in podosome formation compared to cells expressing wild-type DLG1 (27 out of 120 cells, 23%, contained 3 or more podosomes compared to 32 out of 107 cells, 30%, for wild-type). This may be due to the cells' ability to sequester DLG1-T656A and utilize the endogenous DLG1 for podosome formation, and perhaps a more dramatic effect would be seen in cells depleted of the endogenous DLG1. Application of a more stringent threshold for positive podosome scoring, such as 5 podosomes or more per cell, might also yield more differences between the wild-type protein and mutant.

In primary rat astrocytes, DLG1 has been shown to co-localize with PKCζ at the leading edge 4 hours after these cells have begun to migrate to fill a scratch wound (10). To examine whether PKCα is also involved in this process, we stained primary mouse astrocytes for DLG1 and PKCα before and 4 hours after generating a scratch wound. In many cells, PKCα and DLG1 are strongly co-localized at the leading edge of migrating astrocytes (Figure 5.9, middle panels). When these cells are treated with Gö6976 prior to wounding, there is a dramatic reduction in leading edge staining of both proteins (as in Figure 5.9, bottom panels), as well as a reduction in the ability of these cells to migrate to

fill the wound. Figure 5.10 shows a quantification of astrocyte migration during this wound healing assay, with an increase in the percentage of the wound area remaining open, and a concomitant decrease in the area covered, in the presence of cPKC inhibitor, Gö6976. These data support the hypothesis that PKCα/DLG1 signaling module contributes to cytoskeletal rearrangements during migration of primary astrocytes.

In addition to visualizing phospho-Thr656 staining at the podosome-like clusters in COS7 cells formed by exogenous DLG1 and PKCα in response to PMA, we also visualized pronounced staining of phospho-Thr656 overlapping with total DLG staining at the midbody of untransfected COS7 cells (and primary astrocytes, not shown) undergoing cytokinesis (Figure 5.11). This staining is not reversed by the cPKC inhibitor Gö6976 (not shown); so it is not likely PKCα-specific. It has previously been reported that DLG1 accumulates at the midbody of dividing cells ((24), Figure 5.11). Also, the conserved residues surrounding Thr656 comprise a good consensus for BRCT domain binding, with a highly conserved Phe in the +3 position (40). One key protein that participates in cytokinesis, Ect2, is a GEF that contains tandem autoinhibitory N-terminal BRCT domains (41,42). Thus, we sought to determine whether the BRCT domains of Ect2 interact with phosphorylated DLG1. An 18-mer peptide walk, shifting every two amino acids, of the protein sequence of SAP97/DLG1 was arrayed onto an AC-S01 type amino-PEGylated membrane. Peptides containing a phosphorylated Thr residue at position 656 were also arrayed on the membrane. The membrane was overlaid with pure GST-tagged BRCT domains (amino acids 1-333) from Ect2 and incubated with an antibody to GST to detect binding of the BRCT domains to peptides on the array. Figure 5.12A shows selected regions of the peptide walk of DLG1. Peptides containing

phosphorylated Thr656 bind better to the BRCT domains than do peptides containing unphosphorylated Thr656 (Figure 5.12A, compare top two panels). Also notable is a segment in the third PDZ domain of DLG1 containing a serendipitous series of peptides encoding an ExxF motif (bottom panel); these peptides also interact with GST-BRCT in a manner similar to the phospho-Thr 656-containing peptides. It is interesting to note that both the phospho-Thr656 peptides and control ExxF-motif peptides bind with increasing intensity as the motif is positioned closer to the N-terminus of the peptide; this may be due to greater accessibility of the N-terminus of the peptide on the array, as the peptides are attached by the C-terminus to the membrane.

To validate the phospho-specific interaction seen on the peptide array, we added the purified GST-BRCT to lysates from either untreated COS7 cells transfected with CFP-DLG1 or cells transfected with CFP-DLG1 that had been treated with PMA (200 nM, 20 min) and Calyculin A (50 nM, 10 min) to maximize phosphorylation of CFP-DLG1. GST-BRCT was precipitated from solution using GST beads, and bound DLG1 was assessed by immunoblot. GST-BRCT weakly, but selectively, interacts with the phosphorylated DLG1 (Figure 5.12B). Thus, phosphorylation of DLG1 by PKCα creates a consensus site for the BRCT domains of the GEF Ect2, which, in the context of a larger protein complex, may stimulate Rho family GTPase activity. It is plausible that stimulation of Ect2 by the PKCα-DLG1 complex may occur at podosomes and may also occur at the leading edge of migrating astrocytes, contributing to the reorganization of the cytoskeleton at these structures. A different PKC isoform or other kinase may contribute to phosphorylation of DLG1 and stimulation of Ect2 during cytokinesis.

Discussion

Data presented in this chapter uncover a new regulatory mechanism in PKC signaling in which a specific PKC isozyme binds and modifies a scaffold protein to recruit effector proteins that drive cytoskeletal rearrangements. In particular, the data support a model in which PKCα binds the protein scaffold DLG1 and phosphorylates DLG1 at a conserved Thr residue to create a consensus site for the phosphopeptide binding module of the RhoGEF Ect2. Figure 5.13 shows a simplified model of how this signaling scaffold promotes cytoskeletal rearrangements. Specifically, binding of the C-terminal PDZ ligand of PKCα to the third PDZ domain of DLG1 enriches kinase activity at the scaffold and leads to phosphorylation at Thr656. Phospho-Thr656 recruits the BRCT domains of Ect2, which localizes active Rho GTPases in the vicinity of the scaffold, promoting cytoskeletal rearrangements. We show that this mechanism drives podosome formation in Src-transformed fibroblasts and contributes to migration of primary mouse astrocytes.

The DLG family: scaffolds for PKCα

Previous studies determined that PKCα interacts with both SAP97/DLG1 and PSD-95 by co-immunoprecipitation of endogenous proteins from brain extracts (36). However, the authors of this study attributed the binding to a common interacting protein, AKAP79/150. Our studies show that this interaction is direct, and mediated by the PDZ ligand of PKCα and the third PDZ domain of the two scaffold proteins. Concurrent with our study, a large-scale effort to characterize PDZ interactions in the mouse proteome verified this contact point, and demonstrated interactions between PKCα and the entire

DLG sub-family of MAGUK scaffolds (39). In the case of DLG1, PKCα docking to the third PDZ domain likely enriches kinase activity at the scaffold, promoting phosphorylation of Thr656. This may also be the function of PKCα at other MAGUK scaffolds, as most of these contain the highly-conserved phosphorylation motif. However, PSD-95 contains an Ala at the phospho-acceptor site, and the residues surrounding the site are similarly not conserved. PKCα almost certainly docks at the PSD-95 scaffold to phosphorylate other common binding partners, and the elucidation of these substrates would help determine how interacting with PSD-95 influences PKCα signaling.

Phosphorylation of DLG controls recruitment of Ect2

Phosphorylation of Thr656 of DLG1 creates a binding site for the phospho-peptide binding BRCT domains of the RhoGEF, Ect2 (Figure 5.13). Engagement of the BRCT domains has been shown to promote the GEF activity of Ect2 by relieving autoinhibition of the GEF domain (43). During cell division, Ect2 stimulates RhoA at the midbody to promote the formation of a contractile ring of actin; thus, it is a critical participant in cytokinesis (42). Indeed, expression of the BRCT domains alone blocks completion of cytokinesis, probably by competing with the endogenous Ect2 for stimulatory binding partners (44). Intriguingly, phospho-Thr656 staining is strongly localized where DLG1 accumulates at the midbody of cells undergoing cytokinesis, and DLG1 silencing has also been demonstrated to interfere with the completion of cytokinesis (24). A previous study has implicated four Polo-like kinase phosphorylation sites on the midbody protein, HsCyk-4, as the interacting partners for the BRCT domains of Ect2. In these experiments, Ect2 does interact with HsCyk-4 in a phospho-dependent

manner (45). However, these phosphorylation sites do not resemble canonical interaction sites for BRCT domains, which typically prefer to bind a single phosphorylated residue (40). Furthermore, BRCT domains select for peptides containing a Phe residue in the +3 position following the phosphorylatable residue (40), and the Thr656 phosphorylation site on DLG1 fits this consensus perfectly (See Figure 5.6A). A different model consistent with data presented in the previous study is that phosphorylation of HsCyk-4 indirectly promotes phosphorylation of Thr656 on DLG1, and that these proteins are part of a larger complex at the midbody. Alternatively, perhaps both sites are capable of stimulating Ect2, and with one site serving as the primary driving force and the other serving as an accessory to modulate the rate of cleavage furrow ingression.

The PKCα-DLG1 signaling module in podosome formation and astrocyte migration

Consistent with our studies, PKCα has previously been implicated in podosome formation in endothelial cells (11). In fact, constitutively-active PKCα (but not other constitutively-active isoforms) promotes podosomes in this system. However, a role for DLG1 in podosome formation has never been proposed, and neither PKCα nor DLG1 has been demonstrated to be required for the formation of these structures in Src-transformed fibroblasts. Interestingly, however, active RhoA has been demonstrated at podosomes in these cells, and the activity of RhoA is required for their formation (46). Our results show cPKC activity is required for podosome maintenance in Src-transformed fibroblasts as well, which is in agreement with our model placing PKCα-mediated phosphorylation of DLG1 upstream of RhoA activation in this system.

We also show conventional PKC activity to be required for astrocyte migration, and

demonstrate co-localization of PKCα and DLG1 at the leading edge. In a previous study, CDC42-stimulated PKCζ activity was demonstrated to be essential for Rat astrocyte migration, and PKCζ and DLG1 were found to co-localize at the leading edge (10). It may be that the PKCα-DLG-Ect2 signaling module is upstream of CDC-42-stimulated PKCζ activity in this context. While we have not yet investigated whether Ect2 localizes to the leading edge of migrating astrocytes, two of the few published reports of Ect2 activity outside of its well-documented role in cytokinesis are in glioma invasion (47,48). In addition, the placement of PKC isoforms both upstream and downstream of small GTPases could be a mechanism by which an initiating signal is reinforced to promote cell polarity.

PKC-DLG signaling module in control of Rho GTPases

PKC has well-documented actions toward regulators of Rho family GTPases. Specifically, a signaling pathway involving Src and PKC promotes activity of p190RhoGAP, which acts to selectively decrease the activity of RhoA (49). In addition, although Ect2 is often described as a GEF for RhoA (42), the initial characterization of Ect2 demonstrated it can also stimulate Rac and CDC42 (41). An intriguing possibility is that stimulation of the promiscuous GEF, Ect2, by the PKC-DLG signaling scaffold, and concurrent stimulation of the RhoA-specific GAP, p190RhoGAP, by PKC would provide a net effect of selective stimulation of Rac or CDC42 in some cellular contexts. This action would be more in keeping with the localization of the PKC-DLG signaling module to the leading edge of migrating cells, as Rac is implicated in formation of lamellopodia found at the leading edge. However, in some cases, it is entirely possible that RhoA is the target of the PKC-DLG-Ect2 signaling scaffold. As was previously mentioned, active

RhoA has been demonstrated at podosomes, and is critical for the formation of these structures (46). A complex interplay between Rho and Rac is definitely required for the completion of cytokinesis (42,50), and it is interesting to speculate that the recently-defined role for PKCε in cytokinesis (15) might involve phosphorylation of DLG1 and associated proteins.

Evidence for other PKC-DLG signaling modules

Our study provides evidence 1) for interaction between PKCα and DLG family members dictated by a unique PDZ ligand, 2) for cPKC-specific phosphorylation of the endogenous DLG1 scaffold in response to PMA, and 3) for cPKC-specific effects on cytoskeletal rearrangements in certain cellular contexts. However, it is clear that specificity within the PKC family is determined primarily by cellular context rather than by determinants intrinsic to the substrate sequence (51). Thus it is reasonable that other PKC isoforms can complex with DLG family members by other mechanisms and can promote phosphorylation of Thr656 (or the analogous conserved residue in other DLG isoforms) to stimulate the Ect2-mediated cytoskeletal changes. For example, evidence for PKCα in cytokinesis is lacking, but phosphorylated DLG1 does accumulate at the midbody and it is more likely that PKCε could be the upstream kinase in this context (15). Likewise, DLG isoforms in the brain have been implicated not only in coordinating signaling at the post-synaptic density, but also in dendritic spine morphogenesis (52,53). Very recent reports by Fields and colleagues have demonstrated a complex between Par6/PKCι and Ect2 that promotes metastasis in non-small cell lung cancer (54). In these studies, they very clearly define a role for Ect2 outside of cytokinesis in the promotion of cancer invasiveness. In fact, Par6-PKCι promoted redistribution of Ect2 away from the

nucleus. Intriguingly, they show that this PKCι-ECT2 signaling module promotes Rac activation rather than RhoA activation, supporting the idea that PKC can direct specificity amongst members of the Rho family as discussed above. These studies suggest that this PKC-DLG-Ect2 signaling module may be very important in the promotion of Rho family activation outside of the traditionally-defined role of this GEF in cytokinesis, and that this could be a critical signaling module to target in the prevention of tumor metastasis.

Future directions

Future studies are critical to unambiguously determine that this PKCα-DLG1-Ect2 signaling module contributes to normal cellular functions and to promotion of disease. Foremost, it is important to show that Ect2 localizes at podosomes and is necessary for their formation. Also, it is important to show that this complex promotes activation of Rho family members in cells. To define a role for this complex in cell migration, it is important to show that Ect2 is a component of leading edge complexes in primary astrocytes. To support a role for the PDZ-mediated interaction of PKCα and DLG1 in these leading edge complexes, development of a high-affinity peptide inhibitor targeting this interaction would be very helpful. Indeed, certain viruses encode proteins harboring a PDZ ligand that targets the DLG PDZ domains, a feature that is critical for their pathogenesis (55). Studies could also be carried out in cells derived from PKCα$^{-/-}$ or DLG1$^{-/-}$ mice (56,57), or in cells depleted of Ect2, to determine whether these proteins are essential for Rho family activation or for the formation of podosomes in response to Src transformation. These cells could also be supplemented with proteins containing functional mutants to define the roles of specific protein domains. A real challenge to

defining specific roles of PKC and DLG isoforms will likely be that other proteins in the family can compensate for each other, as evidenced by the subtle phenotypes generally observed when silencing members of each family in mice (reviewed in (20,58)), with the exception of PKCι, which is lethal (59), and DLG1, which results in craniofacial dysmorphogenesis (56). Perhaps crossing DLG knock-out mice with PKC knockout mice will yield more answers to the cellular roles of these proteins. Finally, it would be interesting to investigate whether phosphorylation of DLG family members is elevated in metastatic cancer. Candidates would include non-small cell lung cancer, in which levels of PKCι and Ect2 are elevated and are shown to be responsible for the invasive behavior of the cancer (54), or glioma, in which PKCα has been implicated (60-62) and Ect2 has a demonstrated role in invasive behavior (48).

Acknowledgements

I thank Audrey O'Neill for preparing mouse astrocytes and quantifying astrocyte migration. I thank C.J. Allison for preparing the SAP97/DLG1 peptide array, and Erin Garcia for performing the initial PDZ domain array screen. I thank Noel Warfel, Marshall Peterman, Craig Garner, Morgan Sheng, and Mark Dell'Acqua for DNA constructs. I also thank Mark Dell'Acqua, Randy Hall, Maya Kunkel, Gloria Reyes, Verline Justilien, Alan Fields, and Lindsay Lewellyn for helpful discussions.

A)

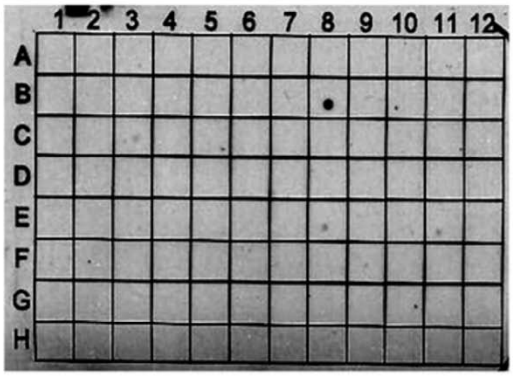

B)

Bin	PDZ Domain	Bin	PDZ Domain	Bin	PDZ Domain
A1	MAGI-1 PDZ1	C9	ERBIN PDZ	F5	MUPP1 PDZ10
A2	MAGI-1 PDZ2	C10	ZO-1 PDZ1	F6	MUPP1 PDZ12
A3	MAGI-1 PDZ3	C11	ZO-1 PDZ2	F7	MUPP1 PDZ13
A4	MAGI-1 PDZ4+5	C12	ZO-1 PDZ3	F8	PTPN13 PDZ1
A5	MAGI-2 PDZ1	D1	ZO-2 PDZ1	F9	PTPN13 PDZ3
A6	MAGI-2 PDZ2	D2	ZO-2 PDZ2	F10	PTPN13 PDZ4+5
A7	MAGI-2 PDZ3	D3	ZO-2 PDZ3	F11	PDZK1 PDZ1
A8	MAGI-2 PDZ4	D4	ZO-3 PDZ1	F12	PDZK1 PDZ2
A9	MAGI-2 PDZ5	D5	ZO-3 PDZ2	G1	PDZK1 PDZ3
A10	MAGI-3 PDZ1	D6	ZO-3 PDZ3	G2	PDZK1 PDZ4
A11	MAGI-3 PDZ2	D7	C2PA PDZ	G3	PDZK2 PDZ1
A12	MAGI-3 PDZ3	D8	GIPC PDZ	G4	PDZK2 PDZ2
B1	MAGI-3 PDZ4	D9	MALS-1 PDZ	G5	PDZK2 PDZ3
B2	MAGI-3 PDZ5	D10	MALS-3 PDZ	G6	PDZK2 PDZ4
B3	NHERF-1 PDZ1	D11	Densin-180 PDZ	G7	LNX1 PDZ1
B4	NHERF-1 PDZ2	D12	Rhophilin-1 PDZ	G8	LNX1 PDZ2
B5	NHERF-2 PDZ1	E1	Rhophilin-2 PDZ	G9	LNX1 PDZ3
B6	NHERF-2 PDZ2	E2	Harmonin PDZ1	G10	LNX1 PDZ4
B7	PSD-95 PDZ1+2	E3	Harmonin PDZ2	G11	LNX2 PDZ1
B8	PSD-95 PDZ3	E4	Neurabin PDZ	G12	LNX2 PDZ2
B9	CNRasGEF PDZ	E5	Spinophilin PDZ	H1	LNX2 PDZ4
B10	CAL PDZ	E6	α1-syntrophin PDZ	H2	PTPN4 PDZ
B11	nNOS PDZ	E7	ß1-syntrophin PDZ	H3	Rho-GEF PDZ
B12	INADL PDZ5	E8	ß2-syntrophin PDZ	H4	RA-GEF PDZ
C1	INADL PDZ6	E9	γ1-syntrophin PDZ	H5	Enigma PDZ
C2	SAP97 PDZ1+2	E10	γ2-syntrophin PDZ	H6	LARG PDZ
C3	SAP97 PDZ3	E11	PAPIN PDZ	H7	PTPN3 PDZ
C4	SAP102 PDZ1+2	E12	MAST-205 PDZ	H8	Shank1 PDZ
C5	SAP102 PDZ3	F1	MUPP1 PDZ1	H9	Tamalin PDZ
C6	Chap110 PDZ1+2	F2	MUPP1 PDZ6	H10	PAR-3 PDZ1
C7	Chap110 PDZ3	F3	MUPP1 PDZ7	H11	PAR-3 PDZ2
C8	E6TP1 PDZ	F4	MUPP1 PDZ8	H12	PAR-3 PDZ3

Figure 5.1. The PDZ ligand of PKCα interacts with the 3rd PDZ domain of both DLG1 and PSD95. *A,* The C-terminal 25 amino acid residues of PKCα fused to an N-terminal GST tag were purified from bacteria and overlaid on an array of 96 purified PDZ domains from a selection of PDZ domain-containing scaffolds. Positive hits were visualized on the array by probing with an antibody to GST. *B,* List of purified PDZ domains on the array. These data appear courtesy of Erin Garcia and Randy Hall.

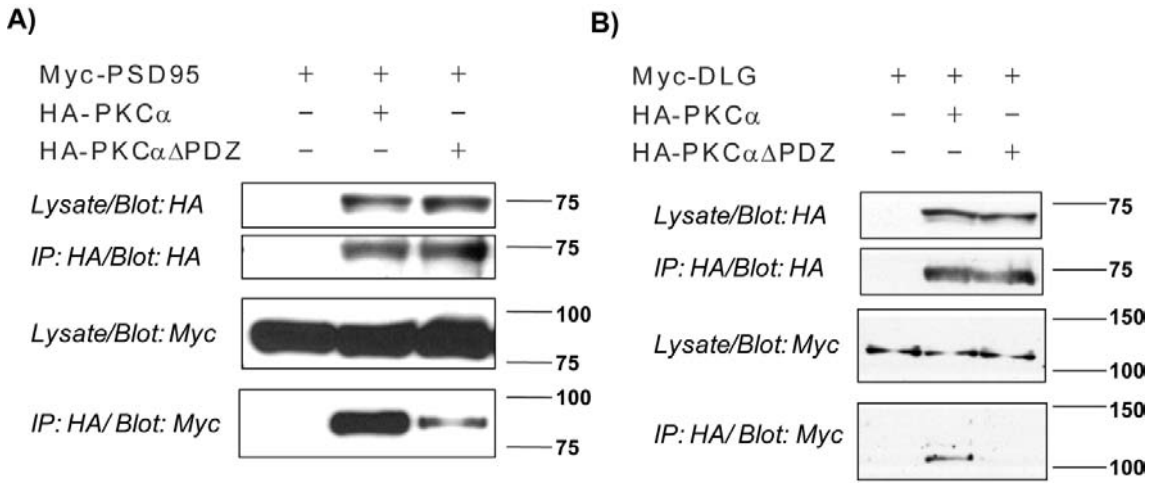

Figure 5.2. The PDZ ligand of PKCα contributes to the interaction between MAGUK scaffolds and PKCα. *A*, HEK 293T cells were transfected with Myc-PSD95 alone, Myc-PSD95 and HA-PKCα, or Myc-PSD95 and HA-PKCαΔPDZ, a construct with the C-terminal three amino acids deleted. *B*, HEK 293T cells were transfected with Myc-DLG1 alone, Myc-DLG1 and HA-PKCα, or Myc-DLG1 and HA-PKCαΔPDZ. An antibody directed against HA was used to immunoprecipitate PKC constructs from detergent-solubilized lysates, and interactions with Myc-tagged scaffolds were assessed by immunoblot. Detergent-solubilized lysates (5% of total) were analyzed by immunoblot to show relative expression levels. Blots are representative of three independent experiments.

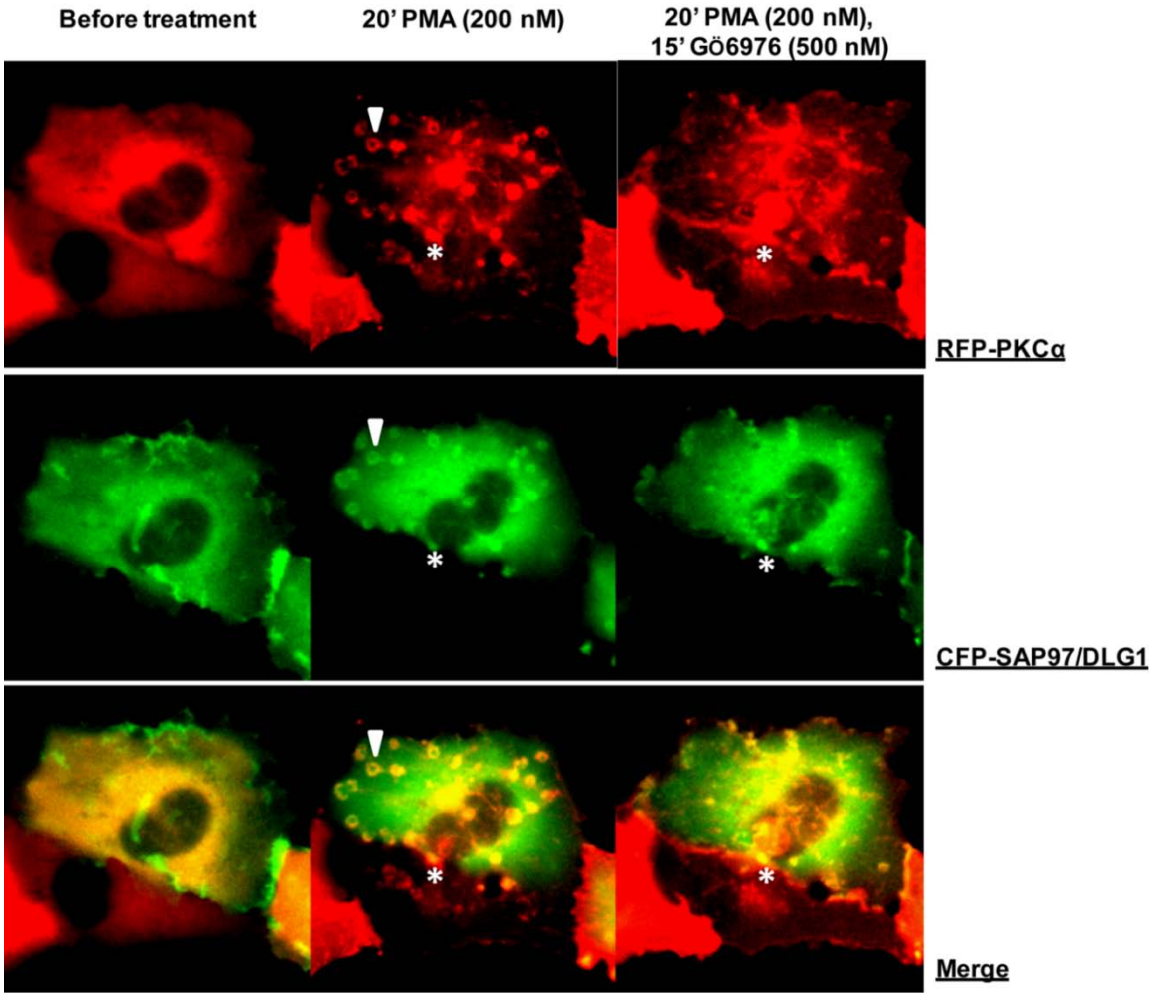

Figure 5.3. CFP-DLG1 and RFP-PKCα form ring-shaped, actin-rich clusters in COS7 cells in a PKC activity-dependent, PDZ ligand-independent manner. *A*, Images of live COS7 cells transfected with CFP-DLG1 (green) and RFP-PKCα (red) acquired before (left column) and after (middle column) treatment with PKC activator PMA (200 nM, 20 min). White arrow indicates ring shaped clusters induced by PMA. Following inhibition of cPKC with Gö6976 (500 nM, 15 min, right column), ring shaped clusters disappear, but amorphous membrane clusters (white asterisk) remain.

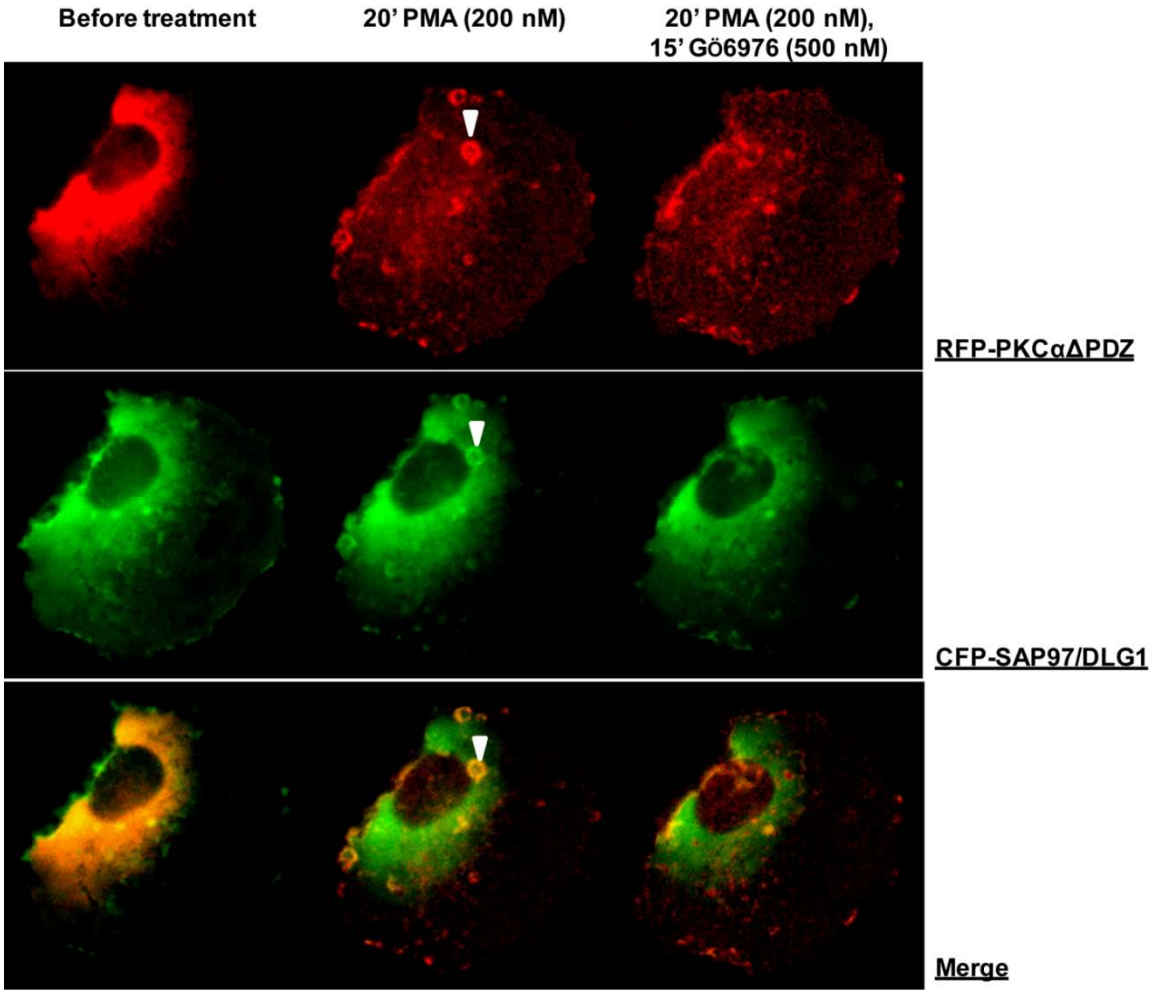

(Figure 5.3, continued.) *B,* Images of live COS7 cells transfected with CFP-DLG1 (green) and RFP-PKCαΔPDZ (red) acquired over the same timecourse of PMA treatment (200 nM, 20 min) followed by Gö6976 (500 nM, 15 min). White arrow indicates ring-shaped clusters.

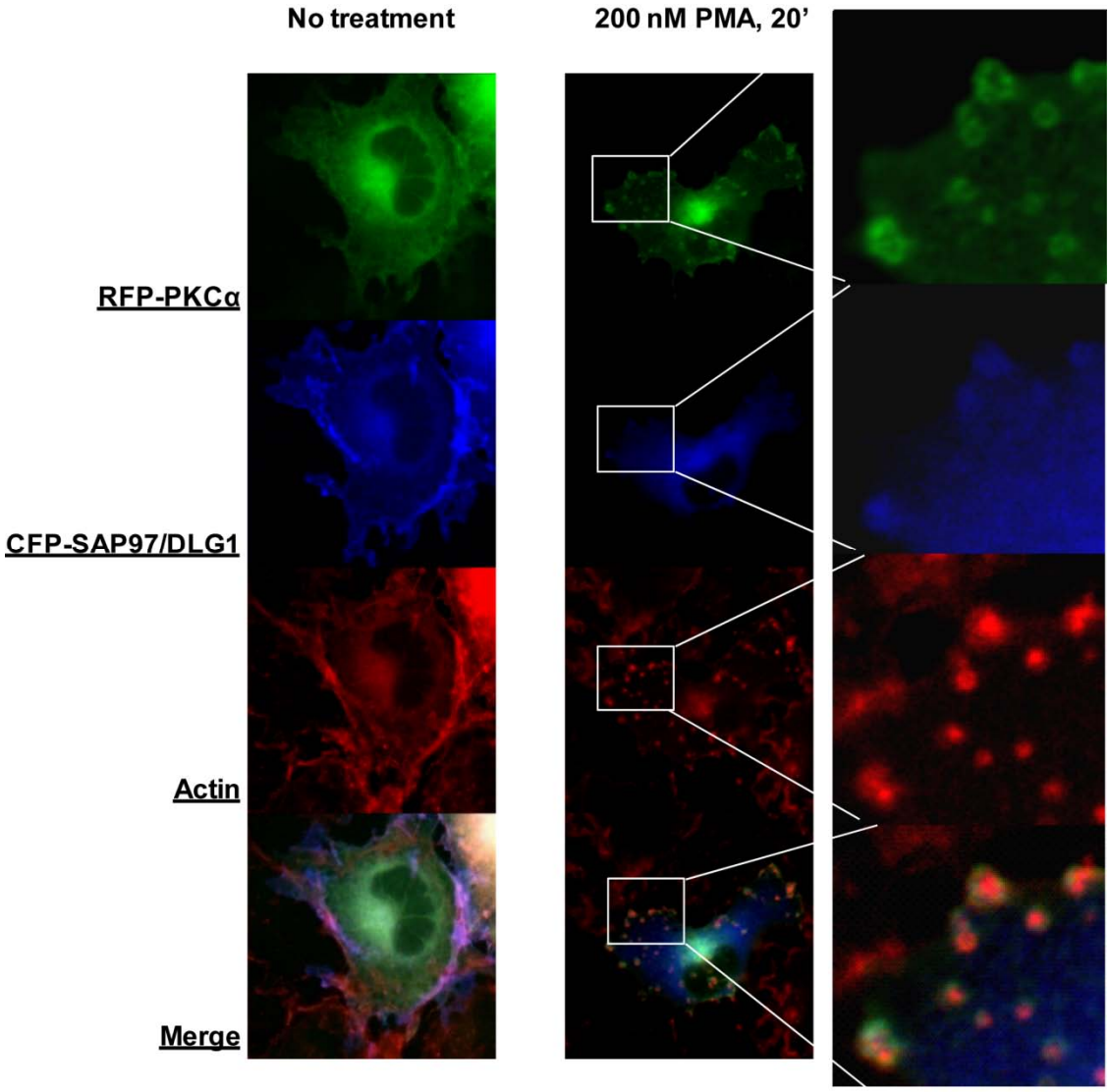

(Figure 5.3, continued) *C*, COS7 cells transfected with RFP-PKCα (visualized with goat anti-rabbit Alexa 488, green) and CFP-DLG1 (visualized with goat anti-mouse Alexa 647 blue) were fixed and stained with phalloidin-568 to visualize actin (red). Ring-shaped clusters of RFP-PKCα and CFP-DLG1 surround the actin core in the merged image (bottom), visualized more clearly in the expanded sections on the right. All images are representative of clusters formed in approximately 30% of transfected cells over more than three independent experiments.

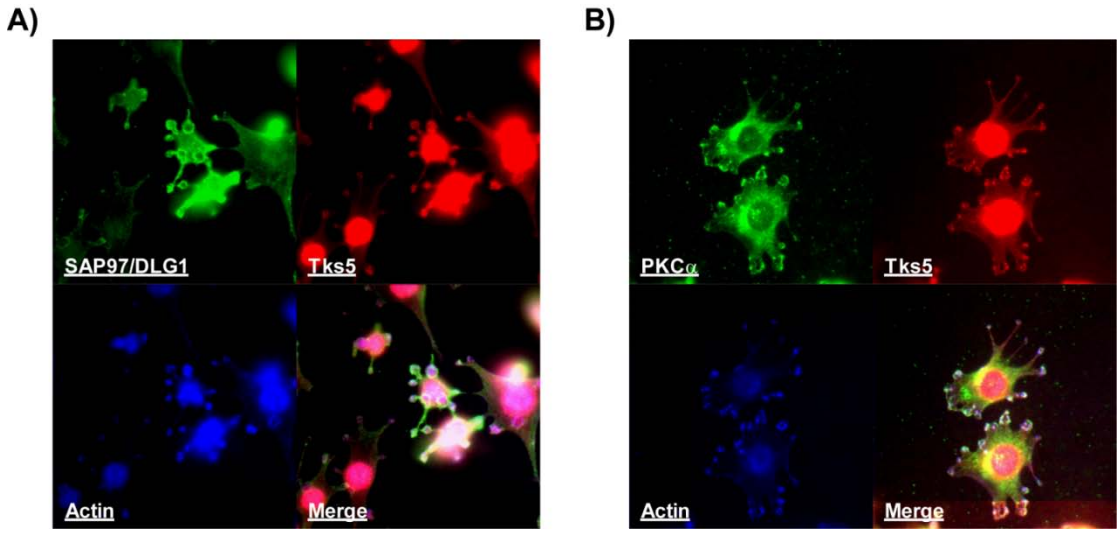

Figure 5.4. Endogenous DLG1 and PKCα staining is enriched at podosomes. Fixed and permeabilized Src-transformed fibroblasts were stained for actin (using phalloidin-647), podosome marker Tks5 (visualized with goat anti-rabbit Alexa 568), and either *A*, DLG1 or *B*, PKCα (visualized with goat anti-mouse Alexa 488). Images are representative of two independent experiments.

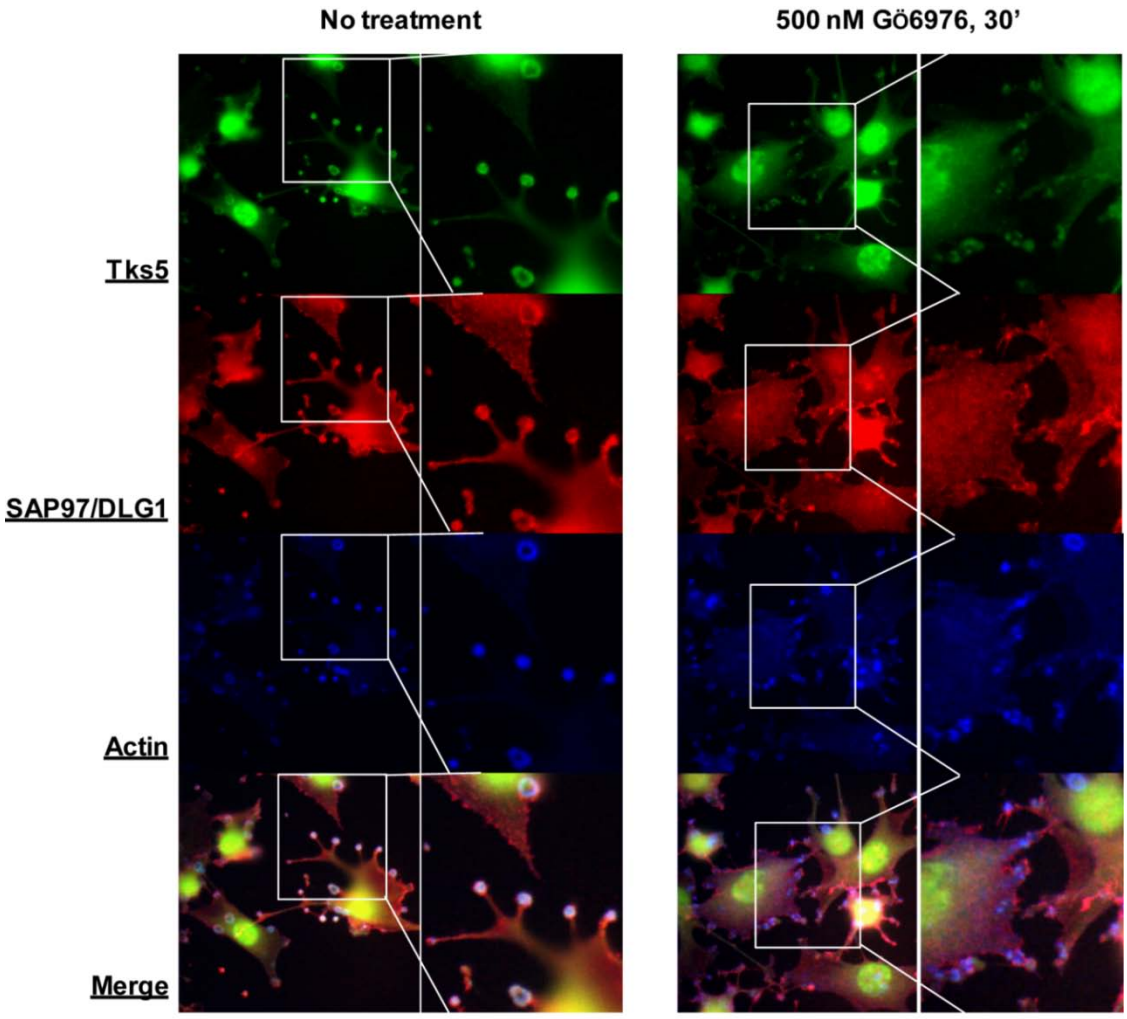

Figure 5.5. Inhibition of conventional PKC reverses podosome formation. Untreated Src-transformed fibroblasts (left columns) and cells treated with Gö6976 (500 nM, 30 min; right columns) were stained for Tks5 (green, top row; visualized with goat anti-rabbit Alexa 488), DLG1 (red, second row; visualized with goat anti-mouse 568), and actin (blue, third row; visualized with phalloidin-647). Merged image (bottom row) shows co-localization in untreated cells, which is dispersed in Gö6976-treated cells.

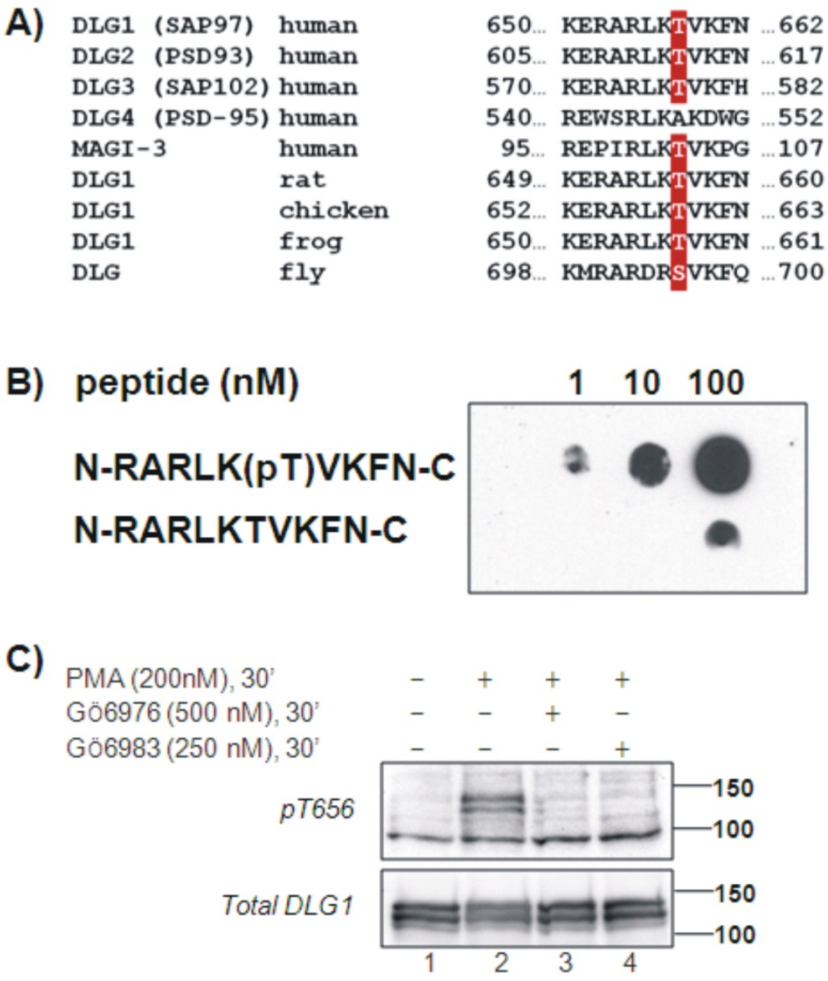

Figure 5.6. Generation of a phospho-specific antibody to PKC phosphorylation site, Thr656 (rat numbering), located in the hinge region of DLG1 and other MAGUK scaffolds. *A*, Partial alignment of a PKC phosphorylation site conserved in MAGUK scaffolds that have been shown to interact with PKCα's C-terminal PDZ ligand (exception: PSD95 contains an Ala residue at the phospho-acceptor site). Twelve residues comprising the phosphorylation site in DLG1 are identically conserved in all vertebrate species examined. *B*, Recognition of increasing concentrations of phosphorylated peptide (top row) compared to unphosphorylated peptide (bottom row) by a phospho-Thr656 antibody generated in rabbits immunized with the following peptide: N-RARLK(pT)VKFN-C. *C*, Immunoblot analysis of whole cell lysates from untreated primary mouse astrocytes (lane 1), or astrocytes treated with PMA (200 nM, 30 min, lanes 2-4); with or without concurrent treatment with Gö6976 (500 nM, lane 3) or Gö6983 (250 nM, lane 4). Top immunoblot is probed with rabbit anti-phospho-Thr 656 antibody; bottom immunoblot is a reprobe of the initial blot using antibodies directed toward total DLG1. Blots are representative of three independent experiments.

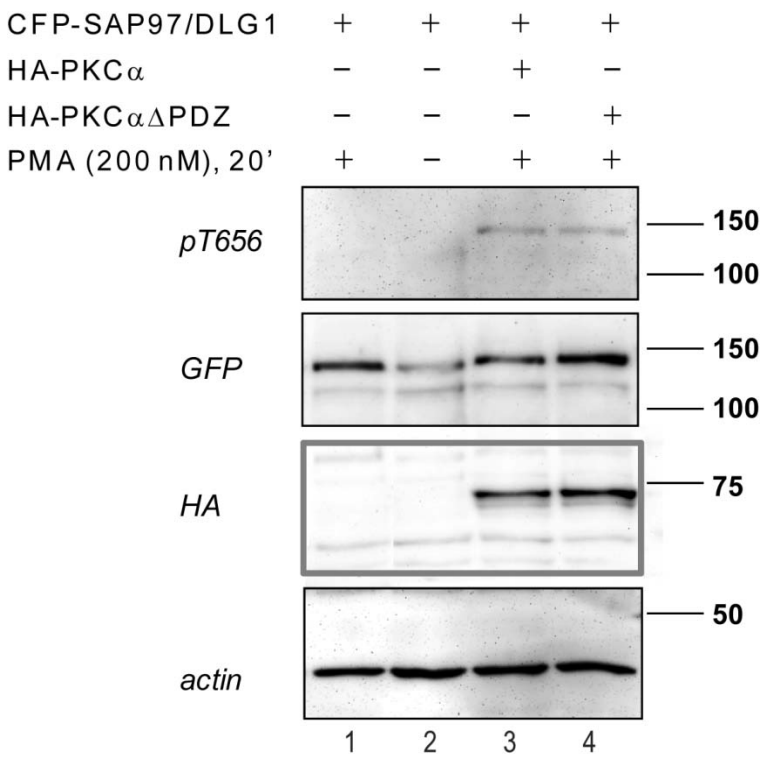

Figure 5.7. PDZ interaction is not essential for phosphorylation of expressed DLG1. COS7 cells were transfected with CFP- DLG1 (lanes 1-2), CFP-DLG1 and HA-PKCα (lane 3), or CFP- DLG1 and HA-PKCαΔPDZ (lane 4) and treated with PdBu (200 nM, 20 min; lanes 1, 3, and 4). Detergent-solubilized lysates were analyzed by immunoblot using antibodies directed against phospho-Thr656, GFP (total expressed DLG1), HA (total expressed PKCα), and actin as a control for loading.

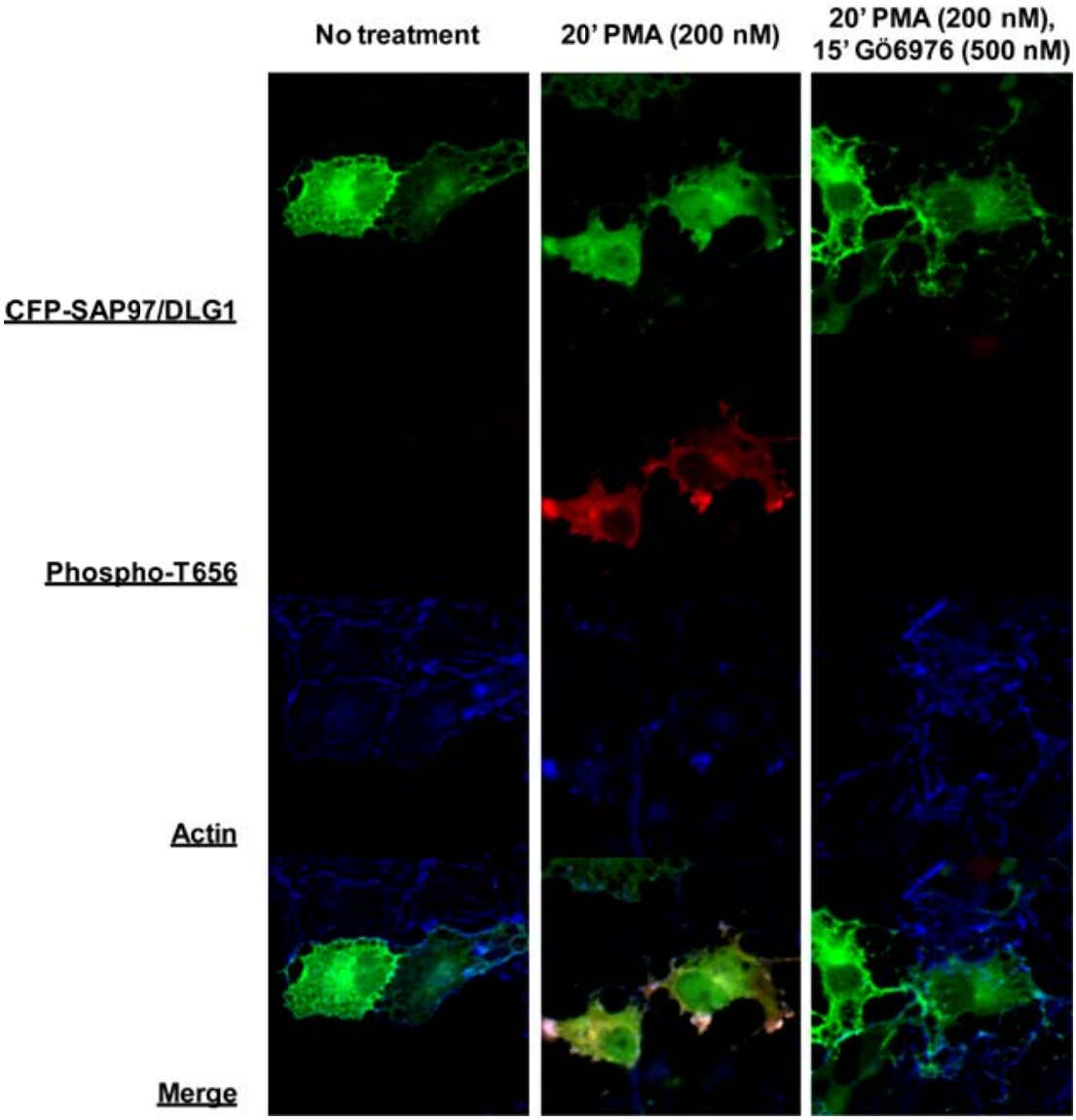

Figure 5.8. Phosphorylation of Thr 656 occurs at podosomes. *A*, COS7 cells transfected with CFP-DLG1 and HA-PKCα (first column) were treated with PMA (200 nM, 30 min; second column) or PMA (200 nM, 30 min) and Gö6976 (500 nM, 30 min; third column). Cells were fixed and stained for total DLG1 (visualized with goat anti mouse 488; green), phospho-Thr 656 (visualized with goat anti-rabbit 568; red), and actin (phalloidin 647; blue). Merged images (bottom row) reveal phosphorylation of DLG1 at podosome-like actin-rich structures formed by PMA treatment.

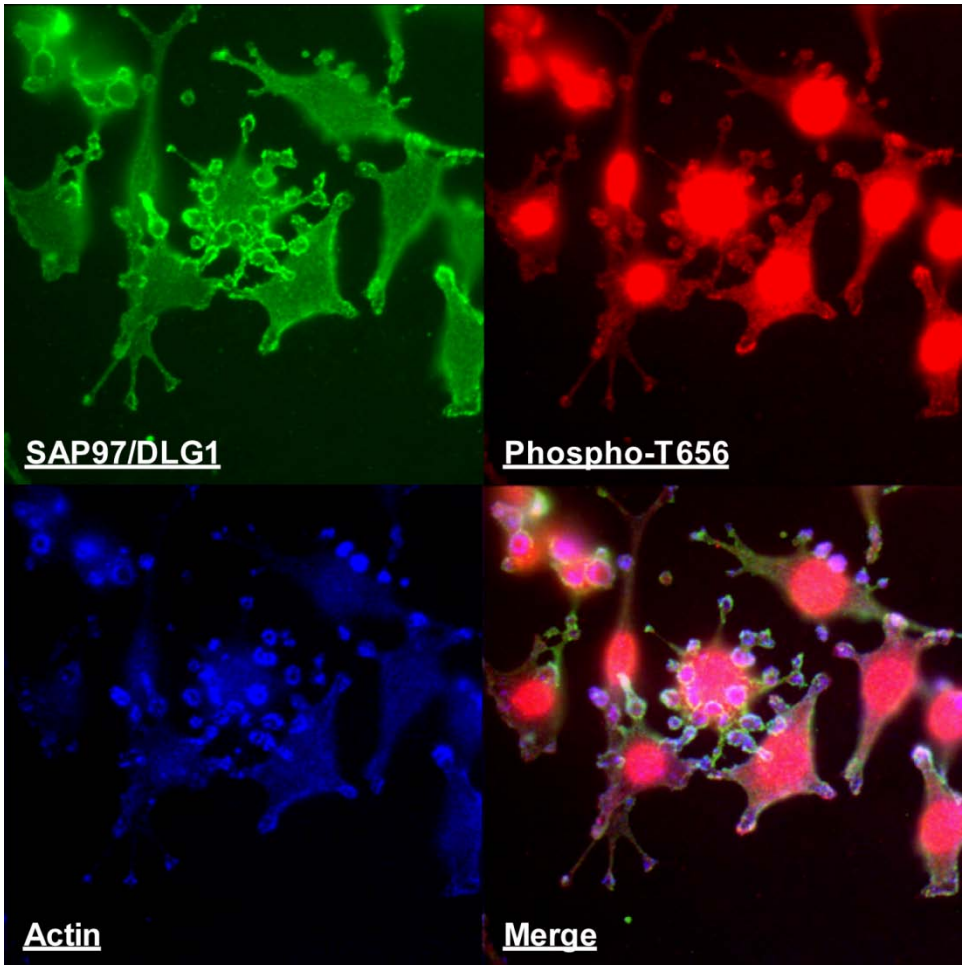

(Figure 5.8, continued) *B,* Fixed and permeabilized Src-transformed fibroblasts were stained for actin (using phalloidin-647), phospho-Thr656 (visualized with goat anti-rabbit Alexa 568), and DLG1 (visualized with goat anti-mouse Alexa 488). Merged image (bottom right corner) reveals co-localization.

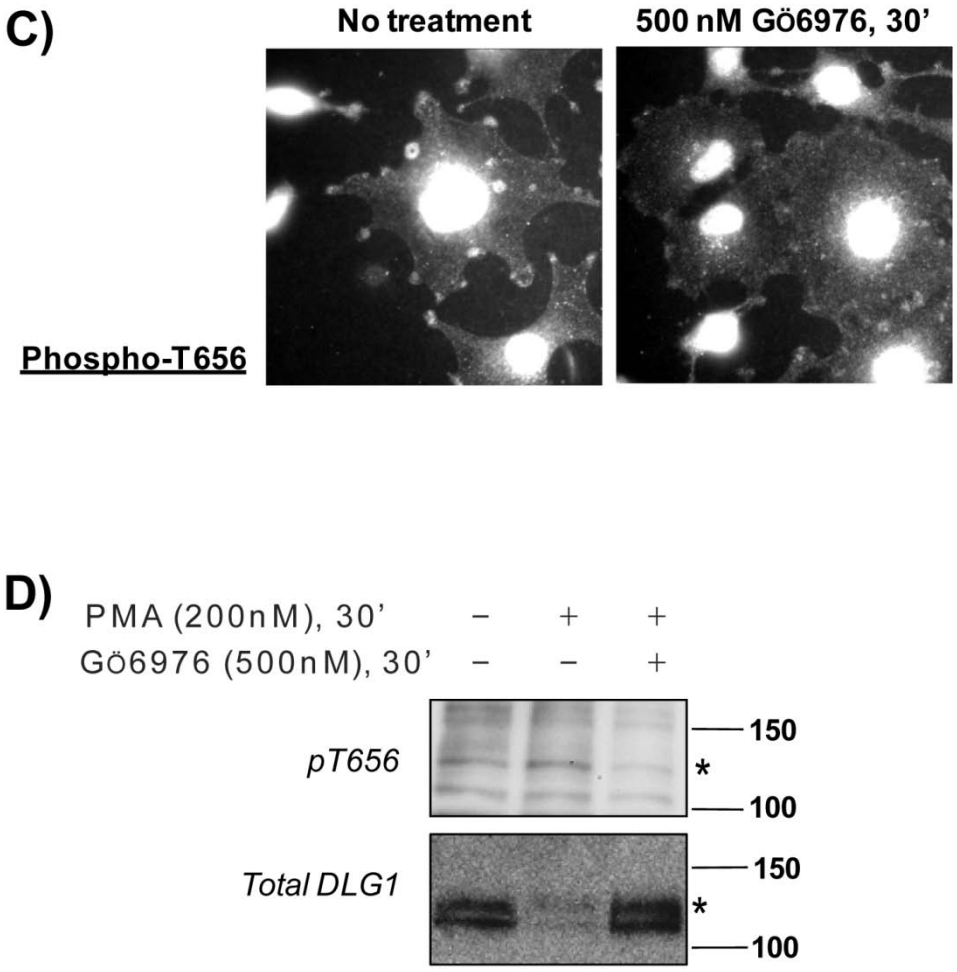

(Figure 5.8, continued) *C,* Images of Src-transformed fibroblasts stained for phospho-Thr 656 in untreated cells (top row) compared to cells treated with Gö6976 (500 nM, 30 min. *D,* Immunoblot of whole cell lysates from Src-transformed fibroblasts (lane 1) treated with PMA (200 nM, 30 min; lane 2) or PMA with Gö6976 (500 nM, lane 3). Top blot is probed with phospho-Thr656 antibody; bottom blot is a reprobe of the same blot with antibody to total DLG1, Black asterisk marks phospho-Thr656 band aligning to upper band on total DLG1 blot.

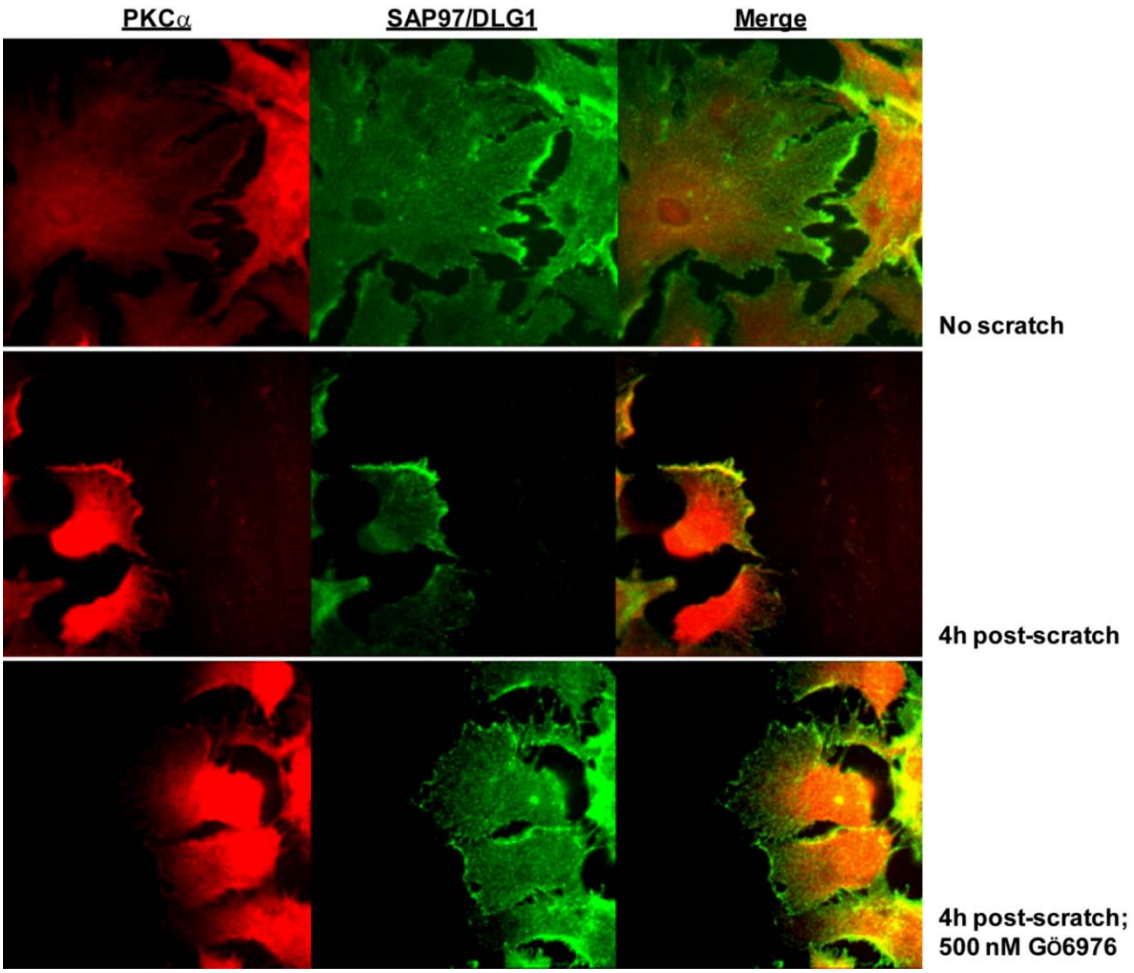

Figure 5.9. Endogenous PKCα and DLG1 co-localize at leading edge of migrating astrocytes in activity-dependent manner. Primary mouse astrocytes were stained for PKCα and DLG1 in confluent cells (top images), 4 hours after scratch (middle images), or 4 hours after scratch in the presence of Gö6976 (bottom images). Merged images (right column) show co-localization of DLG1 and PKCα. Images are representative of cells in three independent experiments.

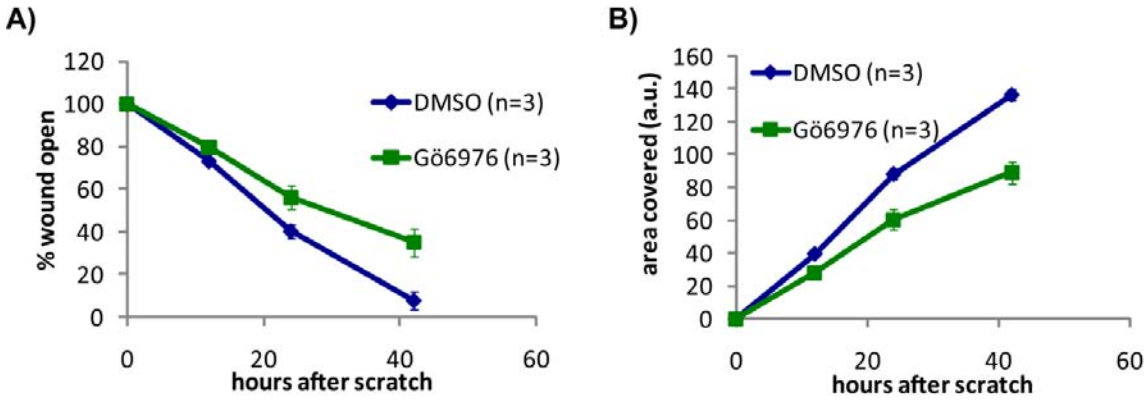

Figure 5.10. Inhibiting cPKCs impairs astrocyte migration. Primary astrocytes grown to confluency were scratched in media containing DMSO or Gö6976. Migration was assessed as *A*, percent open wound and *B*, area covered by measurements taken in ImageJ. Results are from three independent experiments ± S.D. These data appear courtesy of Audrey O'Neill.

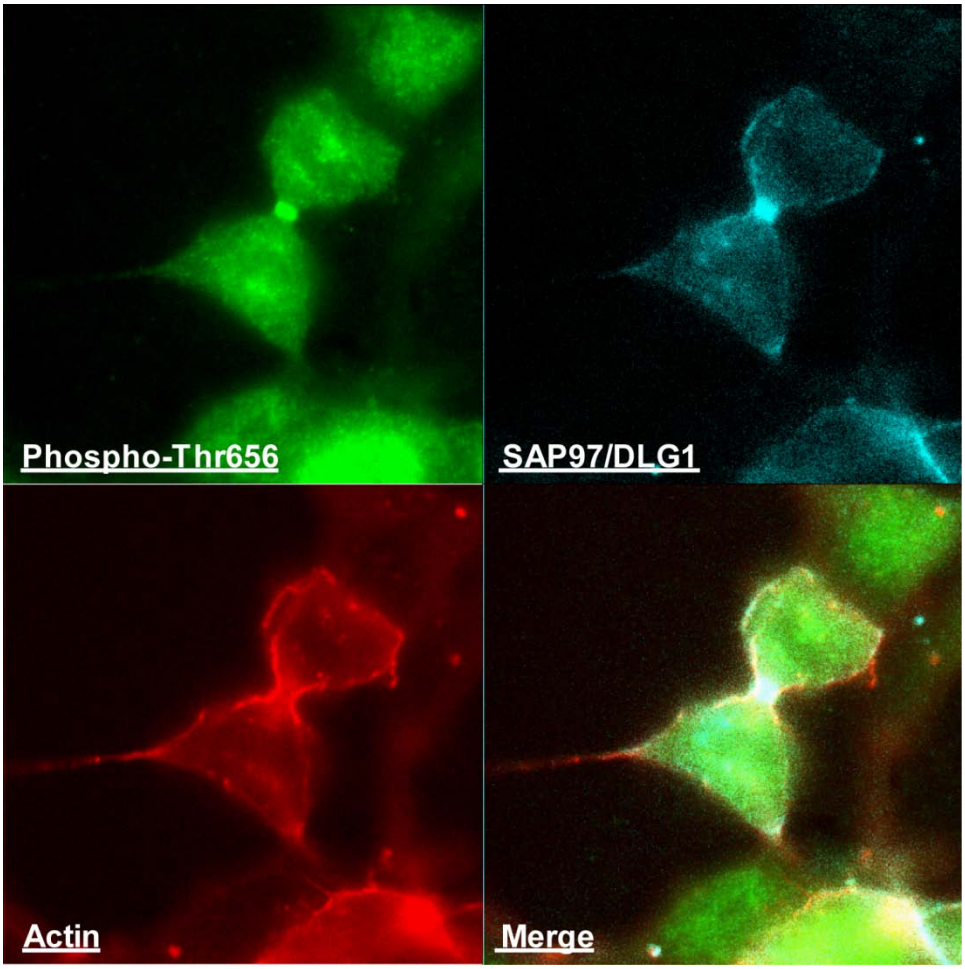

Figure 5.11. Endogenous DLG1 is phosphorylated at the midbody of COS7 cells undergoing cytokinesis. Untransfected COS7 cells were stained with Rabbit anti-phospho-Thr656 (visualized with goat anti-rabbit Alexa fluor 488; green) and total DLG1 (visualized with goat anti-mouse Alexa fluor 647; cyan) and F-actin was stained with phalloidin-Alexa fluor 568 (red). Merged image reveals co-localization at midbody. Images are representative of randomly cycling cells undergoing cytokinesis over three independent experiments.

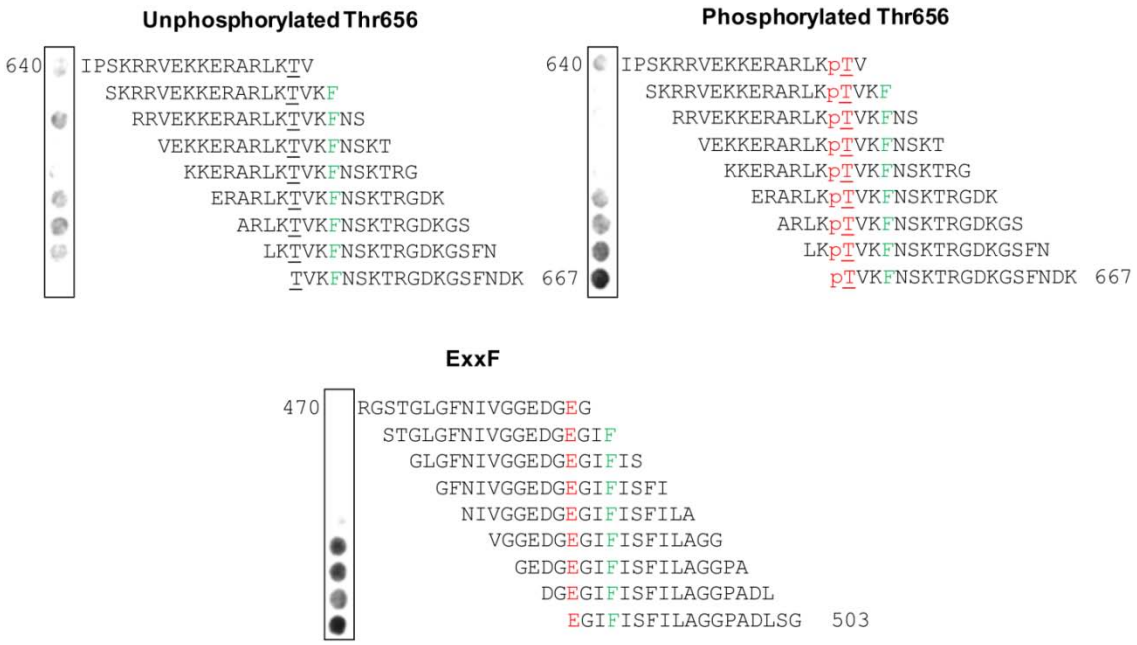

Figure 5.12. Purified GST-tagged BRCT domains from Ect2 bind phospho-Thr656. *A*, An 18-mer peptide walk, shifting every two amino acids, of the protein sequence of SAP97/DLG1 was arrayed onto a membrane. In addition, peptides containing a phosphorylated Thr residue at position 656 were also arrayed on the membrane. The membrane was overlaid with pure GST-tagged BRCT domains (amino acids 1-333) from Ect2 and incubated with an antibody to GST to detect binding of the BRCT domains to peptides on the array. Selected membrane regions are displayed, including peptides encompassing Thr656 (top left panel), phospho-Thr 656 (top right panel), and a serendipitous ExxF motif (bottom panel) that would be predicted to bind BRCT domains.

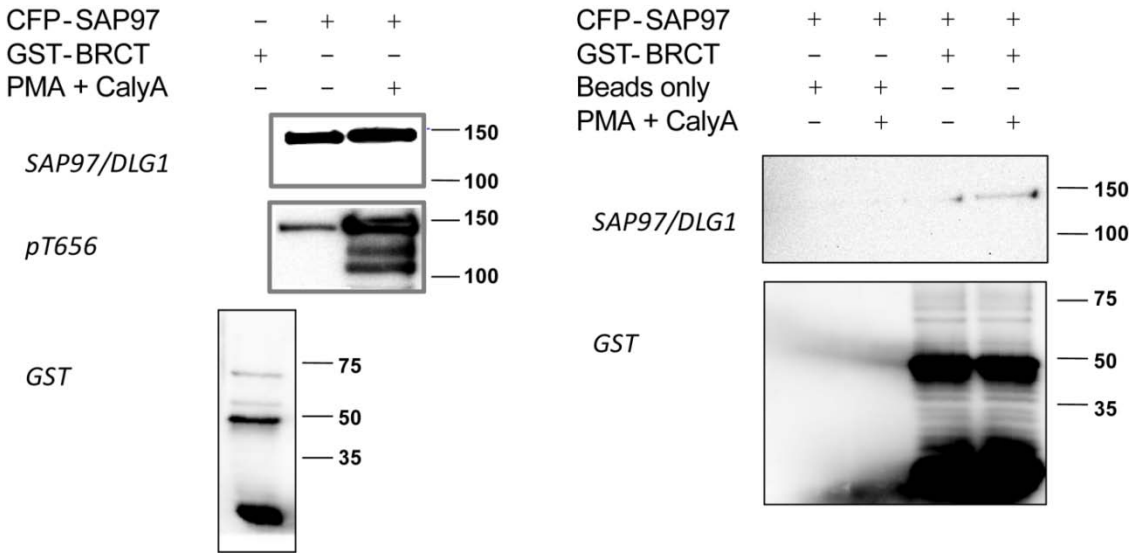

(Figure 5.12, continued) *B,* COS7 cells expressing CFP-DLG1 were treated with PMA (200 nM, 20 min) and Calyculin A (50 nM, 10 min) to maximize phosphorylation of the scaffold. Lysates from untreated cells expressing CFP-DLG1 (second lane, left blot) and from cells expressing CFP-DLG1 treated to maximize phosphorylation (third lane, left blot) were incubated with pure GST-tagged BRCT domains from Ect2 (first lane, left blot). Top right blot shows binding of phosphorylated CFP-DLG (fourth lane), but not unphosphorylated CFP-DLG (third lane), to purified GST-BRCT domains precipitated with GST beads; GST beads alone do not bind DLG (first lane) or phospho-DLG (second lane). Bottom right blot shows equal pull-down of GST-BRCT domains by GST beads.

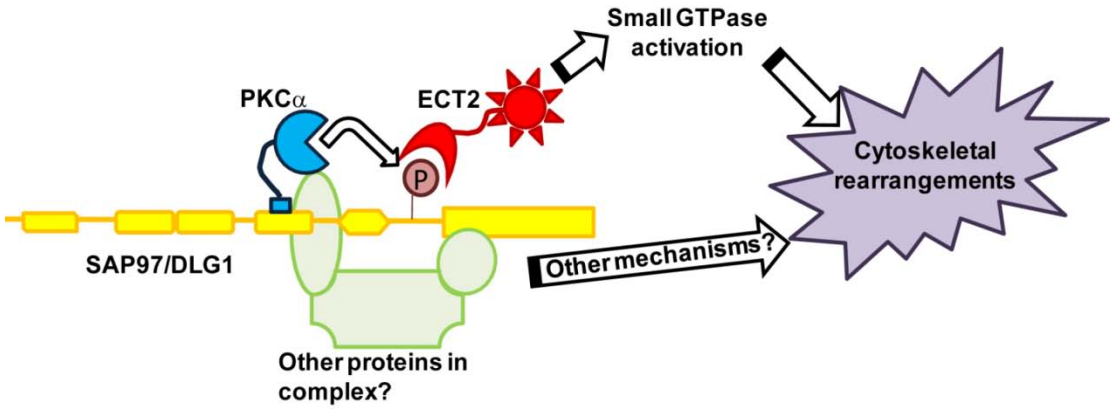

Figure 5.13. Model describing potential molecular mechanism by which PKCα/DLG1 signaling scaffold promotes cytoskeletal rearrangements. The PDZ ligand of PKCα (cyan) interacts with the third PDZ domain of SAP97/DLG1 scaffold (yellow) and phosphorylates it at Thr656 (pink circle). Phosphorylation of SAP97/DLG1 creates a binding site for the BRCT domains of the RhoGEF, Ect2 (red). This phosphorylation event, likely combined with other signaling events poised at the scaffold, contributes to cytoskeletal rearrangements by activating the Rho family of small GTPases.

References

1. Kodama, A., Lechler, T., and Fuchs, E. (2004) *J Cell Biol* **167**(2), 203-207

2. Faguy, D. M., and Doolittle, W. F. (1998) *Curr Biol* **8**(10), R338-341

3. Heasman, S. J., and Ridley, A. J. (2008) *Nat Rev Mol Cell Biol* **9**(9), 690-701

4. Ridley, A. J., and Hall, A. (1992) *Cell* **70**(3), 389-399

5. Ridley, A. J., Paterson, H. F., Johnston, C. L., Diekmann, D., and Hall, A. (1992) *Cell* **70**(3), 401-410

6. Lester, B. R., and McCarthy, J. B. (1992) *Cancer Metastasis Rev* **11**(1), 31-44

7. Schmitz, A. A., Govek, E. E., Bottner, B., and Van Aelst, L. (2000) *Exp Cell Res* **261**(1), 1-12

8. Alto, N. M., Shao, F., Lazar, C. S., Brost, R. L., Chua, G., Mattoo, S., McMahon, S. A., Ghosh, P., Hughes, T. R., Boone, C., and Dixon, J. E. (2006) *Cell* **124**(1), 133-145

9. Meacci, E., Donati, C., Cencetti, F., Romiti, E., and Bruni, P. (2000) *FEBS Lett* **482**(1-2), 97-101

10. Etienne-Manneville, S., Manneville, J. B., Nicholls, S., Ferenczi, M. A., and Hall, A. (2005) *J Cell Biol* **170**(6), 895-901

11. Hai, C. M., Hahne, P., Harrington, E. O., and Gimona, M. (2002) *Exp Cell Res* **280**(1), 64-74

12. Gallegos, L. L., and Newton, A. C. (2008) *IUBMB Life* **60**(12), 782-789

13. Castagna, M., Takai, Y., Kaibuchi, K., Sano, K., Kikkawa, U., and Nishizuka, Y. (1982) *J Biol Chem* **257**(13), 7847-7851

14. Colon-Gonzalez, F., and Kazanietz, M. G. (2006) *Biochim Biophys Acta* **1761**(8), 827-837

15. Saurin, A. T., Durgan, J., Cameron, A. J., Faisal, A., Marber, M. S., and Parker, P. J. (2008) *Nat Cell Biol* **10**(8), 891-901

16. Suzuki, A., and Ohno, S. (2006) *J Cell Sci* **119**(Pt 6), 979-987

17. Chen, D., Purohit, A., Halilovic, E., Doxsey, S. J., and Newton, A. C. (2004) *J Biol Chem* **279**(6), 4829-4839

18. Staudinger, J., Lu, J., and Olson, E. N. (1997) *J Biol Chem* **272**(51), 32019-32024

19. Leitges, M., Kovac, J., Plomann, M., and Linden, D. J. (2004) *Neuron* **44**(4), 585-594

20. Funke, L., Dakoji, S., and Bredt, D. S. (2005) *Annu Rev Biochem* **74**, 219-245

21. Laprise, P., Viel, A., and Rivard, N. (2004) *J Biol Chem* **279**(11), 10157-10166

22. Aoki, C., Miko, I., Oviedo, H., Mikeladze-Dvali, T., Alexandre, L., Sweeney, N., and Bredt, D. S. (2001) *Synapse* **40**(4), 239-257

23. Gardoni, F., Mauceri, D., Marcello, E., Sala, C., Di Luca, M., and Jeromin, A. (2007) *J Biol Chem* **282**(39), 28691-28699

24. Unno, K., Hanada, T., and Chishti, A. H. (2008) *Exp Cell Res* **314**(17), 3118-3129

25. Gardner, L. A., Naren, A. P., and Bahouth, S. W. (2007) *J Biol Chem* **282**(7), 5085-5099

26. Sabio, G., Arthur, J. S., Kuma, Y., Peggie, M., Carr, J., Murray-Tait, V., Centeno, F., Goedert, M., Morrice, N. A., and Cuenda, A. (2005) *Embo J* **24**(6), 1134-1145

27. Paarmann, I., Spangenberg, O., Lavie, A., and Konrad, M. (2002) *J Biol Chem* **277**(43), 40832-40838

28. Hibino, H., Inanobe, A., Tanemoto, M., Fujita, A., Doi, K., Kubo, T., Hata, Y., Takai, Y., and Kurachi, Y. (2000) *Embo J* **19**(1), 78-83

29. Yamada, K. H., Hanada, T., and Chishti, A. H. (2007) *Biochemistry* **46**(35), 10039-10045

30. Nakagawa, T., Futai, K., Lashuel, H. A., Lo, I., Okamoto, K., Walz, T., Hayashi, Y., and Sheng, M. (2004) *Neuron* **44**(3), 453-467

31. Narayan, N., Massimi, P., and Banks, L. (2009) *J Cell Sci* **122**(Pt 1), 65-74

32. Massimi, P., Narayan, N., Cuenda, A., and Banks, L. (2006) *Oncogene* **25**(31), 4276-4285

33. Lau, A. G., and Hall, R. A. (2001) *Biochemistry* **40**(29), 8572-8580

34. Citro, S., Malik, S., Oestreich, E. A., Radeff-Huang, J., Kelley, G. G., Smrcka, A. V., and Brown, J. H. (2007) *Proc Natl Acad Sci U S A* **104**(39), 15543-15548

35. Kunkel, M. T., Garcia, E. L., Kajimoto, T., Hall, R. A., and Newton, A. C. (2009) *J Biol Chem*

36. Colledge, M., Dean, R. A., Scott, G. K., Langeberg, L. K., Huganir, R. L., and Scott, J. D. (2000) *Neuron* **27**(1), 107-119

37. Abram, C. L., Seals, D. F., Pass, I., Salinsky, D., Maurer, L., Roth, T. M., and Courtneidge, S. A. (2003) *J Biol Chem* **278**(19), 16844-16851

38. Obenauer, J. C., Cantley, L. C., and Yaffe, M. B. (2003) *Nucleic Acids Res* **31**(13), 3635-3641

39. Stiffler, M. A., Chen, J. R., Grantcharova, V. P., Lei, Y., Fuchs, D., Allen, J. E., Zaslavskaia, L. A., and MacBeath, G. (2007) *Science* **317**(5836), 364-369

40. Rodriguez, M., Yu, X., Chen, J., and Songyang, Z. (2003) *J Biol Chem* **278**(52), 52914-52918

41. Miki, T., Smith, C. L., Long, J. E., Eva, A., and Fleming, T. P. (1993) *Nature* **362**(6419), 462-465

42. Yuce, O., Piekny, A., and Glotzer, M. (2005) *J Cell Biol* **170**(4), 571-582

43. Kim, J. E., Billadeau, D. D., and Chen, J. (2005) *J Biol Chem* **280**(7), 5733-5739

44. Chalamalasetty, R. B., Hummer, S., Nigg, E. A., and Sillje, H. H. (2006) *J Cell Sci* **119**(Pt 14), 3008-3019

45. Wolfe, B. A., Takaki, T., Petronczki, M., and Glotzer, M. (2009) *PLoS Biol* **7**(5), e1000110

46. Berdeaux, R. L., Diaz, B., Kim, L., and Martin, G. S. (2004) *J Cell Biol* **166**(3), 317-323

47. Sano, M., Genkai, N., Yajima, N., Tsuchiya, N., Homma, J., Tanaka, R., Miki, T., and Yamanaka, R. (2006) *Oncol Rep* **16**(5), 1093-1098

48. Salhia, B., Tran, N. L., Chan, A., Wolf, A., Nakada, M., Rutka, F., Ennis, M., McDonough, W. S., Berens, M. E., Symons, M., and Rutka, J. T. (2008) *Am J Pathol* **173**(6), 1828-1838

49. Miller, L. D., Lee, K. C., Mochly-Rosen, D., and Cartwright, C. A. (2004) *Oncogene* **23**(33), 5682-5686

50. Canman, J. C., Lewellyn, L., Laband, K., Smerdon, S. J., Desai, A., Bowerman, B., and Oegema, K. (2008) *Science* **322**(5907), 1543-1546

51. Nishikawa, K., Toker, A., Johannes, F. J., Songyang, Z., and Cantley, L. C. (1997) *J Biol Chem* **272**(2), 952-960

52. Rumbaugh, G., Sia, G. M., Garner, C. C., and Huganir, R. L. (2003) *J Neurosci* **23**(11), 4567-4576

53. Lee, H. W., Choi, J., Shin, H., Kim, K., Yang, J., Na, M., Choi, S. Y., Kang, G. B., Eom, S. H., Kim, H., and Kim, E. (2008) *J Neurosci* **28**(53), 14546-14556

54. Justilien, V., and Fields, A. P. (2009) *Oncogene*

55. Thomas, M., Glaunsinger, B., Pim, D., Javier, R., and Banks, L. (2001) *Oncogene* **20**(39), 5431-5439

56. Caruana, G., and Bernstein, A. (2001) *Mol Cell Biol* **21**(5), 1475-1483

57. Pfeifhofer, C., Gruber, T., Letschka, T., Thuille, N., Lutz-Nicoladoni, C., Hermann-Kleiter, N., Braun, U., Leitges, M., and Baier, G. (2006) *J Immunol* **176**(10), 6004-6011

58. Leitges, M. (2007) *Biochem Soc Trans* **35**(Pt 5), 1018-1020

59. Matsumoto, M., Ogawa, W., Akimoto, K., Inoue, H., Miyake, K., Furukawa, K., Hayashi, Y., Iguchi, H., Matsuki, Y., Hiramatsu, R., Shimano, H., Yamada, N., Ohno, S., Kasuga, M., and Noda, T. (2003) *J Clin Invest* **112**(6), 935-944

60. Cho, K. K., Mikkelsen, T., Lee, Y. J., Jiang, F., Chopp, M., and Rosenblum, M. L. (1999) *Int J Dev Neurosci* **17**(5-6), 447-461

61. Fan, Q. W., Cheng, C., Knight, Z. A., Haas-Kogan, D., Stokoe, D., James, C. D., McCormick, F., Shokat, K. M., and Weiss, W. A. (2009) *Sci Signal* **2**(55), ra4

62. Amos, S., Mut, M., diPierro, C. G., Carpenter, J. E., Xiao, A., Kohutek, Z. A., Redpath, G. T., Zhao, Y., Wang, J., Shaffrey, M. E., and Hussaini, I. M. (2007) *Cancer Res* **67**(21), 10241-10251

Footnotes

[§]This work was supported by NIH GM43154 and NIH 1F31GM083628.

[*]Abbreviations: DAG, Diacylglycerol; PKC, protein kinase C; C1, PKC conserved region 1; C2, PKC conserved region 2; PB-1, phox and bem-1; CFP, cyan fluorescent protein; RFP, red fluorescent protein; PMA, phorbol myristate acetate; cPKC, conventional PKC; nPKC, novel PKC; aPKC, atypical PKC; PDZ, post-synaptic density-95/discs large/zonula occludens 1; PICK1, protein interacting with kinase 1; MAGUK, membrane-associated guanylate kinase; SH3, Src-homology 3; GK, guanylate kinase homology domain; DLG1-4, discs large homolog, 1-4; PSD-95, post synaptic density protein, 95 kDa; SAP97, synapse-associated protein, 97 kDa; SAP102, synapse-associated protein, 102 kDa; PSD-93, post synaptic density protein, 93 kDa; MAPK, mitogen-activated protein kinase; GKAP, guanylate kinase associated protein; GAKIN, guanylate kinase interacting protein; AKAP79/150, A kinase anchoring protein, 79/150 kDa; GEF, guanine nucleotide exchange factor; GAP, GTPase activating protein; BRCT, BRCA1 C-terminal domain.

Chapter 6

Summary and Conclusions

Underlying cellular functions are complex networks of signaling proteins, with myriad potential for regulation. The breadth of prior knowledge about the PKC family allows us to build upon it as a paradigm for studying detailed regulation of signaling proteins, how this regulation is disrupted in disease states, and how we should target the regulation of this enzyme family in diseases such as cancer (reviewed in (1,2)). Because minimal specificity for cellular PKC substrates is conferred by intrinsic properties of the kinase core (3) we know that the vast majority of specificity of PKC signaling in cells is dependent upon differences in regulatory domains of the PKC isoforms interfacing with contextual cues in cells such as cellular lipids and protein complexes. The studies described within this thesis have built upon previous knowledge about the PKC family in the following significant ways:

Cellular PKC signaling is informed by lipid second messenger dynamics at the level of the organelle.

Our studies in Chapter 2 support that the spatiotemporal dynamics of PKC signaling are chronically and acutely controlled by lipid binding to their membrane-targeting modules, the C1 and C2 domains. Differences in intrinsic affinities and selectivities of these two membrane-targeting modules control the rate, magnitude, duration, and localization of signaling by PKC isozymes. In general, cPKC isoforms respond rapidly at the plasma membrane with the same kinetics as Ca^{2+} formation, driven by rapid recruitment via the C2 domain to the PIP_2-rich plasma membrane, which in turn allows efficient binding of the membrane-embedded ligand DAG via the C1 domain; nPKC isoforms respond more slowly at Golgi, driven by direct recruitment via their C1

domain to Golgi-bound DAG. Conventional PKC activity terminates more rapidly because of faster turnover of DAG at the plasma membrane, whereas nPKC activity is sustained because of prolonged DAG accumulation at the Golgi (4). Fine-tuning of these responses by protein scaffold interactions, allosteric mechanisms, and competition with other proteins for common lipid second messengers gives a unique, cell type-dependent activation signature to each isozyme.

Organization and activation of novel and conventional PKC isoforms is determined by the threshold for engaging the DAG-binding C1b domain

Results from Chapter 3 demonstrate that the affinity of the C1b domains of novel and conventional PKC isozymes for DAG-containing membranes dictates the major cellular differences between the two classes. High affinity DAG-dependent membrane binding allows nPKC to be activated by DAG alone, while cPKC requires pre-targeting via Ca^{2+} dependent interactions with anionic phospholipids via its C2 domain for activation. This difference makes cPKC isozymes coincidence detectors, while nPKCs, in this respect, are not. Also, high affinity for DAG-containing membranes pre-targets nPKC isozymes to the Golgi, while cPKC isozymes are not pre-targeted to this organelle. Incredibly, this difference is predominantly controlled by a single amino acid swap that tunes DAG affinity: position 22 is Tyr in cPKC and Trp in nPKC (5). Thus, a major evolutionary divergence to promote significant functional divergence amongst novel and conventional PKCs occurred in the C1b domain at position 22 to alter affinity for DAG-containing membranes.

Further evidence for evolutionary pressure on the affinity of the C1b domain for DAG-containing membranes is found upon examining a disease with an underlying genetic cause: cancer. In Chapter 4, we mined databases from cancer genome sequencing efforts to find somatic genetic alterations in the PKC family in tumors. In one tumor, a colorectal adenocarcinoma, only two total somatic alterations were identified. One mutation was an established oncogenic activating mutation in K-Ras at Gly 12 (6) and the other occurred in the C1b domain of PKCβ isoforms, Val 144 to Met (V144M). Because PKCβII has clearly defined roles in promoting colon tumorigenesis (7), we were surprised to discover that this putative cancer driver mutation decreased the affinity of the C1 domain for DAG-containing membranes, raising the threshold for activation of the mutant PKC. In colon cancer cells containing activated K-Ras, both PKCβII and PKCβII-V144M promoted proliferation. However, the key difference we found was that PKCβII promoted apoptosis, but PKCβII-V144M did not. Interestingly, PKC has a defined pro-apoptotic role in cells with activated K-Ras: PKC phosphorylates K-Ras at Ser181 to relocate it to mitochondria to promote apoptosis (8). Our results show that decreasing the affinity of PKC for DAG-containing membranes effectively protects tumor cells from apoptosis in the context of oncogenic K-Ras. In addition, the other mutations in PKC family members in colon cancers we discovered while mining the databases all occur together with activating mutations in K-Ras. It will be paramount to the significance of this study to investigate whether there is a trend of de-sensitizing PKC by mutation in the context of K-Ras to protect tumors from apoptosis. However, in support of this model, many studies clearly show a trend of decreased PKC expression in colon cancers (9-11).

The PKC-DLG signaling module as a fundamental mediator of cytoskeletal rearrangements

In addition to its well-characterized lipid-dependent signaling pathways, PKC is also implicated in higher-ordered signaling complexes often associated with cytoskeleton. In Chapter 5, we describe a novel PKCα-DLG1 scaffold signaling module that promotes cytoskeletal rearrangements. Specifically, DLG1 interacts with the PDZ ligand of PKCα, and the proteins form a complex in cells in a cPKC-activity dependent manner. This complex is associated with actin, and forms ring-shaped podosome-like structures. In Src-transformed fibroblasts, which spontaneously form podosomes, endogenous DLG1 and PKCα both co-localize with actin and Tks5, a marker for podosomes. Spontaneous podosomes in Src-transformed fibroblasts are also sensitive to inhibition of conventional PKC. We also discovered a novel PKC phosphorylation site on DLG1, Thr656, and show that the phosphorylated scaffold is present at podosomes. Curiously, phospho-DLG1 also accumulates at the midbody of cells undergoing cytokinesis. One protein that is essential for cytokinesis is a GEF for the Rho family, Ect2. Ect2 contains a phospho-peptide binding BRCT domain, the binding of which promotes GEF activity. We show that this BRCT domain binds the phosphorylated DLG1. Consistent with the hypothesis that Ect2 contributes to podosome formation, previous studies have demonstrated that active RhoA localizes to and is essential for the formation of podosomes (12); in other studies, conventional PKC activity also has been shown to contribute to the formation of podosomes in other cell types (13). However, PKCα does not have documented roles in cytokinesis; here, PKCε plays a prominent role (14). Also, other DLG scaffold family

members have the identical phosphorylation motif contained in DLG1 (see Chapter 4). Thus, it is likely that this PKC-DLG-Ect2 signaling module may have broader roles in orchestrating cytoskeletal rearrangements known to be mediated by the PKC family by stimulating the activity of the Rho family of small GTPases. Clearly, further work to unambiguously determine whether the PKCα-DLG1-Ect2 signaling scaffold activates small GTPases would contribute much to the significance of these studies, and it would also be very interesting to determine whether DLG1 is a PKC substrate that is relevant in invasive cancers.

Technological advances

In these studies, we have advanced the use of FRET-based reporters in a few novel ways. In Chapter 2, we describe a method for ensuring reporters targeted to discrete regions of cells maintain the dynamic range of the initial reporter by summarizing the basal activity (FRET response inhibited from baseline), stimulated activity, and phosphatase-suppressed activity (FRET response upon adding phosphatase inhibitors to maximize phosphorylation of the reporter in cells). This characterization is important to ensure that responses altered by targeting reporters to discrete regions are a result of a different signaling environment rather than an effect on the range of the reporter. Indeed, for one reporter, Mito-CKAR, we did see an altered range as a result of targeting (1). In Chapter 3, we encountered a problem with comparing magnitude of responses from cells transfected with a reporter for DAG in which the CFP and YFP were not located on the same polypeptide. This challenge was overcome by adding a subsequent stimulus, PdBu, which maximized the FRET response and allowed us to

determine the range for each individual cell. Individual responses could thus be normalized for the range of the cell prior to averaging across similar experiments. This analysis allowed us to compare the magnitude of DAG-dependent responses between different C1b domains that would have otherwise been impossible (5). This method could be extended to other non-ratiometric FRET reporter systems, provided that a maximal stimulus for the system is known. Finally, in Chapter 4, we used CKAR as the readout in a dose-response assay in order to compare the effects of mutations in PKC on kinase activity in cells over-expressing the functional mutants, the expression levels of which can be monitored by tagging with a non-interfering fluorescent protein such as mCherry. This has not been attempted using CKAR prior to this report. This cellular assay for the effects of mutation on PKC activity has an advantage over *in vitro* studies in that no protein purification is necessary and it does not require radioactivity. Also, there less ambiguity regarding whether even minor differences observed would be relevant in a cellular setting, since the responses monitored are downstream of endogenous receptors.

<u>Major unanswered question: how do cells bridge the gap between acute lipid-stimulated signaling and prolonged signaling at protein complexes?</u>

The effects of PKC signaling at protein complexes can be monitored and perturbed artificially using the many tools at our disposal, but endogenous inputs to these complexes are often less well-understood. Indeed, these protein complexes are typically discovered using broad screening approaches (14-16), and the biochemical mechanism for PKC activation in these complexes often remains to be elucidated (17). However, perturbation of these complexes may underlie many pathophysiological roles of PKC,

and thus, it is important to begin to bridge the gap between what is known about acute stimulation of PKC in response to phospholipid hydrolysis and how these signals are maintained to inform roles of PKC isoforms in protein complexes. For example, the time course of PKC activation via receptor-mediated lipid signaling often attenuates within 15 minutes at the plasma membrane (1), yet cellular functions involving PKC in protein complexes near the plasma membrane seem to occur over much longer periods of time. How is the signal from the receptor maintained and amplified in protein complexes? PKCε provides one example, with stabilization of the open conformation by proteins interacting with the hinge region providing prolonged activation in the absence of membrane-binding (14). Perhaps studies on atypical PKCs will better inform efforts to understand prolonged signaling events, since these isozymes appear to be primarily regulated by protein interactions, but the involvement of conventional and novel PKC isoforms in processes such as migration (18), which can take hours (17), suggests that prolonged modes of activation may also occur for these isoforms.

Therapeutic implications of this work

Colon cancer driver mutations in PKC appear to be inactivating ones (see chapter 4). If our preliminary studies are correct, this provides evidence of a feedback loop from PKC to K-Ras that is intact in early colon cancer progression. The reduction of this feedback loop, either by reduced expression of PKC or by mutation, may allow colon tumor progression. PKC inhibitors are currently in clinical trials for the treatment of colon cancer. According to our results, one might expect a bell-shaped curve of tumor progression in the presence increasing doses of PKC inhibitor, with low concentrations of

inhibitor promoting tumor growth (by disrupting the apoptosis feedback loop), and high concentrations blocking tumor progression (by blocking proliferation). If characterization of additional colon cancer driver mutations in other PKC isoforms clearly shows a trend of mild desensitization in the presence of K-Ras, this should be taken into consideration when thinking about preventative strategies involving low-dose PKC inhibition. Still this does not rule out using a higher dose of PKC inhibitor that more completely blocks PKC to inhibit the pro-proliferative signaling in the prevention of colon cancer, which is the strategy that has been evaluated in mouse models of colon cancer (19).

Evidence has recently been presented in support of a PKC-Ect2 connection in non small cell lung cancer (NSCLC). Specifically, Ect2 is coordinately amplified with PKCι in NSCLC tumors. Also, depletion of Ect2 by RNAi inhibits Rac activity and affects the invasive behavior of the NSCLC cells; invasive behavior can be restored by an active mutant of Rac. In these cells, Ect2 is located outside of the nucleus, and the role of Ect2 in transformation and invasion is demonstrated to be independent from its well-characterized role in cytokinesis (20). Evidently, the physical interaction between the PKCι-Par6 complex and Ect2 is mediated by different mechanism than the PDZ interaction-mediated PKCα-DLG-Ect2 connection we describe in chapter 5, which is specific to PKCα. However, the PKCα-DLG1 signaling module may stimulate Ect2 in other cancers such as glioma; PKCα has been demonstrated to promote either invasion or proliferation in glioma cells (21-23), and Ect2 is essential for invasive phenotype of glioma (24). Also, we show evidence that the PKCα-DLG1 signaling module may be

important for migration in primary astrocytes. If a link between PKCα, DLG1, and Ect2 is demonstrated in cancer, it is possible that the PDZ interaction could be targeted in the design of anti-cancer therapeutics. Efforts to develop therapeutic compounds targeting PDZ interactions are ongoing for other protein-scaffold interactions (reviewed in (25)). Additionally, characterization of the mode of interaction of PKCι-Par6 and Ect2 might provide strategies to target this complex in metastasis apart from developing aPKC kinase inhibitors (26).

Summary

The work described in this thesis employs many different techniques, including novel FRET-based technology, to investigate the regulation of PKC in normal cellular states and in disease (summarized in Figure 6.1). We have determined the spatiotemporal signature of PKC activation in cells in response to G_q-coupled receptor signaling at the level of the organelle, showing rapid, brief kinetics of activation at the plasma membrane compared to slower, prolonged signaling at the Golgi (4). We also studied how the binding affinity of the C1b domain of novel and conventional PKC isozymes directs cellular signaling, showing that the identity of a single residue influences affinity for DAG-containing membranes and resulting sub-cellular localization of novel PKCs (5). In addition to examining properties of the C1b domain in normal cellular signaling, we show that a cancer driver mutation occurring in the C1b domain of PKCβ isozymes desensitizes them to DAG-dependent signaling. This has the surprising effect of tipping the balance toward tumor cell survival by disengaging a feedback loop in which PKC normally phosphorylates K-Ras to promote apoptosis (8). Finally, in a search for novel

interacting partners for PKCα's C-terminal PDZ ligand, we uncover a signaling scaffold composed of PKCα, DLG1, and Ect2, which promotes podosome formation and possibly other cellular functions involving cytoskeletal rearrangements, likely via activation of Rho family GTPases (12). The advances made with this research will hopefully lead to a better understanding of PKC signaling in diseases such as cancer, in which PKC is emerging as a key component in later stages by promoting metastasis and invasion (27).

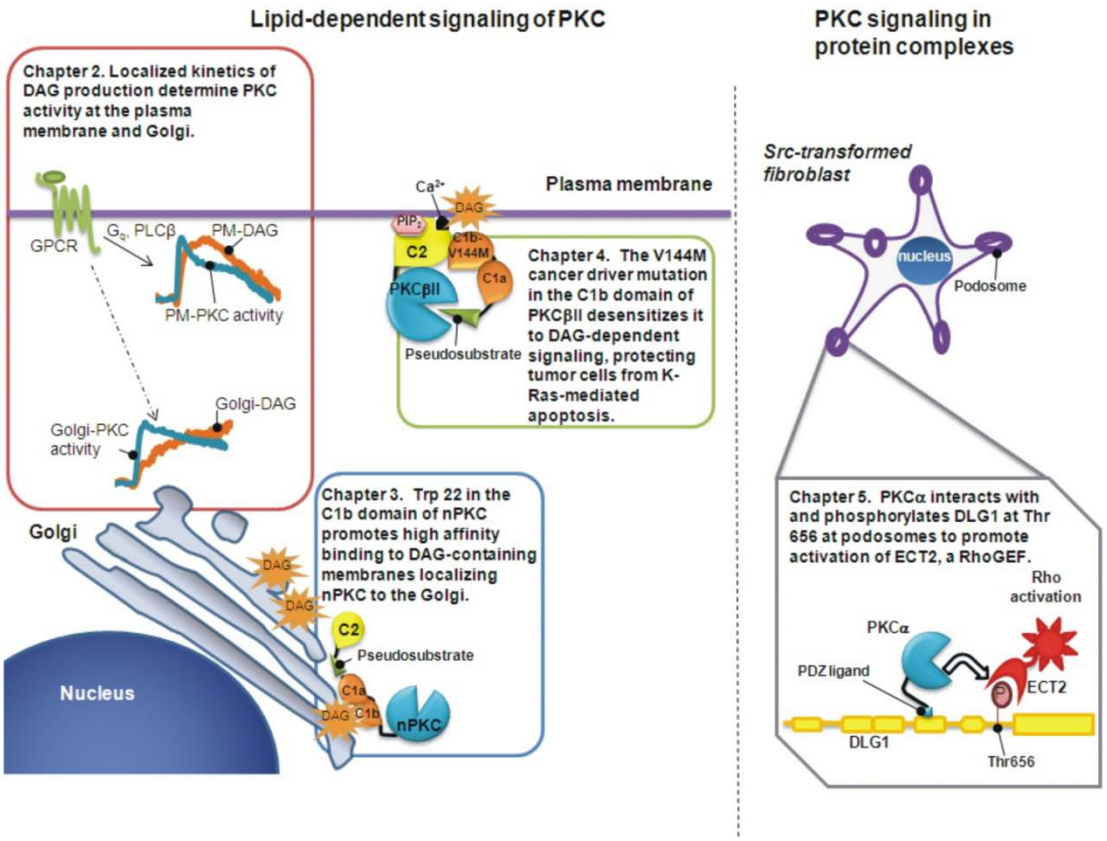

Figure 6.1. Summary of thesis work examining spatio-temporal dynamics of PKC signaling. In Chapter 2, we used FRET-based imaging to visualize the spatial and temporal profile of PKC signaling at cellular organelles. Specifically, we found the kinetics of phosphorylation at the Golgi were prolonged compared to at the plasma membrane, and were governed by localized differences in DAG. In Chapter 3, we discovered that the identity of a single residue at position 22 in the C1b domain of novel and conventional PKC isoforms governs the affinity of the domain for DAG. Trp at this position provides high affinity for DAG membranes and thus targets nPKC isoforms to the Golgi. In Chapter 4, we characterize the effects of a cancer driver mutation, V144M, occurring in the C1b domain of PKCβII, and show that this desensitizes it to DAG-dependent signaling and protects cells from K-Ras-mediated apoptosis. In Chapter 5, we uncover a novel protein scaffold for PKCα, SAP97/DLG1, and reveal how phosphorylation of the scaffold by PKC contributes to cytoskeletal rearrangements during podosome formation, likely by activation of the RhoGEF, Ect2.

References

1. Gallegos, L. L., and Newton, A. C. (2008) *IUBMB Life* **60**(12), 782-789

2. Gould, C. M., and Newton, A. C. (2008) *Curr Drug Targets* **9**(8), 614-625

3. Nishikawa, K., Toker, A., Johannes, F. J., Songyang, Z., and Cantley, L. C. (1997) *J Biol Chem* **272**(2), 952-960

4. Gallegos, L. L., Kunkel, M. T., and Newton, A. C. (2006) *J Biol Chem* **281**(41), 30947-30956

5. Dries, D. R., Gallegos, L. L., and Newton, A. C. (2007) *J Biol Chem* **282**(2), 826-830

6. Tabin, C. J., Bradley, S. M., Bargmann, C. I., Weinberg, R. A., Papageorge, A. G., Scolnick, E. M., Dhar, R., Lowy, D. R., and Chang, E. H. (1982) *Nature* **300**(5888), 143-149

7. Murray, N. R., Weems, J., Braun, U., Leitges, M., and Fields, A. P. (2009) *Cancer Res* **69**(2), 656-662

8. Bivona, T. G., Quatela, S. E., Bodemann, B. O., Ahearn, I. M., Soskis, M. J., Mor, A., Miura, J., Wiener, H. H., Wright, L., Saba, S. G., Yim, D., Fein, A., Perez de Castro, I., Li, C., Thompson, C. B., Cox, A. D., and Philips, M. R. (2006) *Mol Cell* **21**(4), 481-493

9. Levy, M. F., Pocsidio, J., Guillem, J. G., Forde, K., LoGerfo, P., and Weinstein, I. B. (1993) *Dis Colon Rectum* **36**(10), 913-921

10. Doi, S., Goldstein, D., Hug, H., and Weinstein, I. B. (1994) *Mol Carcinog* **11**(4), 197-203

11. Ki, D. H., Jeung, H. C., Park, C. H., Kang, S. H., Lee, G. Y., Lee, W. S., Kim, N. K., Chung, H. C., and Rha, S. Y. (2007) *Int J Cancer* **121**(9), 2005-2012

12. Berdeaux, R. L., Diaz, B., Kim, L., and Martin, G. S. (2004) *J Cell Biol* **166**(3), 317-323

13. Hai, C. M., Hahne, P., Harrington, E. O., and Gimona, M. (2002) *Exp Cell Res* **280**(1), 64-74

14. Saurin, A. T., Durgan, J., Cameron, A. J., Faisal, A., Marber, M. S., and Parker, P. J. (2008) *Nat Cell Biol* **10**(8), 891-901

15. Staudinger, J., Zhou, J., Burgess, R., Elledge, S. J., and Olson, E. N. (1995) *J Cell Biol* **128**(3), 263-271

16. Watts, J. L., Etemad-Moghadam, B., Guo, S., Boyd, L., Draper, B. W., Mello, C. C., Priess, J. R., and Kemphues, K. J. (1996) *Development* **122**(10), 3133-3140

17. Etienne-Manneville, S., Manneville, J. B., Nicholls, S., Ferenczi, M. A., and Hall, A. (2005) *J Cell Biol* **170**(6), 895-901

18. Simpson, K. J., Selfors, L. M., Bui, J., Reynolds, A., Leake, D., Khvorova, A., and Brugge, J. S. (2008) *Nat Cell Biol* **10**(9), 1027-1038

19. Fields, A. P., Calcagno, S. R., Krishna, M., Rak, S., Leitges, M., and Murray, N. R. (2009) *Cancer Res* **69**(4), 1643-1650

20. Justilien, V., and Fields, A. P. (2009) *Oncogene*

21. Cho, K. K., Mikkelsen, T., Lee, Y. J., Jiang, F., Chopp, M., and Rosenblum, M. L. (1999) *Int J Dev Neurosci* **17**(5-6), 447-461

22. Fan, Q. W., Cheng, C., Knight, Z. A., Haas-Kogan, D., Stokoe, D., James, C. D., McCormick, F., Shokat, K. M., and Weiss, W. A. (2009) *Sci Signal* **2**(55), ra4

23. Amos, S., Mut, M., diPierro, C. G., Carpenter, J. E., Xiao, A., Kohutek, Z. A., Redpath, G. T., Zhao, Y., Wang, J., Shaffrey, M. E., and Hussaini, I. M. (2007) *Cancer Res* **67**(21), 10241-10251

24. Salhia, B., Tran, N. L., Chan, A., Wolf, A., Nakada, M., Rutka, F., Ennis, M., McDonough, W. S., Berens, M. E., Symons, M., and Rutka, J. T. (2008) *Am J Pathol* **173**(6), 1828-1838

25. Wang, N. X., Lee, H. J., and Zheng, J. J. (2008) *Drug News Perspect* **21**(3), 137-141

26. Jin, Y. T., Ying, X. X., Hu, Y. H., Zou, Q., Wang, H. Y., and Xu, Y. H. (2008) *Oncol Res* **17**(2), 59-68

27. Fields, A. P., and Regala, R. P. (2007) *Pharmacol Res* **55**(6), 487-497